STUDY OF FORMABILITY AND FRACTURE OF ALUMINUM ALLOYS

STUDY OF FORMABILITY AND FRACTURE OF ALUMINUM ALLOYS

By

BAL. K. SAREEN, M.Tech.

A Thesis

Submitted to the School of Graduate Studies

in Partial Fulfillment of the Requirements

for the Degree

Master of Engineering

McMaster University

March 1976

MASTER OF ENGINEERING (1976) McMASTER UNIVERSITY
(Mechanical Engineering) Hamilton, Ontario

TITLE: Study of Formability and Fracture of Aluminum Alloys

AUTHOR: Bal Krishan Sareen, B.Sc.(Mech. Eng.) Ranchi University
M.Tech.(Prod. and Ind. Eng.) I.I.T. Delhi.

SUPERVISOR: Dr. R. Sowerby

NUMBER OF PAGES: xiv; 142

SCOPE AND CONTENTS:

High strength to weight ratio materials are becoming of increasing importance in the automotive industry. Some aluminum alloys offer strength equivalent to low carbon sheet steel at one third its weight. However, for these alloys no production experience exists. The present work involves the study of formability of three important grades of formable aluminum alloys. Strain distributions have been examined for the materials deformed under different conditions of biaxial straining. In particular the maximum useful strains (limit strains) have been obtained as well as the fracture strains.

A detailed description of fundamental property tests and simulative tests have been provided in this thesis.

Computer programs developed by the author to compute plastic properties of the materials from the test data are also provided.

Some instability analyses have been examined with particular reference to their ability to assess the influence of material properties and the loading system on the useful forming limits.

ACKNOWLEDGEMENTS

I would like to express my gratitude to Dr. R. Sowerby, who as my supervisor has been immensely helpful throughout the duration of this work.

Many thanks are also extended to Dr. J.L. Duncan and Dr. J. Kolodzieski whose support and continued interest contributed to the success of this work.

The author also wishes to express his appreciation to Mrs. Lorraine Felbel for her expert typing of the manuscript.

Finally, I wish to thank the Canadian Commonwealth Scholarship and Fellowship Committee on whose financial support I was able to complete this work.

TABLE OF CONTENTS

LIST OF SYMBOLS

		UNITS
σ	Normal Stress	FL^{-2}
P	Tensile Load	F
A	Cross Section Area	L^2
ℓ	Gauge Length	L
ε	Normal Strain (logarithmic)	-
p	Hydrostatic bulge pressure	FL^{-2}
R	Radius of Curvature	L
t	Thickness	L
r	Plastic strain ratio	-
K	Strength Coefficient	FL^{-2}
m	Strain Rate Sensitivity index	-
n	Strain Hardening Index	-
ε_o	Pre-strain	-
$\dot{\varepsilon}$	Strain rate	T^{-1}
$\bar{\sigma}$	Equivalent stress	FL^{-2}
$\bar{\varepsilon}$	Equivalent strain	-
τ	Shear stress	FL^{-2}
γ	Shear strain	-
ε_f	Fracture strain	-
ε^*	Limit strain	-
ε^*_ℓ	Limit strain in localized necking	-
ε^*_d	Limit strain in diffuse necking	-
a	Strain ratio ($\varepsilon_2/\varepsilon_1$)	-

α	Stress ratio (σ_2/σ_1)	-
f	Inhomogeneity index	-
$\varepsilon_{1(o)}$	Limit strain normal to the groove in a state of plain strain	-

LIST OF SUBSCRIPT

X,Y,Z	Refer to general components of stress and strain in a Cartesian Co-ordinate System.
1,2,3	Refer to principal directions of stresses and strains.
0,45,90	Angle of specimen orientation w.r to the rolling direction of sheet metal.
A	Region outside Marciniak Groove.
B	Region inside Marciniak Groove.
0	Initial Condition.

LIST OF FIGURES

LIST OF TABLES

CHAPTER I

INTRODUCTION

Formability is one of the most important properties of metals. Generally it is regarded as that property of a material which permits plastic deformation to proceed without failure by fracture, buckling, wrinkling, necking, etc.

Formability is an elusive quality to measure since there is no single index that will enable the formability of a specific material to be reliably predicted for all production conditions. Both material parameters and process parameters influence the final behaviour of the material.

Over the last five decades, low carbon sheet steel has been the most dominant material in consumer industries because it can be stamped into inexpensive, complex components at very high production rates. Recently, however more attention is being paid, particularly in the automotive industry, to materials offering greater strength to weight ratios. Mainly two classes of materials viz; High Strength Low Alloy Steels (HSLA steels) and High Strength Aluminum Alloys fall under this category. The purpose of this project is to investigate material parameters and assess formability of some aluminum alloys, of interest to the automotive industry.

Some aluminum alloy sheets offer strength equivalent to low carbon sheet steel but at one third of the weight. Apart from low density, aluminum differs from steel in many other properties. It has a lower melting point and poor resistance to creep at elevated temperatures. On the other hand, at low temperatures where steel becomes brittle, aluminum alloys may actually increase in ductility. In most situations aluminum alloys exhibit greater corrosion resistance than steel due to the formation of a protective oxide layer on the surface. In addition aluminum has high thermal and electrical conductivity and is non-magnetic.

The modulus of elasticity of aluminum is three times less than that of steel. This can lead to higher spring back in forming, higher stored strain energy (at the same stress level), which may influence fracture propagation and lower resistance to deflection and buckling, other things being equal.

From a microstructural point of view aluminum has a face-centred cubic crystal structure (f.c.c.) and steel at room temperature has a body-centred cubic crystal structure (b.c.c.). The f.c.c. structure has more available slip systems and is therefore intrinsically more isotropic than b.c.c.

In conventional steels the important strengthening mechanisms are strain hardening, grain refinement and the

presence of interstitials like carbon and nitrogen.

Pure aluminum is soft and ductile, the higher strength is principally obtained by addition of alloying elements. Further strengthening is possible by various degrees of cold working in non-heat treatable alloys, whereas for heat treatable alloys additional strengthening is possible by solution heat treatment and precipitation hardening.

A wide variety of aluminum both in non-heat treatable and heat treatable alloys are available. For aluminum to replace low carbon steel, these alloys are required to have good strength and good formability characteristics, so that they are suitable for use in automotive industry, which is certainly one of the largest consumers of sheet metal.

The forming characteristics of the group of alloys selected is of interest to Alcan, General Motors and Chrysler and some work is being undertaken within these companies. Hopefully, all of these investigations will lead to a more meaningful comparison between the performance of individual alloys as well as that of mild steel. The behaviour of these alloys vis a vis that of mild steel is of interest since dies, tooling etc. and the whole sequencing of the processing operations has been designed around steel. No doubt certain features of existing tooling and production lines will have to be modified if aluminum replaces mild steel.

Formability has been extensively studied for low carbon steels. A Forming Limit Diagram (FLD), originally developed by S.P. Keelar [1,2] and then extended by Goodwin [3], was proposed to understand steel behaviour in sheet forming process. The FLD has taken on some significance as a diagnostic tool.

Much work has been done to correlate basic material parameters to its behaviour in drawing and/or stretching, both empirically [4-7] and theoretically [8-12].

In recent years the FLD together with material parameters have been utilized to assess the formability of newly developed aluminum alloys. Hecker [13,14] and others [15] have compared the formability of different aluminum alloys both with that of steel and among themselves. It has generally been concluded that the aluminums have poorer forming capabilities than mild steel and the FLD is quite different for different alloys.

Some aluminum alloys have been tested previously at McMaster and a comparative performance of these alloys and Aluminum Killed Drawing Quality (AKDQ) steel during deep drawing of square cups has been assessed [16]. It was shown that the performance of aluminum alloys can not be predicted from normal tensile data. However, ductile fracture properties in high strength aluminum alloys appears to influence the behaviour in the cup drawing process.

With the present work it is proposed to look into the behaviour of aluminum alloys both in fundamental material property tests e.g. the tensile test and certain simulative tests. These latter tests rarely duplicate the real forming operation (this only occurs in the actual press trials) but are simulations carried out under controlled laboratory conditions involving certain stretching and drawing operations. The tests performed are described in greater detail in Chapters 2 and 4. It is the aim of the work to reveal data about the useful forming limits (prior to failure) as well as the fracture characteristics of the individual alloys as a function of the straining path.

CHAPTER II

DESCRIPTION OF TESTS

In the study of formability of sheet metal both fundamental material tests and simulative tests are required to be performed. This chapter defines the most important material parameters and techniques of determining them from fundamental material tests like the Tensile Test, Bulge Test and In-Plane Torsion Test.

Simulative tests which aid to assess the material behaviour in a particular sheet metal forming operation under simulated processing conditions are discussed later in this chapter.

2.1 Fundamental Material Property Test

2.1.1 Tensile Test

The tensile test is perhaps the most widely employed test for the determination of mechanical property data. The test is so well known that a little space need be devoted here to its description.

While the test is often used to evaluate the elastic constants of a material, these are not the most pertinent parameters in assessing material formability. The parameters significant to formability are: yield stress, ultimate tensile strength, work hardening index, strain rate sensi-

tivity index, plastic strain ratio, limit strain, total elongation and fracture strain. These quantities are described in greater detail in Section 2.1.2.

Computer programs have been developed by the author (discussed in the Art.4.8 &9 of Chapter IV) which are designed to compute true stress and true strain from load-extension data obtained from a tensile test. These true stress and true strain values are then used to compute the constitutive equation of the form

$$\sigma = K(\varepsilon + \varepsilon_o)^n \quad *$$

2.1.2 Definition of Some Important Material Parameters Which Can be Determined From the Tensile Test

(i) Yield Stress is the stress required to induce plastic flow in the material.

a) Some materials exhibit clearly the yield point on a load vs. extension plot. Thus, yield stress is numerically equal to

$$YS = \frac{\text{Yield Point Load}}{\text{Original Cross Section Area}} \qquad (2.1)$$

Some materials exhibit an upper and lower yield point stress, for this kind of material the extension is associated with discontinuous yielding which occurs at approximately constant load following the onset of plastic flow. Such an elongation

---

* For symbols refer to nomenclature given at the beginning of this thesis.

is called "yield point elongation" and is associated with the propagation of Luder's lines or bands.

b) Some materials do not exhibit a clear yield point. In such a case so called 0.2% Yield Stress is a measure of the stress required to cause plastic deformation. The load used to calculate it is determined as shown in Fig. 1. The required load (P_y) is found at the intersection of the line drawn on the load-extension graph parallel to the initial slope but offset from it by an extension of 0.2% with the load-extension curve. Thus, 0.2% Yield Stress is numerically equal to

$$0.2\%\ YS = \frac{P_y}{\text{Original Cross Section Area}} \qquad (2.2)$$

(ii) Ultimate Tensile Strength

The ultimate tensile strength is the indication of the maximum strength of a material. This parameter is, according to Fig. 1, determined as follows

$$UTS = \frac{\text{Maximum Load}}{\text{Original Cross Section Area}} \qquad (2.3)$$

The ultimate strength, because it is based on the original cross sectional area of the test piece, is not always a good indicator of the material plastic behaviour. This objection can be overcome by calculating the true stress at the point of maximum load, obtained by dividing the maximum load by the current cross sectional area just prior to the onset of

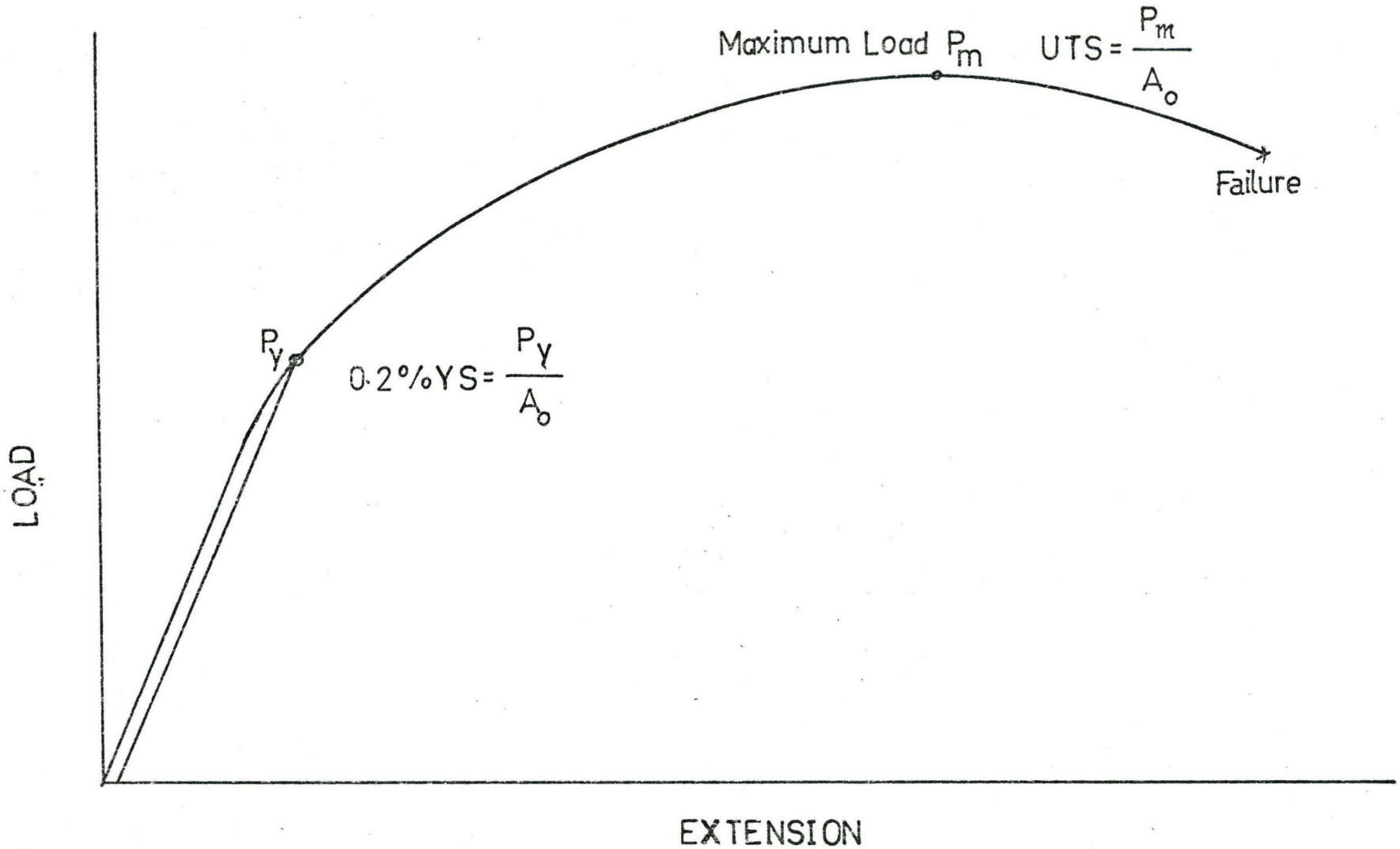

FIGURE 1 DETERMINATION OF 0.2% YS. AND UTS.

diffuse necking.

(iii) Work Hardening Index

Most materials exhibit an increase in strength and hardness during the plastic deformation process. The common measure of work hardening ability is the strain hardening index or n-value obtained by fitting the true stress-natural strain data with the generalized material behaviour law

$$\sigma = k\ (\varepsilon_o + \varepsilon)^n\ \dot{\varepsilon}^{\ m} \qquad (2.4)$$

where $\dot{\varepsilon}$ - strain rate

σ - flow stress of material

ε - logarithmic strain

k - strength constant

n - work hardening index

m - strain rate sensitivity factor

ε_o - initial strain

This equation was chosen for its mathematical convenience, it is easy to handle in theoretical analyses and it is able to fit many monotonically increasing curves quite reasonably.

It was found that in certain cases the n-value remains essentially constant for different orientation with respect to the rolling direction of sheet metal. For materials in which n-value alters as a function of orientation it has become customary to designate the direction in which "n" was determined.

In many cases the strain rate sensitivity of the material may be neglected so that the equation 2.4 takes form

$$\sigma = k\ (\varepsilon_o + \varepsilon)^n \qquad (2.5)$$

(iv) Strain Rate Sensitivity Factor

Strain rate sensitivity factor or m-value is a measure of the degree to which plastic flow of the material is affected by changes in deformation rate. It may be expressed numerically by the equation

$$m = \frac{\ln \frac{\sigma_1}{\sigma_2}}{\ln \frac{\dot{\varepsilon}_1}{\dot{\varepsilon}_2}} \qquad (2.6)$$

where σ_1, $\dot{\varepsilon}_1$, σ_2, $\dot{\varepsilon}_2$ stresses and corresponding strain rates at the same level of strain in tensile test.

It has been found that in most cases the m-value remains essentially constant for the range of plastic strains up to the point of instability, and for the range of strain rates encountered in industrial practice. The m-value may alter as a function of the direction in the plane of the sheet. In this case it is necessary to designate the direction, with respect to that of rolling, in which "m" was determined.

(v) Plastic Strain Ratio (r value)

Invariably all metal working processes introduce some directionality (or preferred orientation) to the crystal

structure. It is now recognized that crystallographic texture is the primary source of anisotropic behaviour of the material.

Starting with two (or more) different pole figures, techniques are now available to provide a mathematical description of the texture existing in a given cubic metal [17]. However, these methods are reasonably complex and it has become customary to obtain a mechanical index of the degree of plastic anisotropy through the "r" value. This quantity is defined as the ratio of true width strain to true thickness strain determined from tests on tensile specimens cut from different orientations in the plane of a sheet material.

Numerically "r" is given by

$$r = \frac{\varepsilon_w}{\varepsilon_t} = \frac{\ln {}^{w}/_{w_o}}{\ln {}^{t}/_{t_o}} \qquad (2.7)$$

where "w" and "t" represents the width and thickness respectively and the subscript "o" represents the original dimension.

It has been found that in certain cases the ratio remains essentially constant for the range of plastic strains up to the point of instability in the tensile test.

For materials in which "r" alters as a function of strain, it has become customary to use a superscript to

designate the strain level at which "r" is determined. Thus, if the strain level of 20 per cent was employed then this would appear as r^{20}.

In addition to the possibility that "r" can vary with strain, it can (and invariably does) vary with the orientation within the plane of the sheet. Again, it has become customary to refer all orientations with respect to the rolling direction and to use a subscript to define the orientation such as r_o, r_{45}, r_{90}, etc. Thus

$$r_o^{20}$$

would define the "r" value determined at 20 per cent strain for a specimen orientated along the rolling direction.

If all "r" values are constant within the plane of the sheet the material is said to possess Planar Isotropy. This does not imply that the material as a whole is isotropic; this would only arise when "r" was equal to unity. A material exhibiting planar isotropy but with "r" greater than unity shows improved thickness strength and better deep drawing characteristics vis a vis the isotropic material. The reverse is true when $r < 1$.

As already mentioned more often than not "r" does vary with the orientation. However, recourse is often made to some averaging technique based on the variation in "r" with orientation in order to specify an average value for the material and this is usually designated, $\bar{r}$. See section

2.1.2(x).

Depending upon the magnitude of $\bar{r}$ so determined, the thickness strength and deep drawability characteristics are interpreted in the same way as if the material did possess planar isotropy.

(vi) Limit Strain

Limit strain is defined as the maximum uniform strain measured as close as possible to the necked zone. The value of limit strain depends upon both the properties of the deformed material and mode of loading.

(vii) Total Elongation

Total elongation is a parameter measured in a tensile test used as a measure of ductility and is defined as

$$\varepsilon_t(\%) = \frac{\text{final gauge length - original gauge length}}{\text{original gauge length}} \times 100 \quad (2.8)$$

The magnitude of total elongation is influenced very strongly by the gauge length, so that it is necessary to designate the original gauge length used.

It has become customary to use a 2" gauge length.

(viii) Fracture Stress

Fracture stress is the true stress at fracture which is the load for fracture divided by final cross section area.

(ix) Fracture Strain

Fracture strain is the natural strain at fracture defined by the relationship,

$$\varepsilon_f = \ln \left(\frac{\text{initial cross section area}}{\text{final cross section area}}\right) \qquad (2.9)$$

or alternately and the more commonly used (for rectangular specimens) thickness strain

$$\varepsilon_{3f} = \ln \left(\frac{\text{initial thickness}}{\text{final thickness}}\right) \qquad (2.10)$$

It is worthwhile emphasizing that it has not been clearly established how the fracture strain alters as a function of the loading condition for a wide class of materials. There is apparently a great deal of attention being paid to this question but as yet very few results have found their way into the technical literature.

(x) Weighted Average

The average values of the parameters is obtained through a weighted average if x is the parameter reported then

$$x_{av} = \frac{x_o + 2\,x_{45} + x_{90}}{4} \qquad (2.11)$$

Where suffix 0, 45 and 90 are angles in degrees at which the specimen was cut with respect to the rolling direction.

Other variations on the above averaging techniques are available depending upon the number of directions in which the tensile tests are made. It is to be noted, the values are not weighted in any true statistical sense.

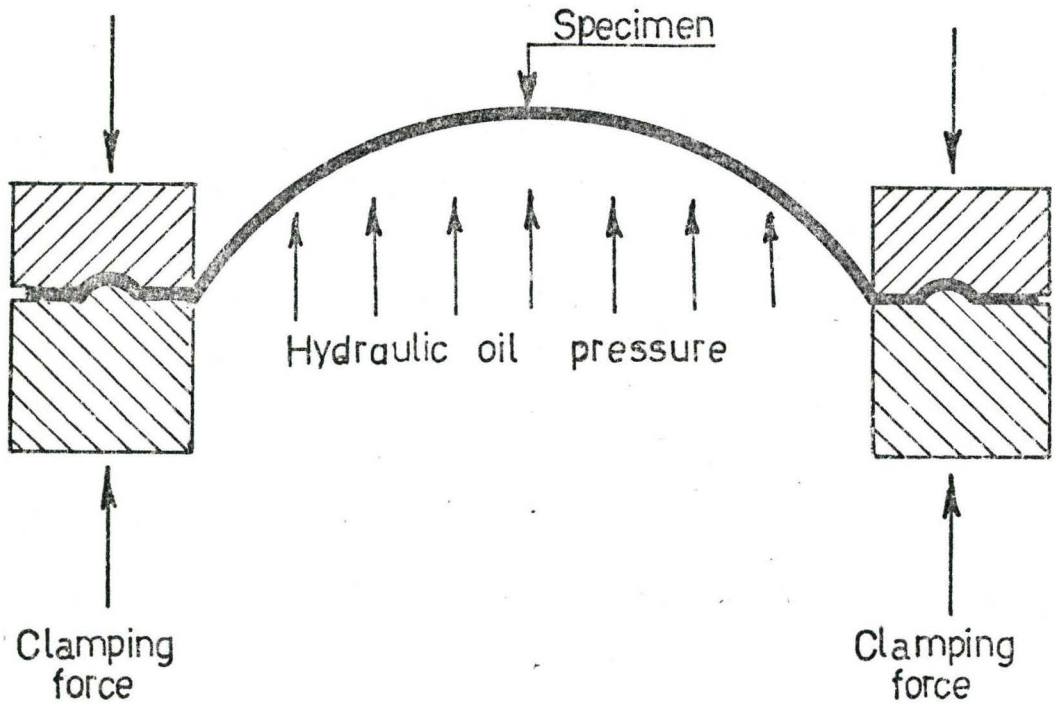

FIGURE 2 SCHEMATIC DIAGRAM OF BULGE TEST

2.1.3 Bulge Test

The maximum uniform strain of the specimen stretched uniaxially in tensile test is limited by the onset of diffuse necking. For most materials the uniform strain achieved is of the order of work hardening index. This limitation can, however, be overcome by testing the material in balanced biaxial tension using a hydrostatic bulge test [8].

In this test a sheet clamped at the circumference is bulged by oil pressure applied to one side of the specimen (see Fig. 2). Stress - strain data up to the point of fracture is obtained by using a pressure gauge and a mechanical spherometer and extensometer which sits at the top of the specimen [18]. For an isotropic material a plot of membrane stress versus thickness strain should be equivalent to the stress strain curve for uniaxial test.

The bulge test enables the range of the true stress-strain curve to be extended beyond that obtainable from the uniaxial tensile test. This is particularly noticeable for material having a low strain hardening index. For example, 3003-H14 aluminum exhibited a maximum uniform strain of 0.02 in uniaxial tension and a uniform strain of 0.54 in the bulge test. Clearly this material has considerable ductility which is not apparent from the tensile test.

2.1.4 In-Plane Torsion Test

The determination of the "n" value on the basis of

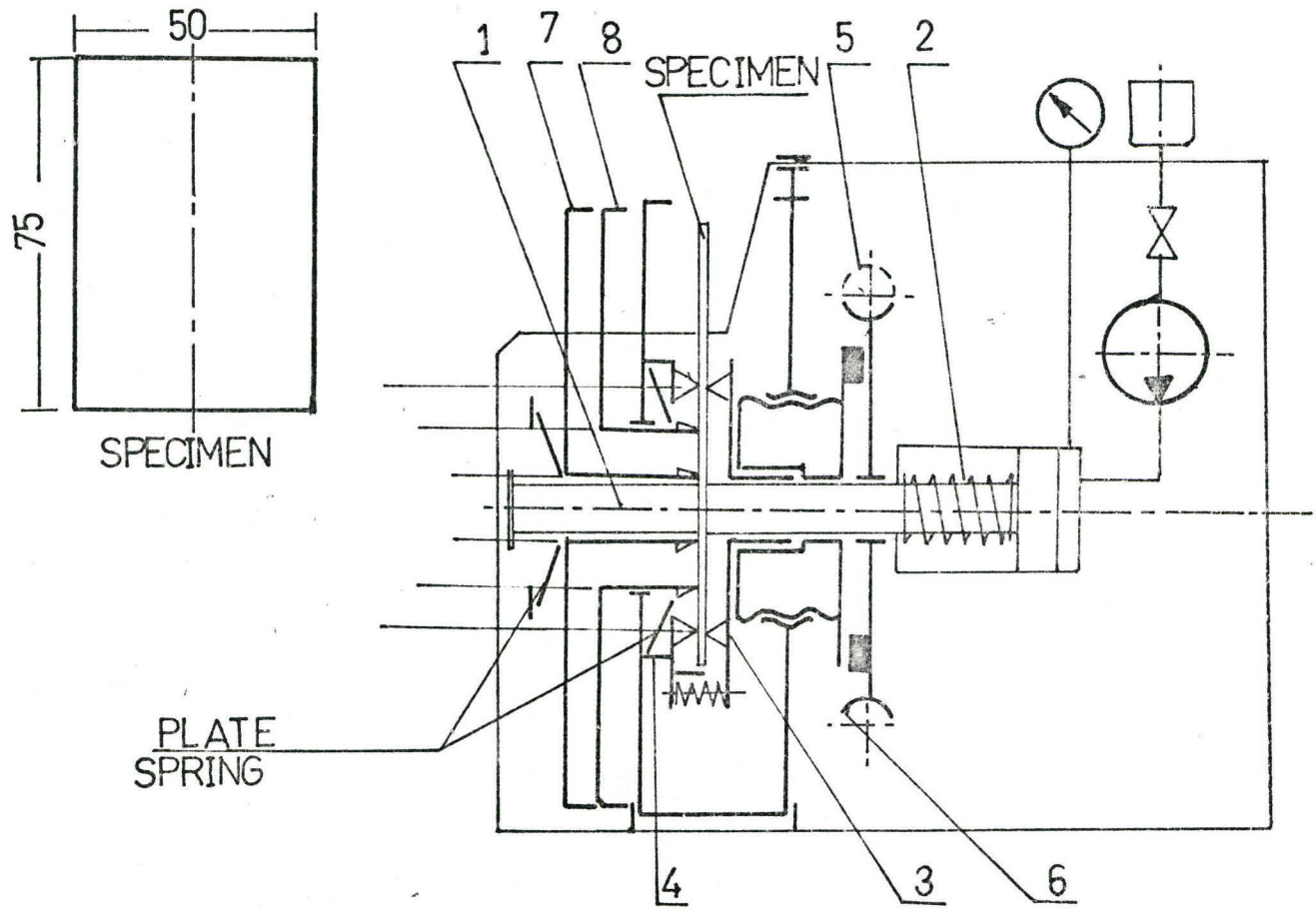

1,2	INNER ANVIL
3,4	OUTER ANVIL
5	WORM
6	WORM WHEEL
7,8	MEASURING DRUM

FIGURE - 3 SCHEMATIC DIAGRAM FOR IN-PLANE TORSION TEST

the tensile or bulge test is easy and accurate but can be time consuming. However, the evaluation of fracture strain from these two tests causes more serious difficulties for the following reasons.

i) direct measurements of sheet metal thickness at the failure site is troublesome and the results obtained are subject to great errors particularly when thin sheets are to be measured.

ii) the stress state in the groove, which preceeds fracture is not constant but is subject to change during the deformation process.

A test designed to overcome the above mentioned difficulties is described in reference [19] and is termed the "In-Plane Torsion Test". A pair of opposed annular clamps grip a coupon of the test material. Within the annular clamps, and concentric with them, a pair of opposed anvils grip the sheet and twist it until fracture occurs. The fracture strain as well as the work hardening index can be readily evaluated from the test as described in reference [9]. Fig. 3 illustrates the essential features of the equipment.

It is worthwhile repeating a comment made in Chapter I, namely that very little data exists regarding the influence of the straining process on the fracture strain. A comparison of the fracture strains ensuing from the various tests described here will therefore be of interest and is one

of the objectives of this thesis.

2.2 Simulative Tests

The tests described so far can be considered as a fundamental property test. These tests are distinct from the so called simulative tests which purport to simulate some aspect of the actual processing condition.

In all practical sheet metal forming operations, the material experiences some degree of stretching and/or drawing. Simulative tests are designed therefore to induce a certain amount of stretch and/or draw to the material and to monitor the material response to these tests under controlled laboratory conditions.

2.2.1 Swift Cupping Test

This test simulates a 100% drawing operation and is often considered to be most useful in distinguishing the drawing properties of sheet metal. The parameter most often referred to in the context of the Swift Cup Test is the "Limiting Drawing Ratio" (LDR). A circular specimen is drawn through a circular die by a circular flat bottomed punch of 2" diameter, See Fig. 4. A series of blanks, increasing in diameter by small increments are drawn, until a specimen fails. The maximum size of the blank that was drawn successfully is the limiting blank size and the LDR is given as follows,

$$LDR = \frac{\text{Limiting Blank Diameter}}{\text{Punch Diameter}}$$

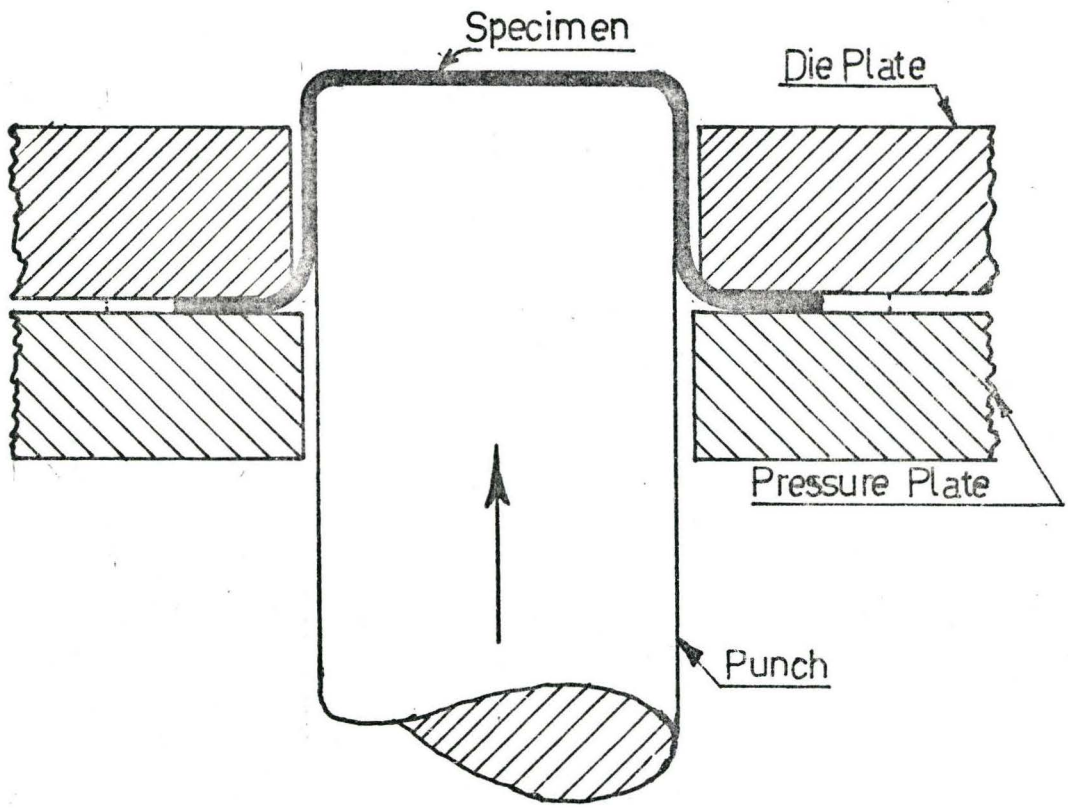

FIGURE 4 SCHEMATIC DIAGRAM FOR SWIFT CUP TEST

The results of this test have been found to be highly dependent upon the lubrication of the specimen and blank holder pressure.

It was shown by Whitely [6] and others [20] that there is a good correlation between LDR and the "r" value. LDR increases for a material with a higher "r" value.

2.2.2 Stretch Bend Test

In the stretch bend test a specimen in the form of a strip is rigidly clamped at each end, as shown schematically in Fig. 5, and bent at the centre using a radiused punch until transverse cracking of the specimen occurs. The process variables are the punch radius, r, specimen thickness t, and the unsupported length, l, of the specimen. All these parameters influence the ensuing strain distribution in the specimen and the depth of punch penetration before fracture occurs. This test simulates the bending and stretching of the material over a die radius. Further details of the test can be found in reference 21.

2.2.3 Fukui Test

In this test, a circular specimen of given diameter (for a particular thickness range) is drawn through a conical die. The test involves drawing and stretching and the test value is given by the following,

$$\text{FUKUI VALUE} = \frac{\text{Average diameter of the test piece after fracture}}{\text{Blank diameter}}$$

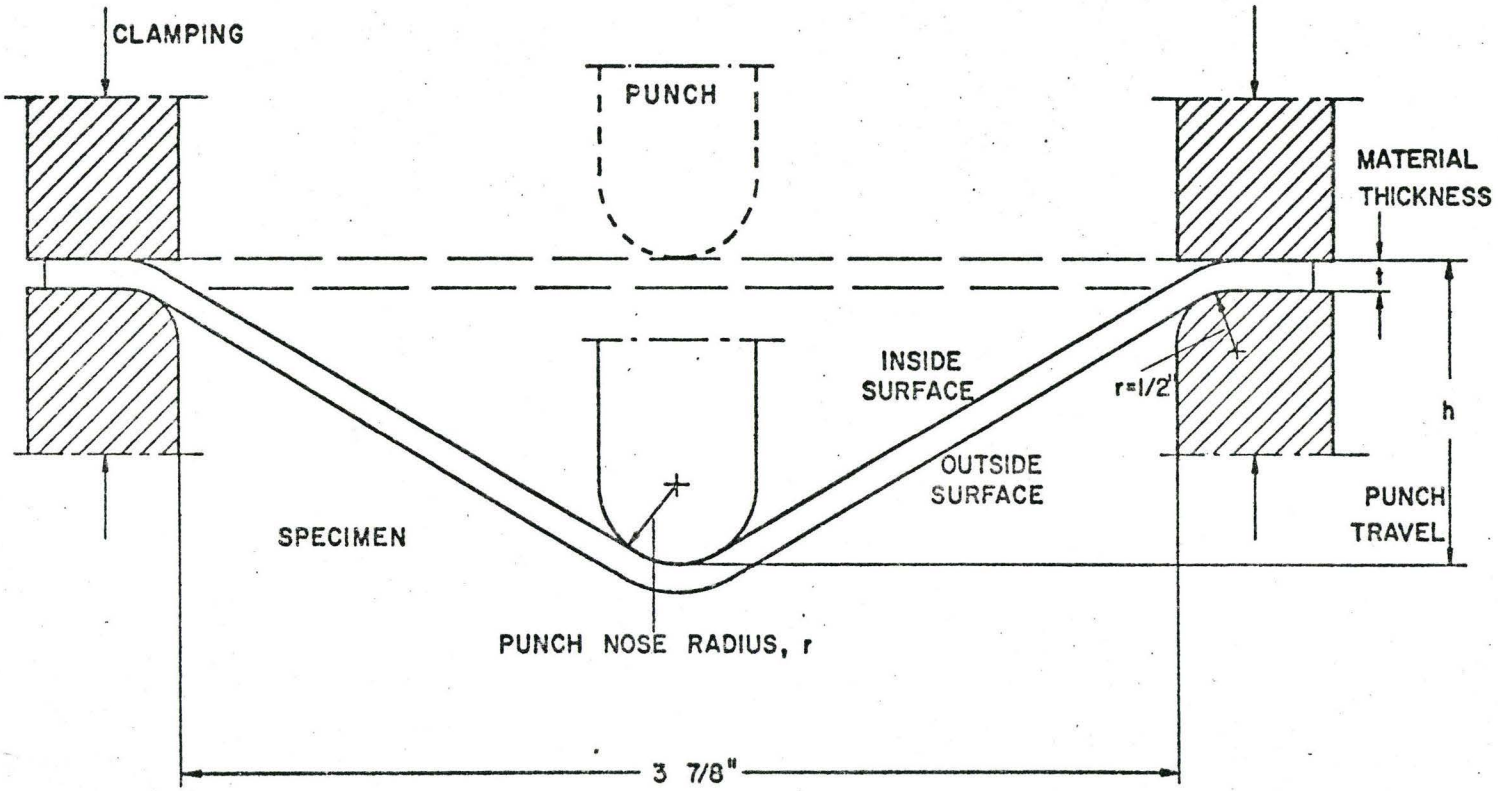

FIGURE 5 SCHEMATIC DIAGRAM OF STRETCH BEND TEST

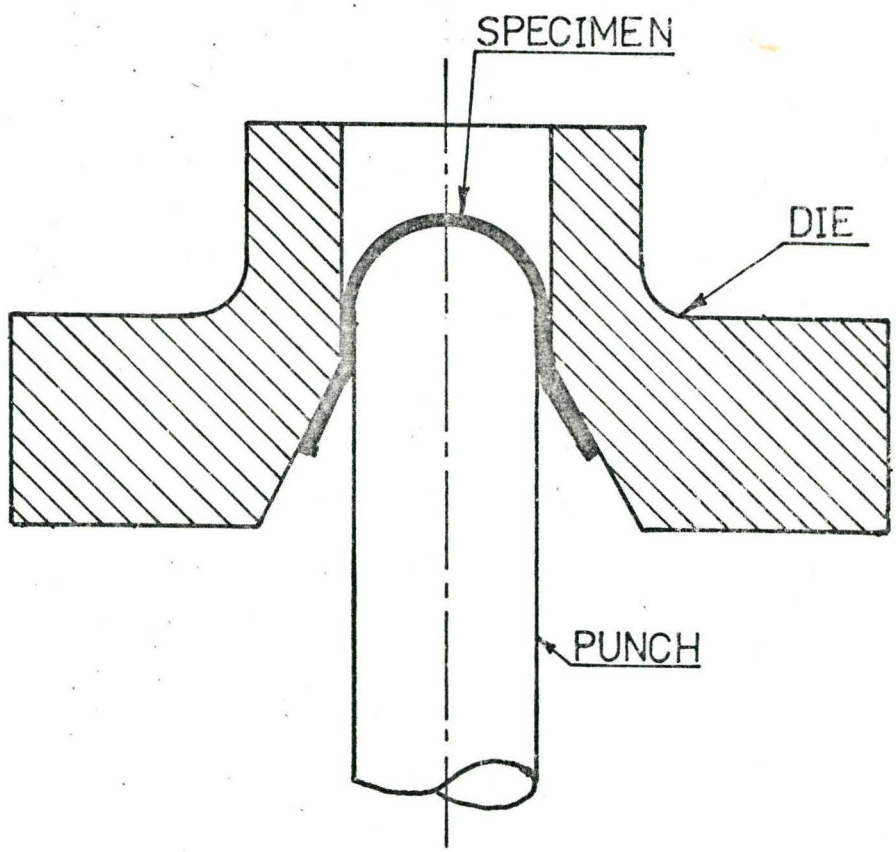

FIGURE 6 FUKUI TEST

Due to earing the periphery of the test piece is non circular. The diameter across the ears and in the hollows are measured and then the average diameter is computed. The process is shown schematically in Fig. 6.

2.2.4 Erichsen and Olsen Tests

The Erichsen test is commonly used in Europe. A steel ball of 20 mm diameter is pushed through a die until the specimen fractures. The test piece, which is generally a strip specimen is clamped (1000 kg load) to prevent drawing-in, refer to Fig. 7. The depth of indentation is measured in mm. This test has commercial significance in that it is widely used as a quality control procedure.

The Olsen test is an American version of the Erichsen test and uses a 7/8" ball. In this case the measurement made is that between the bottom surface of the specimen and the top of the bulge. It therefore takes thinning into account.

These tests are usually regarded as 100% stretch tests. However, there has been some claim that the Erichsen and Olsen tests are not able to give good correlation with actual production stampings because of the following reasons.

(a) insufficient size of the penetrator

(b) inability to prevent inadvertent drawing-in of the flange

and (c) inconsistent lubrication.

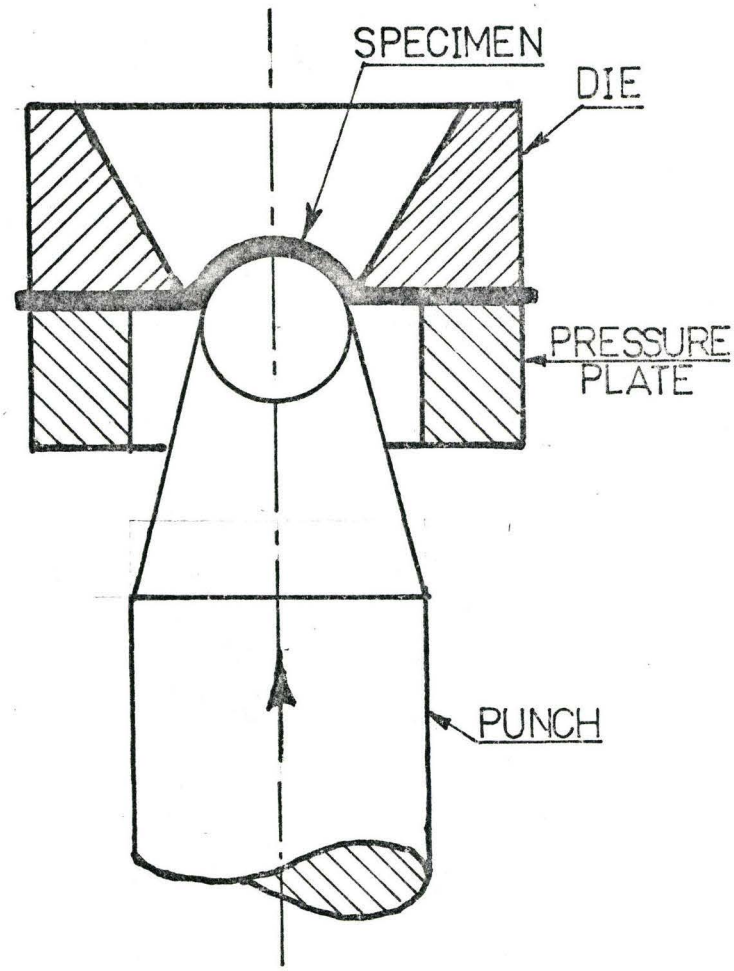

FIGURE 7 ERICHSEN/OLSEN TEST

2.2.5 Hecker Cup Test

Because the Erichsen and Olsen tests have not been entirely satisfactory in their ability to assess stretchability another cup method was developed by Hecker [22] which is a scaled up version of the Erichsen and Olsen tests. It uses a 4" hemispherical punch and a very positive clamping arrangement to prevent drawing-in*. For steel sheet Hecker showed that the cup height could be successfully correlated to the "n" value. For other materials such as brass, aluminum and zinc however, total elongation in uniaxial tension correlated well with cup height.

2.2.6 Plane Strain Test

The test developed by Marciniak et al [12] consists of in-plane stretching of the sheet metal. The method adopted in this test consists of applying to a plane piece of sheet biaxial tension in such a manner that the value of the ratio of the principal strains is essentially constant, ($a = \frac{\varepsilon_2}{\varepsilon_1}$), over a finite region in the plane of a sheet. The test is shown schematically in Fig. 9. In order to facilitate proportional straining in the plane of the test piece a secondary piece of sheet material is employed. This auxiliary sheet has a hole cut in its centre which approximates to the shape of the punch. The two pieces of sheet material are clamped together around their periphery and penetrated by the punch. The punch is in contact with the

---

* Fig. 8 shows the schematic diagram of the test set up.

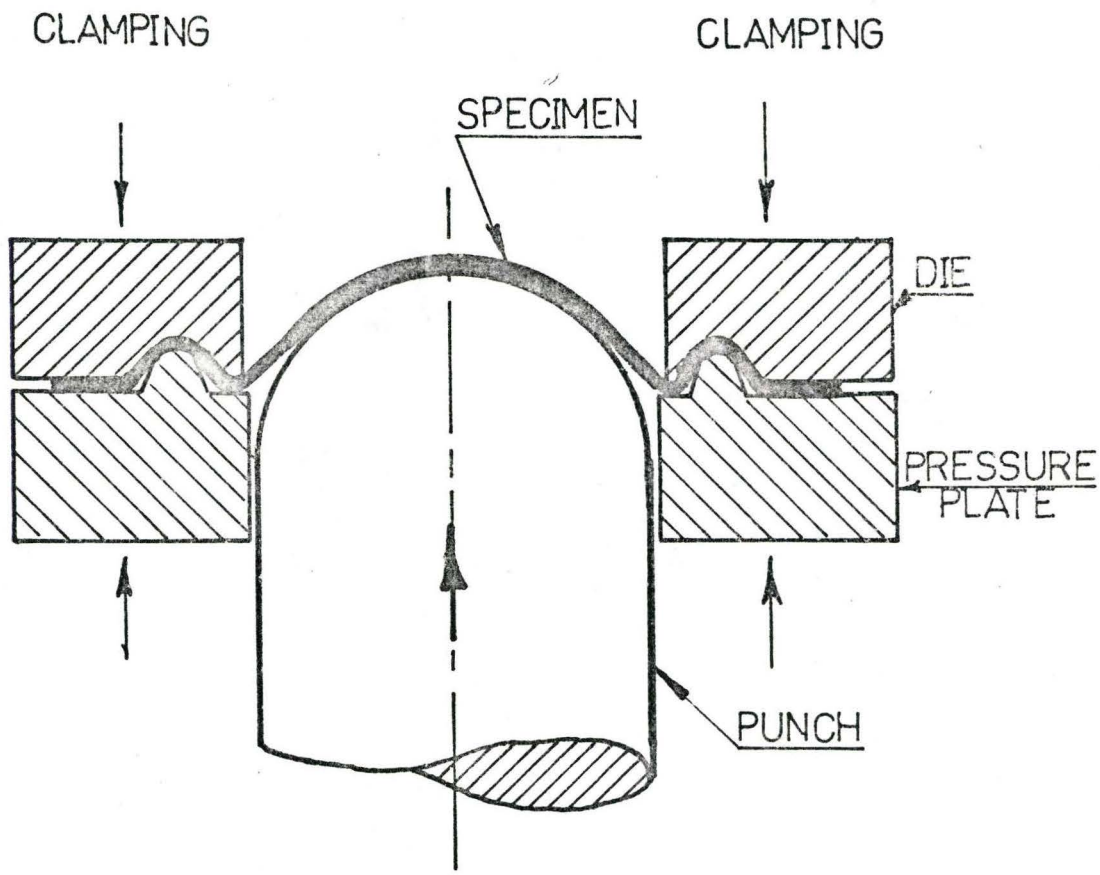

FIGURE 8 HECKER CUP TEST

secondary sheet which, because of the presence of the hole, wants to stretch at a faster rate than the actual specimen. This tendency facilitates the deformation of the actual test piece; note that this is achieved by the frictional forces between the auxiliary sheet and test piece over the region where the two are in contact.

By altering the shape of the punch and die and the hole in the secondary test piece different degrees of proportional straining can be achieved in the test piece.

In the present case to achieve a condition of plane strain (a = o) a rectangular punch whose sides were in the ratio, $\ell_1/\ell_2 = 4.6$, was employed. This equipment is shown in Fig. 10.

2.3 Forming Limit Diagram

The Forming Limit Diagram depicts the extent of the maximum useful straining (i.e. prior to visible necking, wrinkling, fracture, etc.) that a material can exhibit. The FLD is invariably presented as a curve employing the principal surface strains (ε_1 and ε_2) as co-ordinate axis as shown schematically in Figure 11. As illustrated in Figure 11 the curve represents a Fail-Safe envelope of surface strains. Obviously no material behaves in such a way that a single line can represent the region between safety and failure. Consequently, in reality a transition zone (which might be represented by a band on Figure 11) exists. The width of this "uncertainty band" could be taken to represent the

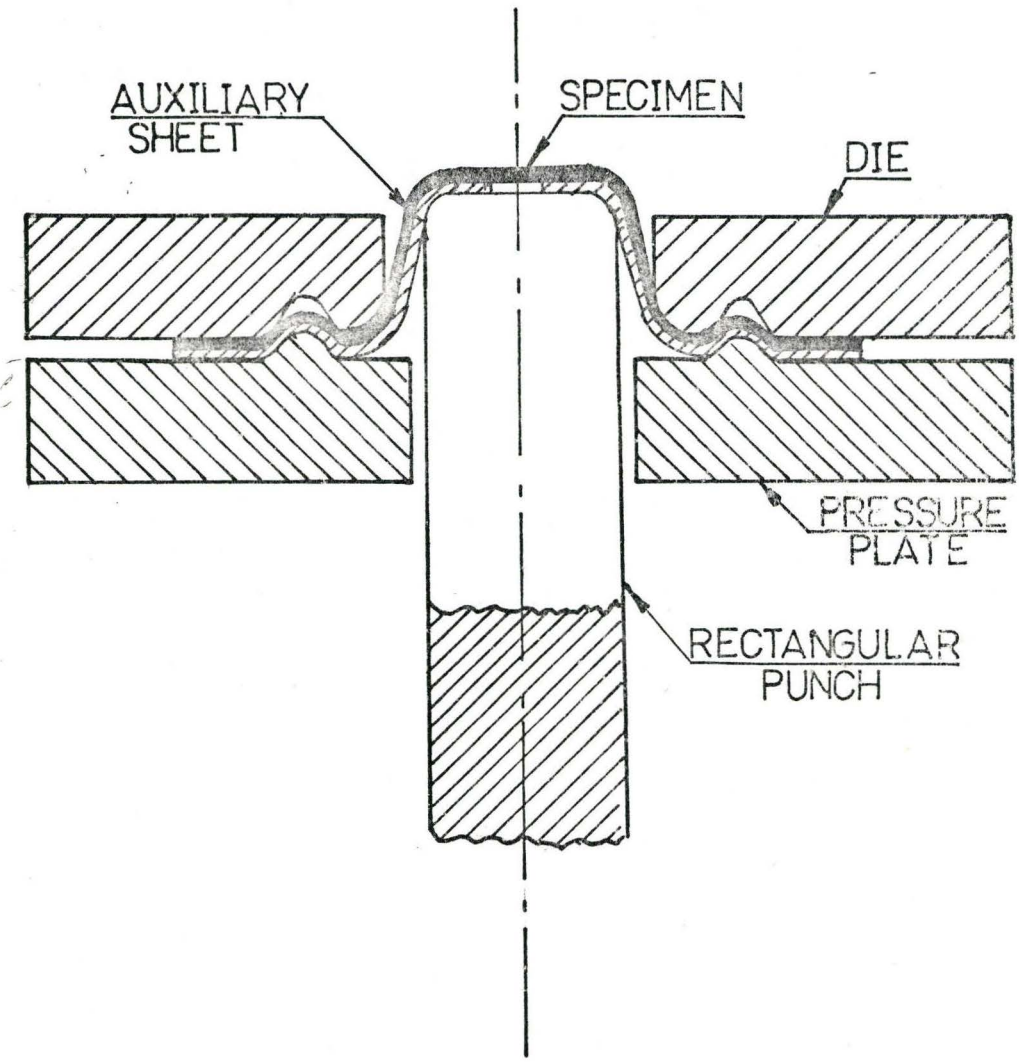

FIGURE 9 PLANE STRAIN TEST

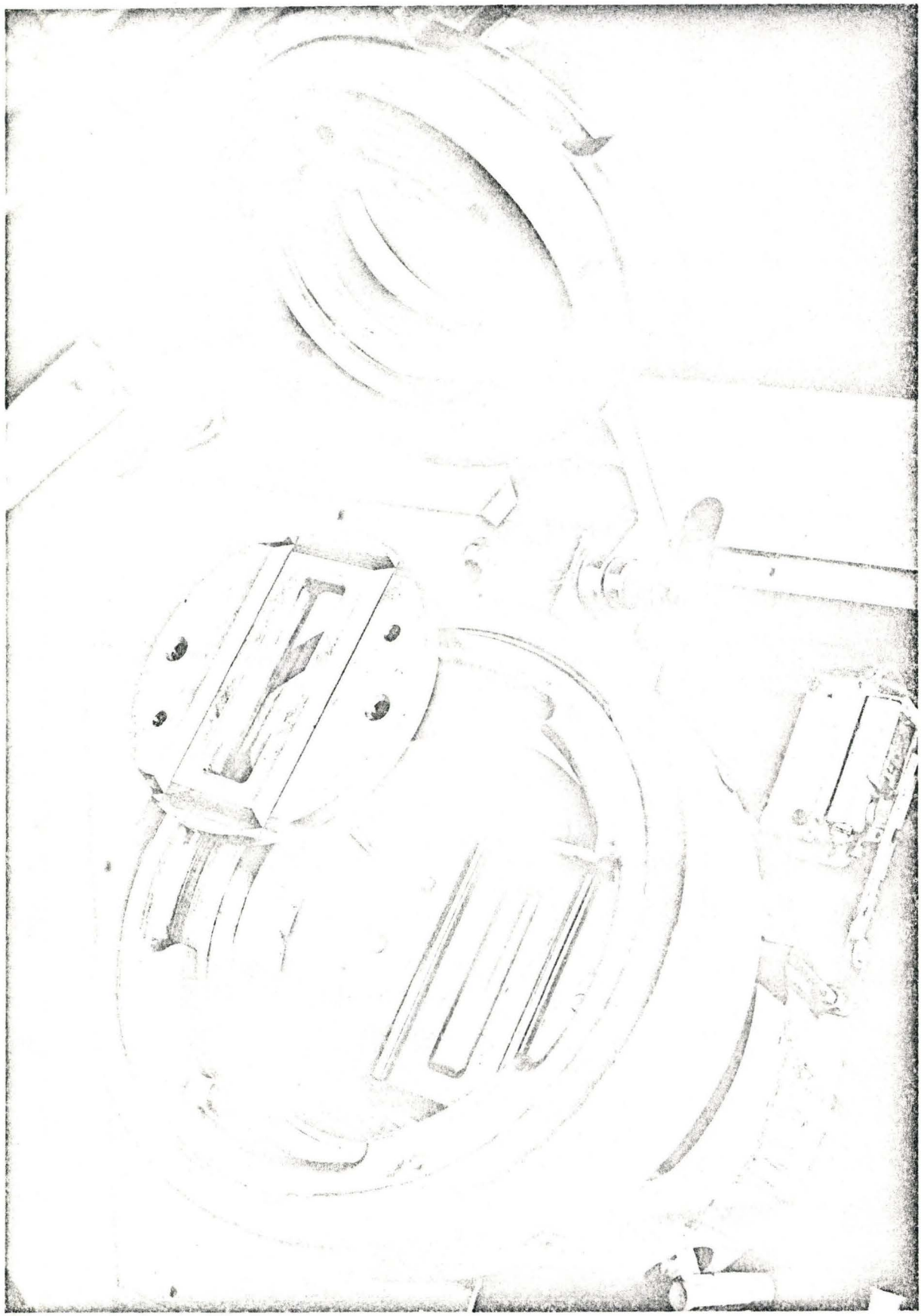

FIGURE 10 SET UP FOR PLANE STRAIN TEST

variability of the behaviour of the material. It is to be noted that the overall shape of the FLD is also important both in the level of strains that can be achieved and the manner in which it changes for different materials.

Hence the essential features of the test to determine the FLD should be

(a) The test should be capable of producing a strain ratio "a" covering a wide range i.e. $-\frac{1}{2} < a < 1$.

(b) There should be an easy method for determination of surface strain in and around the zone of failure.

(c) The strain path should be close to proportional loading and should be monotonically increasing.

(d) The lubrication conditions and deformation mode of the test piece should simulate the actual production conditions. (This is rarely achieved in the laboratory).

One such test is developed by Hecker [13], and discussed in detail below, is a modification of the stretch test described in section 2.3.5.

2.3.1 A Test to Determine a FLD

The cup test developed by Hecker, described in Section 2.2.5, can form the basic equipment for the determination of a FLD. As in the cup test sheet specimens are securely clamped at their periphery and stretched to failure over a hemispherical punch. By altering the width of the test pieces and the lubrication conditions a range of strain

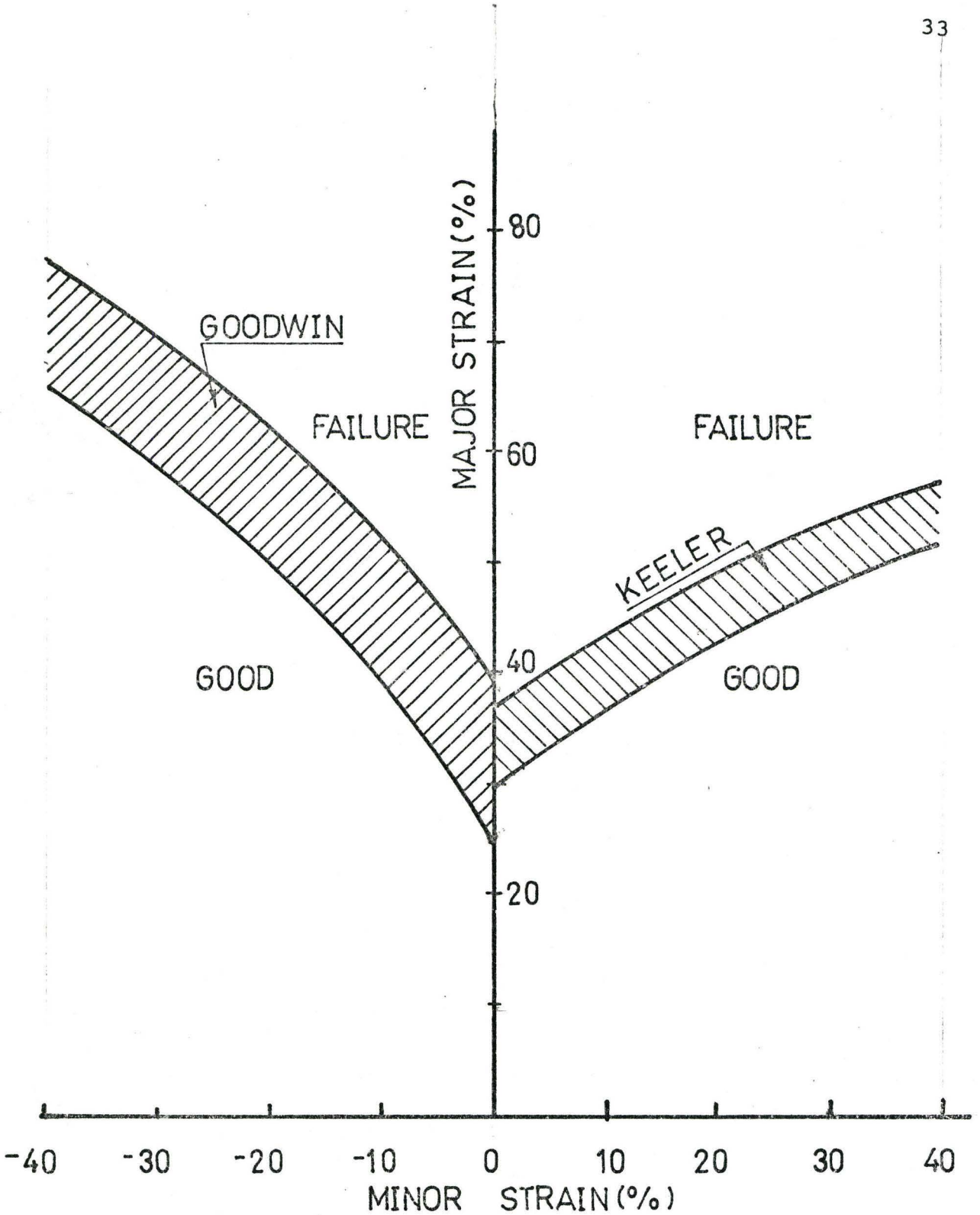

FIGURE 11 FORMING LIMIT DIAGRAM

ratios ($a = \varepsilon_2/\varepsilon_1$) can be achieved at which failure takes place. This is illustrated schematically in Fig. 12.

All the specimens are gridded using either an electro-etching or photo-resist technique. Invariably, circular grid patterns are employed which are transformed into elliptical shapes as the specimen deforms. Measurement of the major and minor diameters of the resulting ellipse enables the principal surface strains at that point to be evaluated.

There is still a degree of uncertainty as to the actual value taken for the limit strain and plotted as part of the FLD. It is generally accepted that the limit strain is taken close to but not actually within a necked and fractured zone. Hence, the degree of uncertainty since it depends upon the experimentors judgement as to what constitutes "close". The severity of the strain gradient in the fractured region can also influence the final value recorded. The more painstaking investigations follow the technique of Hecker [22] and plot the FLD as shown in Fig. 13.

The open circles represent a strain state for grid circles that are close to but not within a necked or fracture affected zone. The half solid symbols represent grids in a necked or fracture affected zones and the solid symbols represent a fractured grid.

The FLD is drawn above the acceptable (open) data

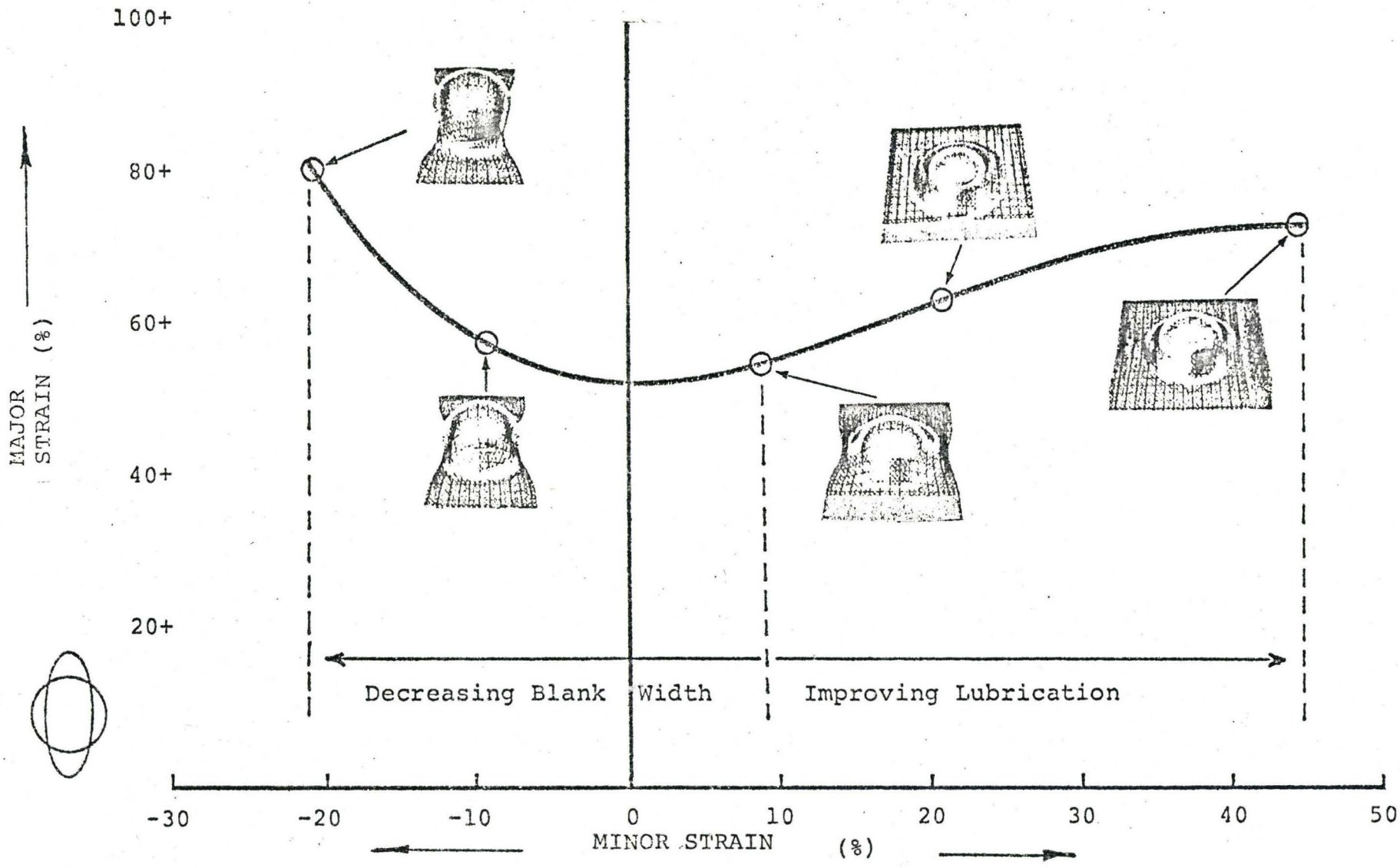

FIGURE 12 DETERMINATION OF FLD.

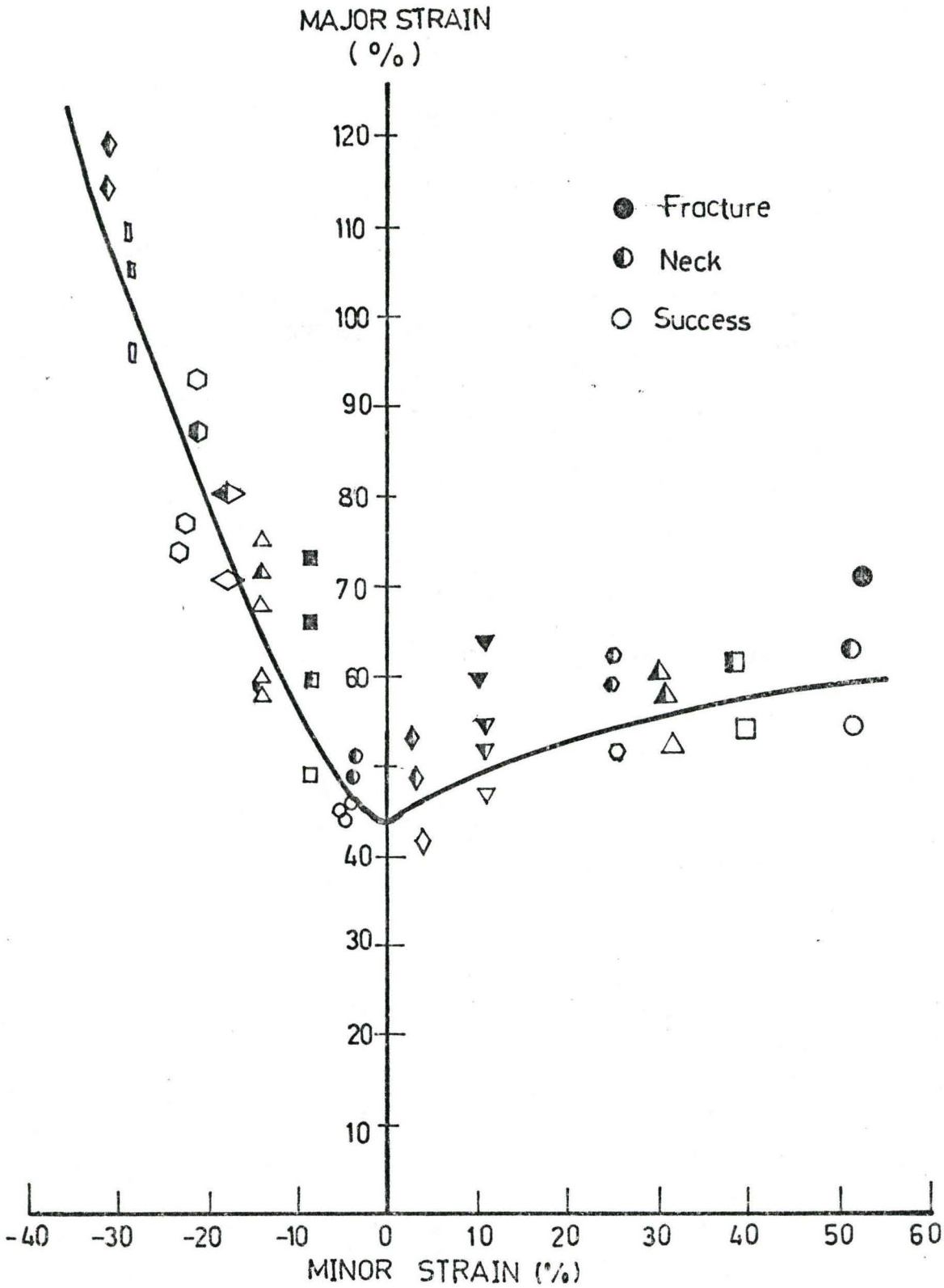

FIGURE 13 FLD FOR AKDQ STEEL(Ref 13)

points and below the necked or fracture affected (half solid) data points as shown in Fig. 13. This definition of a FLD is consistent with the press shop definition of maximum useful deformation.

CHAPTER III

INSTABILITY

3.1 Introduction

In sheet metal forming operations where the principal surface strains are positive, one has to be careful to avoid visible necking and/or fracture of the sheet metal. In other words the strains developed in the workpiece at any point should be within the safe levels or below the FLD.

As already mentioned in Chapter 2,the material properties and process conditions like lubrication and loading path influence the shape and position of FLD.

Ideally one would like to predict the Forming Limits theoretically by using a mathematical model which would take into account all pertinent material parameters that influence formability plus the induced straining path. Obviously, such a task is not an easy one, since even in the simplest case of uniaxial stretching one could encounter three types of failure (or instability leading to fracture) modes depending upon the material characteristics.

1) Abrupt failure with no significant necking of material, a type of brittle fracture.

2) The classical, so called diffuse neck, in which the material is straining at a faster rate than in

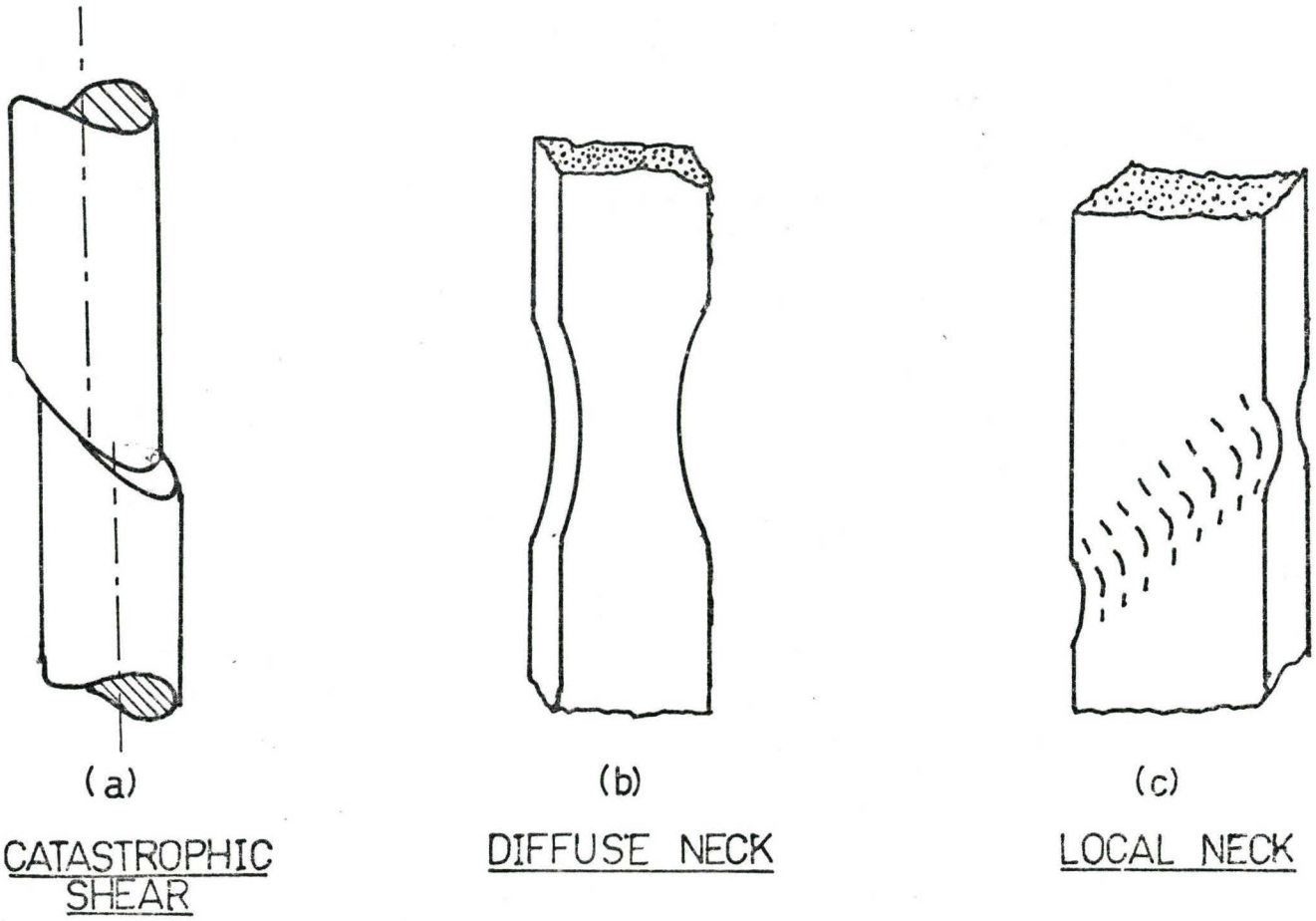

FIGURE- 14 MODES OF FAILURE IN UNIAXIAL TENSION

other regions but this zone of thinning is spread over finite region.

3) Localized necking is which a very definite concentration of straining takes place. This observation is usually associated with rectangular specimens whose width is wide compared with its thickness.

These different modes of failure in uniaxial stretching are depicted schematically in Figure 14. Figure 14a shows that the material has failed abruptly after suffering some plastic strains. Such a failure is called catastrophic shear failure. This may have been caused by the presence of second phase particles or heavy prestraining of material [23].

Figure 14b shows a material instability due to the formation of a diffuse neck. Diffuse necking is common for most ductile materials, although the actual shape of the neck is strongly influenced by the material parameters. Once a diffuse neck begins to form the stress state within the neck is no longer simple uniaxial tension but in general (particularly for round specimens) a triaxial stress system is developed. This stress state can also influence the developing shape of the neck and the point of fracture. With rectangular specimens it can sometimes be observed that a local neck or region of high strain concentration develops within a zone of diffuse necking. It is considered that this

is often the case in general press forming operations, although the onset of diffuse necking is not usually apparent in complex pressings. However, once the localized neck appears fracture is imminent.

In Figure 14c the deformation of the localized neck tends to be a feature of the specimen geometry. The large width of the specimen tends to restrict any transverse drawing-in locally. In fact, the material necks or thins through the thickness along a direction in the plane of the specimen that is currently undergoing no straining.

From this brief discussion of the uniaxial tensile test notwithstanding the rheological behaviour of the material arising through structural irregularities, the material properties, stress state and specimen geometry (which in turn influences the stress state) all control the mode of deformation.

3.2 Instability in Uniaxial Tension

One of the first attempts to analyse the extent of useful straining of a bar in uniaxial tension is due to Considere in 1885 [24]. He identified the limit of uniform straining with the attainment of the maximum load i.e. just prior to the development of a diffuse neck (as shown in Fig. 14b). The instant at which the neck appears is referred to as the point of instability and marks the beginning of non-uniform straining of the material. Material strains faster in the necked zone than its neighbouring zones after

the neck appears.

Obviously, the failure mode shown in Figure 14a would not be obtained at a maximum load but would generally take place under a rising load.

In a similar manner failure mode shown in Figure 14c would show a load maximum corresponding to formation of the local neck.

3.2.1 Diffuse Instability

As already stated, Considere is generally accepted as the first person to analyse the onset of diffuse necking.

Following Considere, it can be shown that at maximum load

$$\frac{1}{\sigma}\ \frac{d\sigma}{d\varepsilon} = 1 \qquad (3.1)$$

for material having constitutive equation of the form

$$\sigma = k\ (\varepsilon_o+\varepsilon)^n \qquad (3.2)$$

then

$$\frac{1}{\sigma}\ \frac{d\sigma}{d\varepsilon} = \frac{n}{\varepsilon+\varepsilon_o} \qquad (3.3)$$

from 3.1 and 3.3

$$\varepsilon_d^* = \varepsilon_1 = n-\varepsilon_o \qquad (3.4)$$

Empirical constitutive equations can be formed for the rate sensitive materials often having the following form

$$\sigma = k(\varepsilon_o+\varepsilon)^n\ \dot{\varepsilon}^{\,m} \qquad (3.5)$$

The rather remarkable extensible behaviour of the so called "superplastic alloys" obeying a constitutive equation of the form

$$\sigma = k\,\dot{\varepsilon}^{m} \tag{3.6}$$

has been attributed to having a large value of the strain rate sensitive index m ($\simeq 0.5$) [25].

However, the same influence has not been found with equations of type (3.5) if it is postulated that instability is the attainment of a point of load maximum.

3.2.2 Localized Instability

Hill [28] was apparently the first person to analyse the formation of a localized neck in uniaxial tension for thin sheet. He reasoned for a local neck to develop,

(a) the principal strains are of opposite sign

(b) the neck is formed in a direction in the plane of sheet where the current strain increment is equal to zero.

Instability was again based on surface traction achieving a maximum value in the direction perpendicular to the groove or neck.

For a material having constitutive equation of the form

$$\sigma = k\,\varepsilon^{n}$$

the uniform limit strain was given by

$$\varepsilon_{\ell}^{*} = \varepsilon_{1} = 2n \tag{3.7}$$

In comparing the two stability modes, it is seen that critical strains for the localized necking are twice as much as that in the diffuse neck, thus a localized neck may occur in a region where a diffuse neck has already developed. Note the comment to this effect made earlier in this chapter.

3.3 Instability in Biaxial Loading

In his original article Hill [26] analyzed the case of biaxial loading i.e. the plane stress case, where the sheet is loaded in its plane and the principal stress normal to the sheet is zero ($\sigma_3=0$). Altering the degree of biaxiality of the loading altered the orientation of neck up to a limiting value of $\frac{\sigma_2}{\sigma_1} \leq \frac{1}{2}$ or $\frac{\sigma_1}{\sigma_2} \leq \frac{1}{2}$. Beyond this point there was no direction within the sheet at which zero strain increment was taking place, as can be verified in its simplest terms by constructing Mohr's (incremental) strain circle, see Fig. 15.

About the same time as Hill published his paper Swift [27],in an independent investigation,had extended the original hypothesis of Considere to cover the biaxial stressing condition for the onset of diffuse necking.

It is to be remembered that all of these analyses are based on the attainment of a load maximum. Other proposals have been made, generally based on energy considerations [28]. These are more complex mathematically and in general

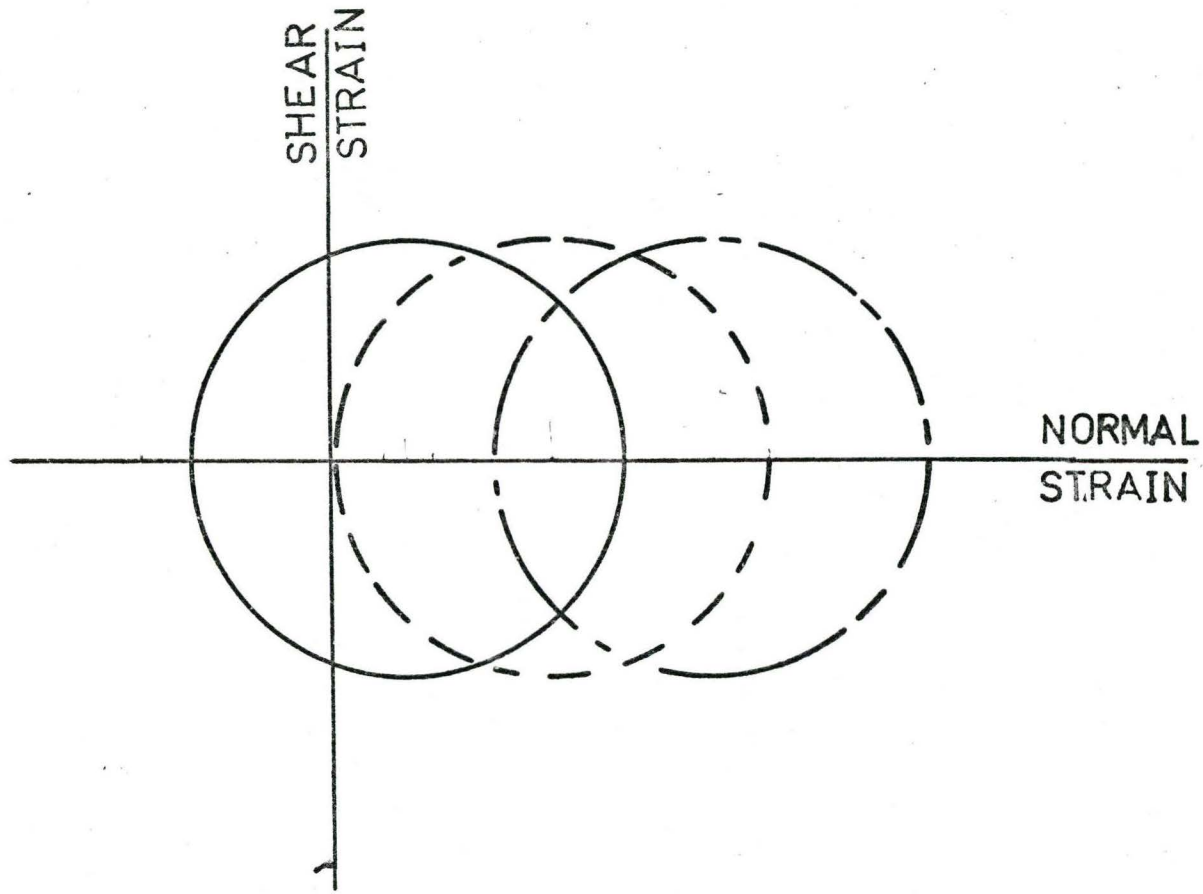

a UNIAXIAL TENSION (a=-1/2)
b PLANE STRAIN (a=0)
c BOTH STRAINS +ive (a>0)

FIGURE 15 MOHR'S (INCREMENTAL) STRAIN CIRCLE

have not produced results that are of more practical use than the simpler analytical models.

There is no need to develop in full the analysis of Hill and Swift here since the original papers can be consulted. The resulting expressions for the instability strains for both isotropic and anisotropic materials is given in the Art. 3.5 of this chapter. It will be seen that the expressions can be used to plot a Forming Limit Diagram. The results are not entirely satisfactory particularly in the stretch-stretch quadrant of the FLD where the Swift analysis tends to be very conservative particularly in the region of balanced biaxial tension.

The original theories of Hill and Swift do not take into account the geometry of workpiece and implicity the problem was treated as if all the deformation was taking place in the plane of the sheet (biaxial loading).

A classical illustration of the effect that the geometry of deformation can have on the useful surface strains is that of the hydrostatic bulge test. The test has already been referred to in Chapter II (Article 2.1.3) and some of the analytical results are given below.

3.3.1 Bulge Test

A circular metal diaphragm clamped at the circumference is subjected to hydraulic pressure on one side. At the pole of the bulged dome the straining process is one of balanced biaxial tension, but since the specimen deforms as

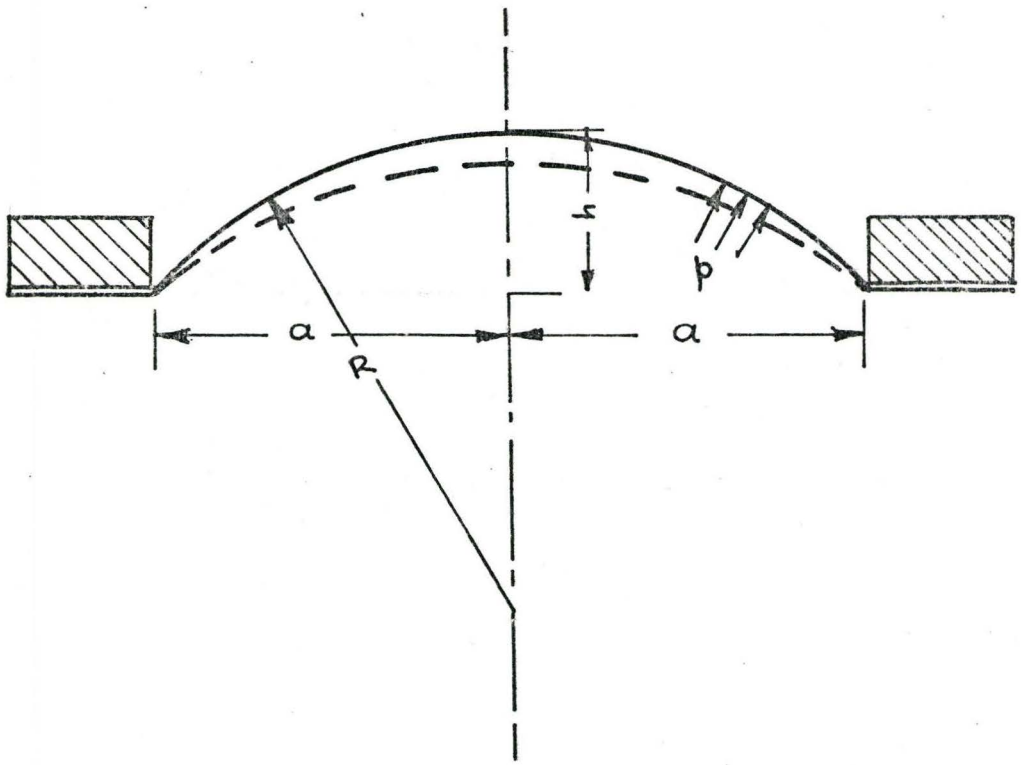

$$a^2 = h(2R - h)$$

FIGURE-16 GEOMETRY OF BULGED SPECIMEN (Ref. 29)

a dome, there exists a strain gradient from the clamped edge to the pole of the dome.

The process analysed by Hill [29] assumed that instability occurred when the pressure achieved a maximum. However, one crucial consideration was that Hill attempted to take into account the geometry of deformation of the dome. He assumed that the current dome was part of a large spherical shell and thus the radius of curvature decreased as dome height increased, refer to Figure 16.

It was on this basis that Hill predicted the limit surface strains at the pole. A treatment of Hill's original work can also be found in Johnson and Mellor [30], who demonstrated that for a material with a constitutive equation

$$\sigma = k\varepsilon^{n} ,$$

the limit strain at the pole in the thickness direction is given by

$$\varepsilon_t^* = \varepsilon_3^* = \frac{4}{11} (2n + 1) . \qquad (3.8)$$

This is rather a remarkable result since it predicts that material with a low "n" value still show appreciable straining in the hydrostatic bulge test. It has been observed for aluminum 3003-H14 with n value of 0.06 showed the limit strain of 0.54 in Bulge Test. This has only been possible because of the geometry of deformation.

As demonstrated above, the instability in the material certainly depends on the geometry of deformation.

Most of the theories of instability do not take this effect into account and as a result we expect the limit strains to be different under different conditions of material processing.

Likewise it is to be noted that no theories exist which predict the behaviour of the material from the initial region of say uniform straining, to then determine the onset of a bifurcation of the deformation field and to continue to predict the ensuing deformation mode for the whole specimen. In other words to predict when a neck would develop in say,a uniaxial test and to describe the continuing shape changes.

It is worthwhile reiterating that the aforementioned theories of Considere, Hill and Swift predict a load instability; the formation of a neck or some equivalent change in the deformation field is invariably associated with this point of instability. None of the theories proport to predict the ensuing deformation mode and the point of fracture.

An alternative approach, developed by Marciniak [31], is that some surface irregularity (geometric irregularity) or zone of weakness is postulated to exist in material right from the very onset. An analysis has been developed to look into stresses and strains in this zone of weakness right from the beginning to the fracture. The Marciniak analysis

can be used to predict a FLD as described by Sowerby and Duncan [32].

3.4 Marciniak Theoretical Analysis of FLD

The basis of the Marciniak analysis is a pre-existing material inhomogeneity. This inhomogeneity has been pictorially represented as a pre-existing groove, in the surface of material that under continued deformation becomes a site for strain concentration and fracture. This inhomogeneity could be an inclusion, void or any material imperfection.

Marciniak's theoretical FLD analysis is presented in reference [11,12]. Essentially the theory is composed of six basic axioms. The three generally accepted axioms obtained from anisotropic plasticity theory are:

i) The anisotropic yield function due to Hill [33] (which reduces to the Von Mises criterion for isotropic materials),

ii) an associated flow rule,

iii) representative strain for the anisotropic model.

iv) The degree of biaxiality based on the strain ratio $a = d\varepsilon_2/d\varepsilon_1$; for proportional straining $a = d\varepsilon_2/d\varepsilon_1 = \varepsilon_2/\varepsilon_1 =$ constant.

v) The constitutive equation used to describe the material properties is of the form that the flow stress is a function of both strain and strain rate,

$$\sigma = k(\varepsilon_o+\varepsilon)^n \dot{\varepsilon}^m$$

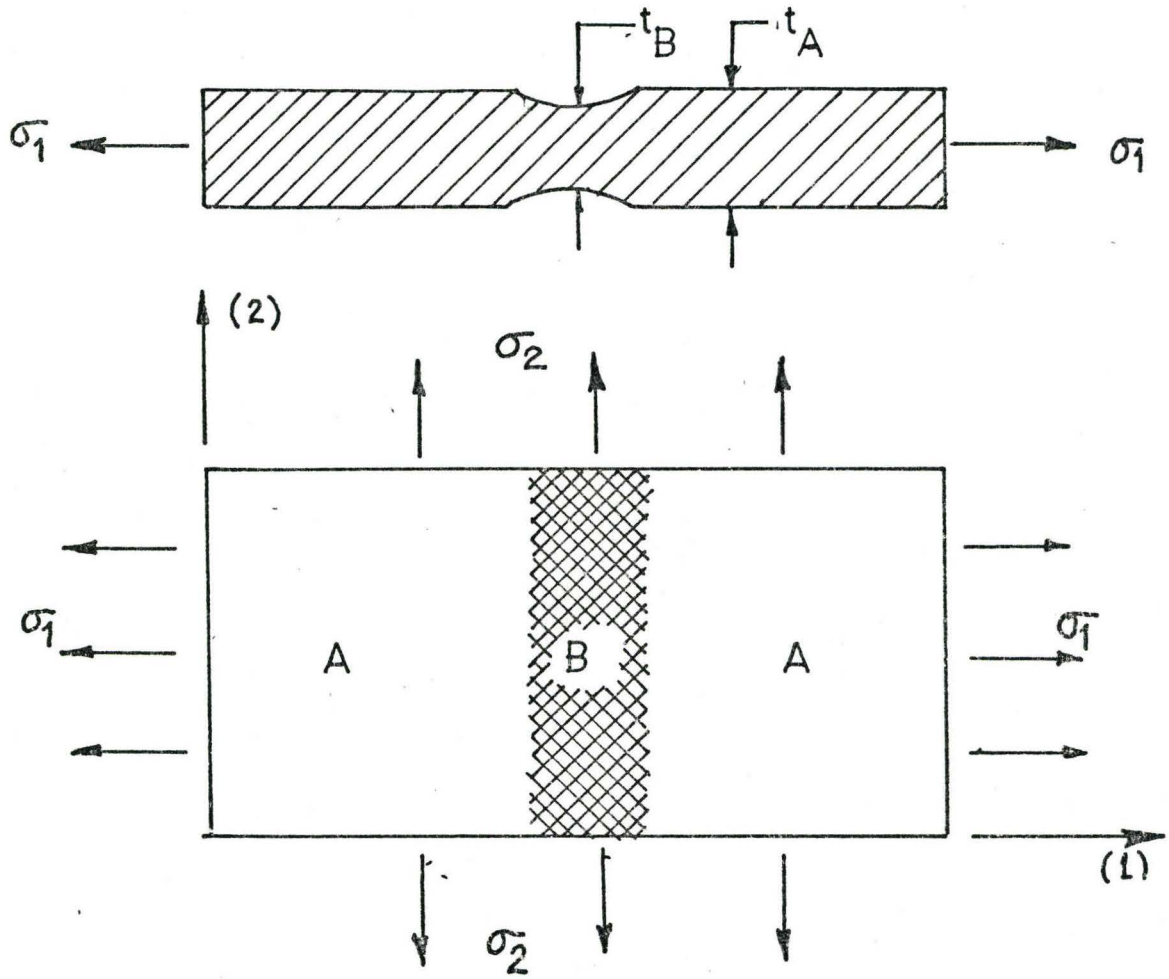

FIGURE 17 SCHEMATIC PRESENTATION OF MARCINIAK GROOVE IN AN ELEMENT

vi) The definition of the coefficient of inhomogeneity, refer to Fig. (17).

$$f = \frac{t_{0B}\, k_B}{t_{0A}\, k_A} \tag{3.9}$$

Subscript B refers to a section of material in the realm of the inhomogeneity (in the groove), and the subscript A refers to a section of material outside the realm of the inhomogeneity(outside the groove).

Employing a force balance between section A and B establishes the initial expression upon which the forming model is constructed. After substitution of the six axioms into the force balance and subsequent algebric manipulation a system of two differential equations is obtained that requires the following material parameters viz. n, m, $\bar{r}$, ε_o, ε_{3f} and f.

The assumption stated by Marciniak in this analysis are:

(1) The thickness strain at fracture, ε_{3f}, is independent of degree of biaxiality "a" and

(2) the strain in the groove ε_{2B} and outside the groove, ε_{2A}, parallel to the groove direction are equal.

A numerical solution to the Marciniak equations can be obtained by employing the Runge-Kutta Method. Marciniak's analysis can be used to plot a FLD as demonstrated by Sowerby and Duncan [32]. In reference [12] a number of FLD's are provided with different material parameters. Some of

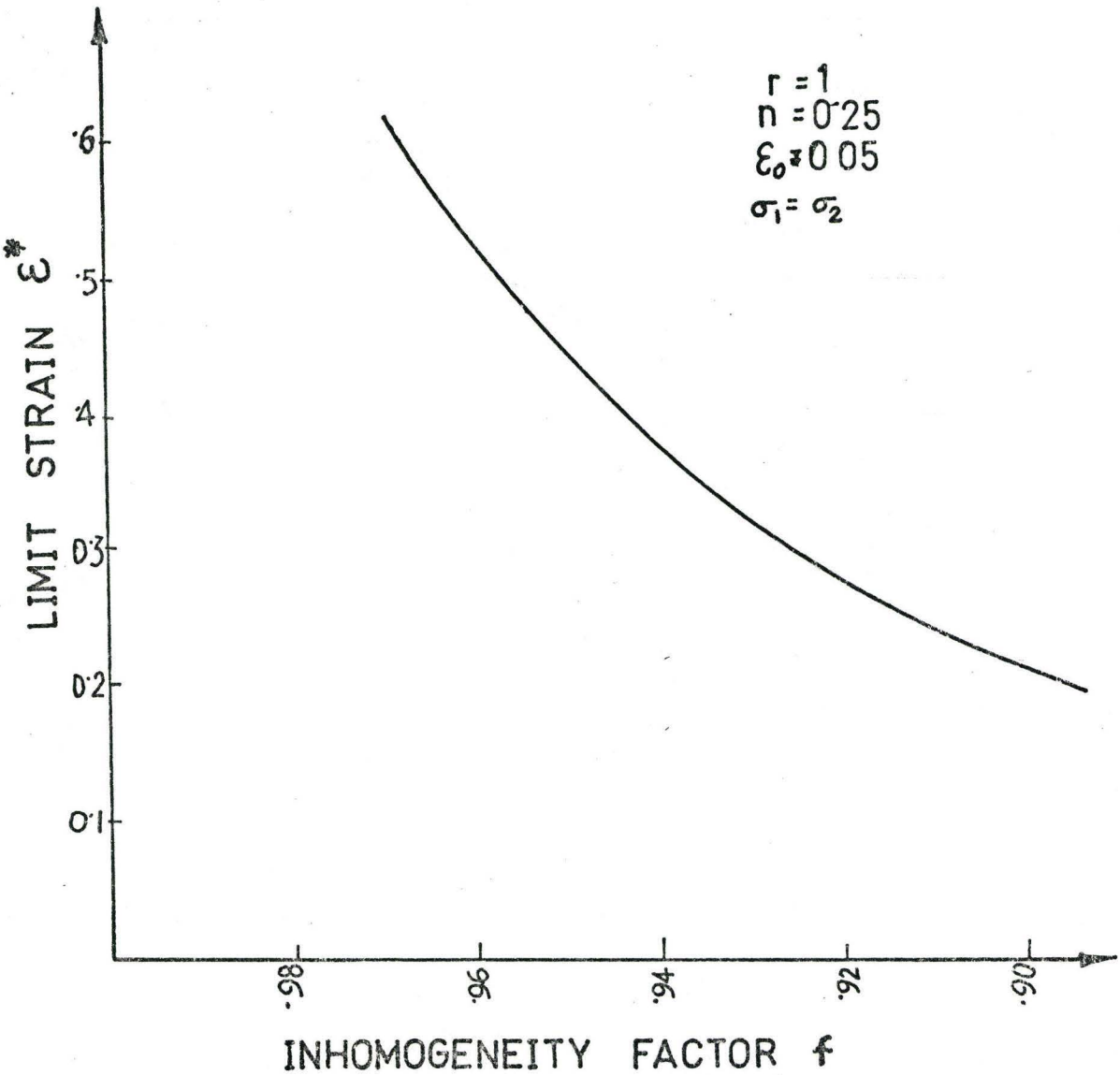

FIGURE 18 INFLUENCE OF f ON ε^*

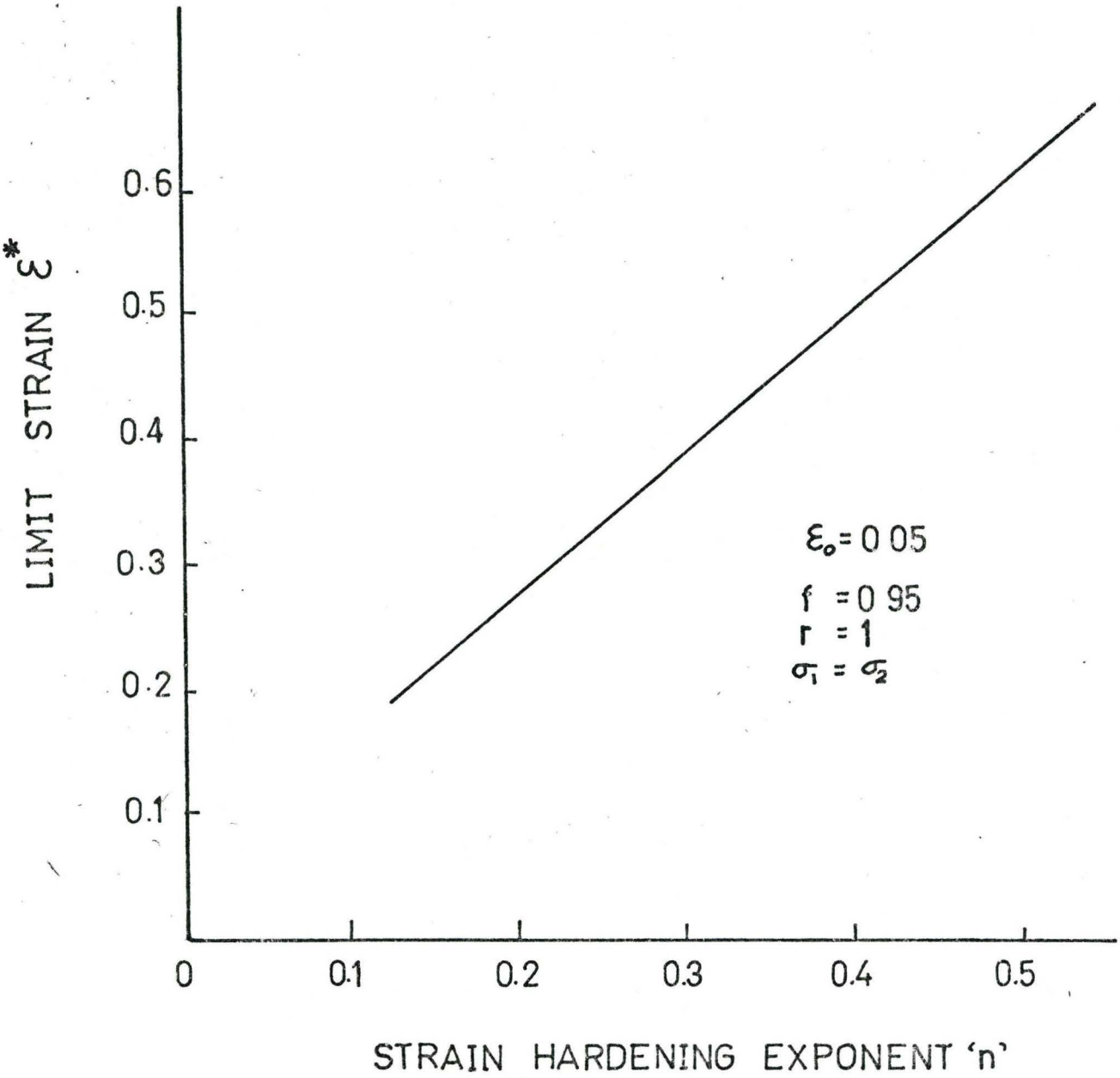

FIGURE 19 INFLUENCE OF 'n' ON ε^*

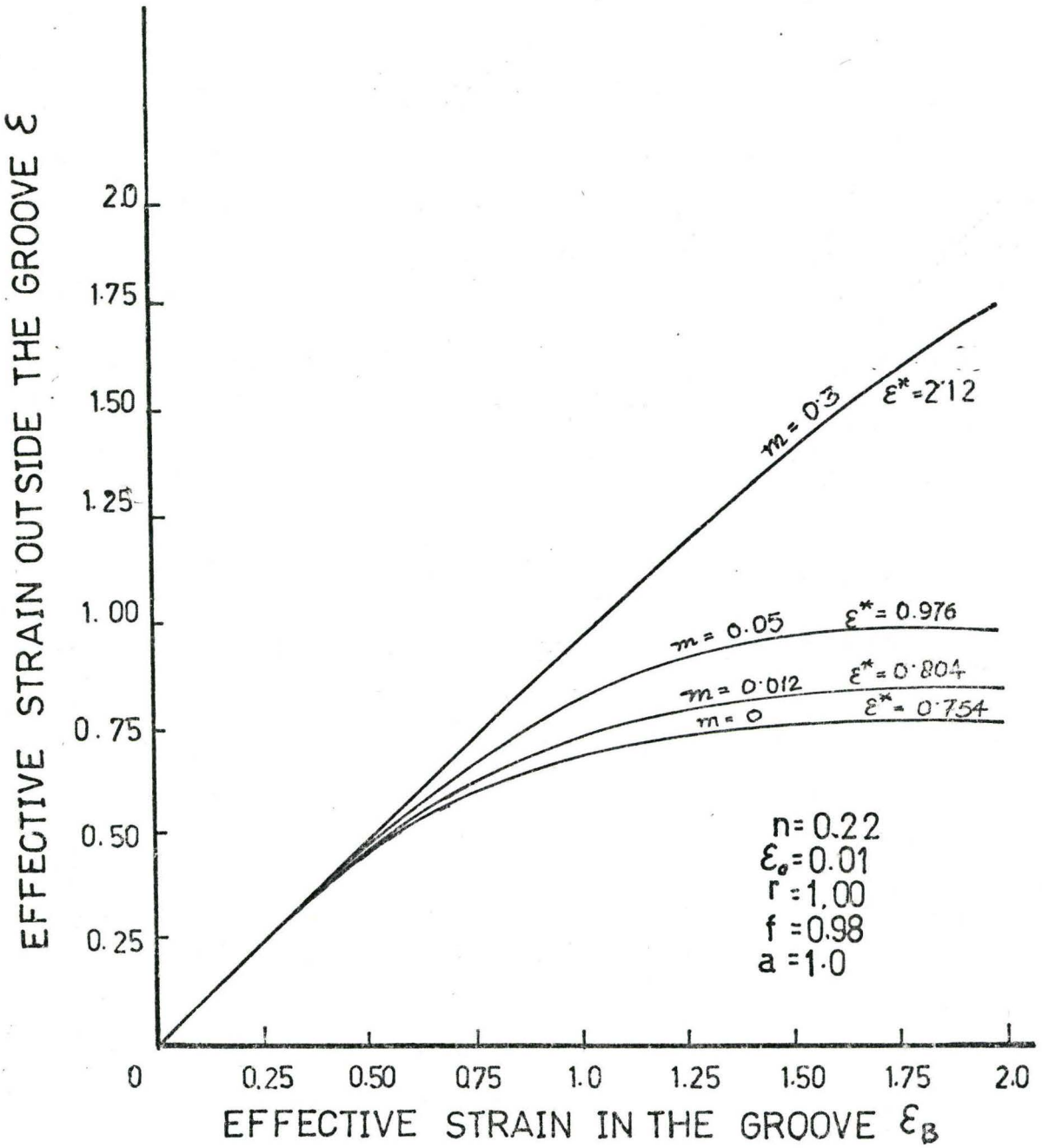

FIGURE 20 INFLUENCE OF 'm' ON THE DEFORMATION PROCESS

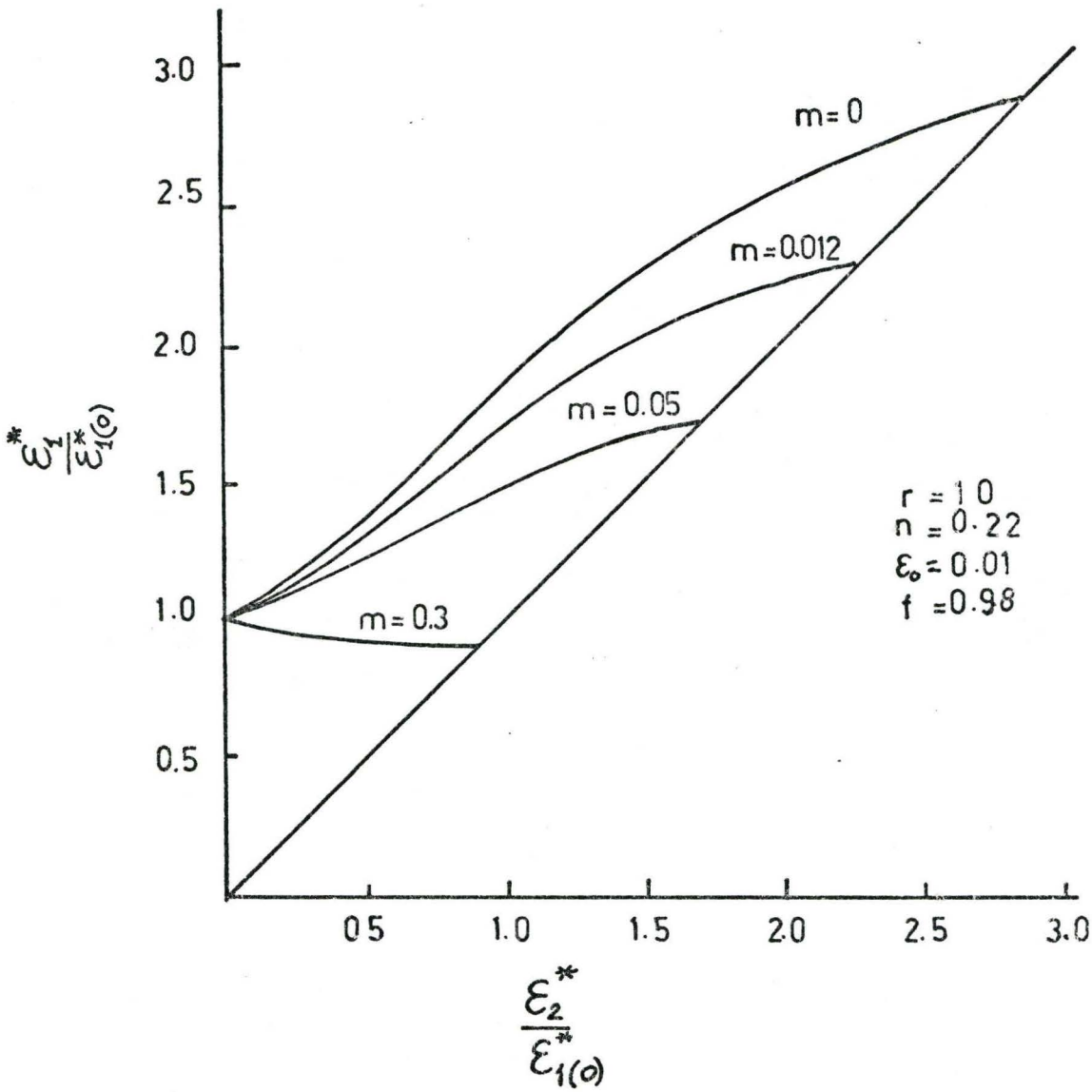

FIGURE 21 INFLUENCE OF 'm' ON FLD.

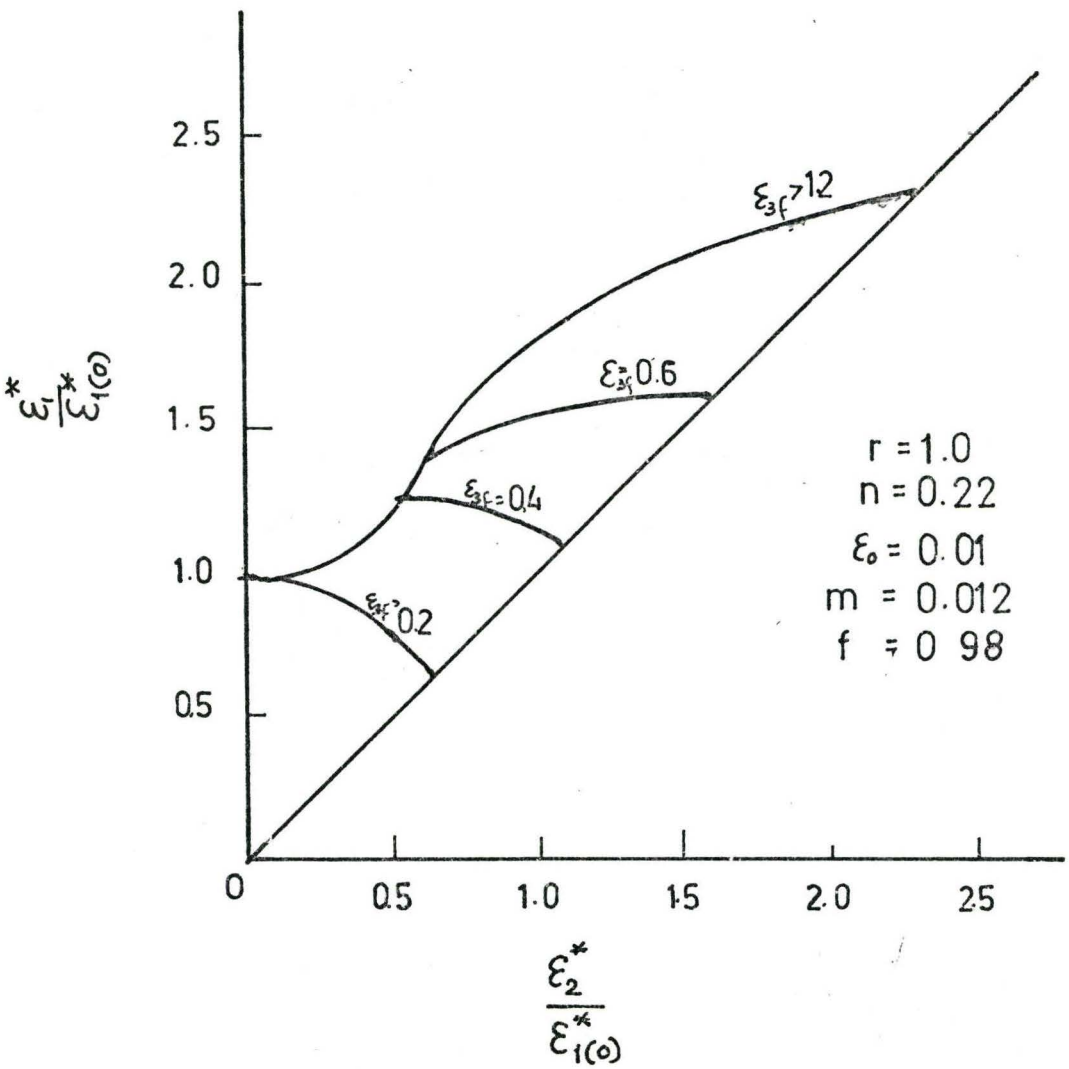

FIGURE 22 INFLUENCE OF ε_{3f} ON FLD

these effects are discussed below and a number of diagrams taken from reference [25] are provided to illustrate the point.

3.4.1 Influence of Material Properties on Limit Strain and Shape of Forming Limit Diagram

The limit strain depends both on the strain ratio "a" and material properties such as:

1. strain hardening index, n;
2. strain rate sensitivity, m;
3. inhomogeneity, f';
4. anisotropy, $\bar{r}$;
5. ductility, ε_{3f}.

The influence of a particular material parameter on the limit strain can be investigated by keeping all other parameters constant and choosing a value for a (say a = 1).

The material inhomogeneity f is the one which exerts the greatest influence on the limit strain ε^*, this is shown in Figure 18. The value of the limit strain increases very rapidly as the material inhomogeneity diminishes i.e. as f increases.

Figure 19 shows that an increase in n causes an increase in limit strain.

The influence of strain rate sensitivity on the deformation process is shown in Figure 20. It is seen that with an increasing value of m the process of localized strain

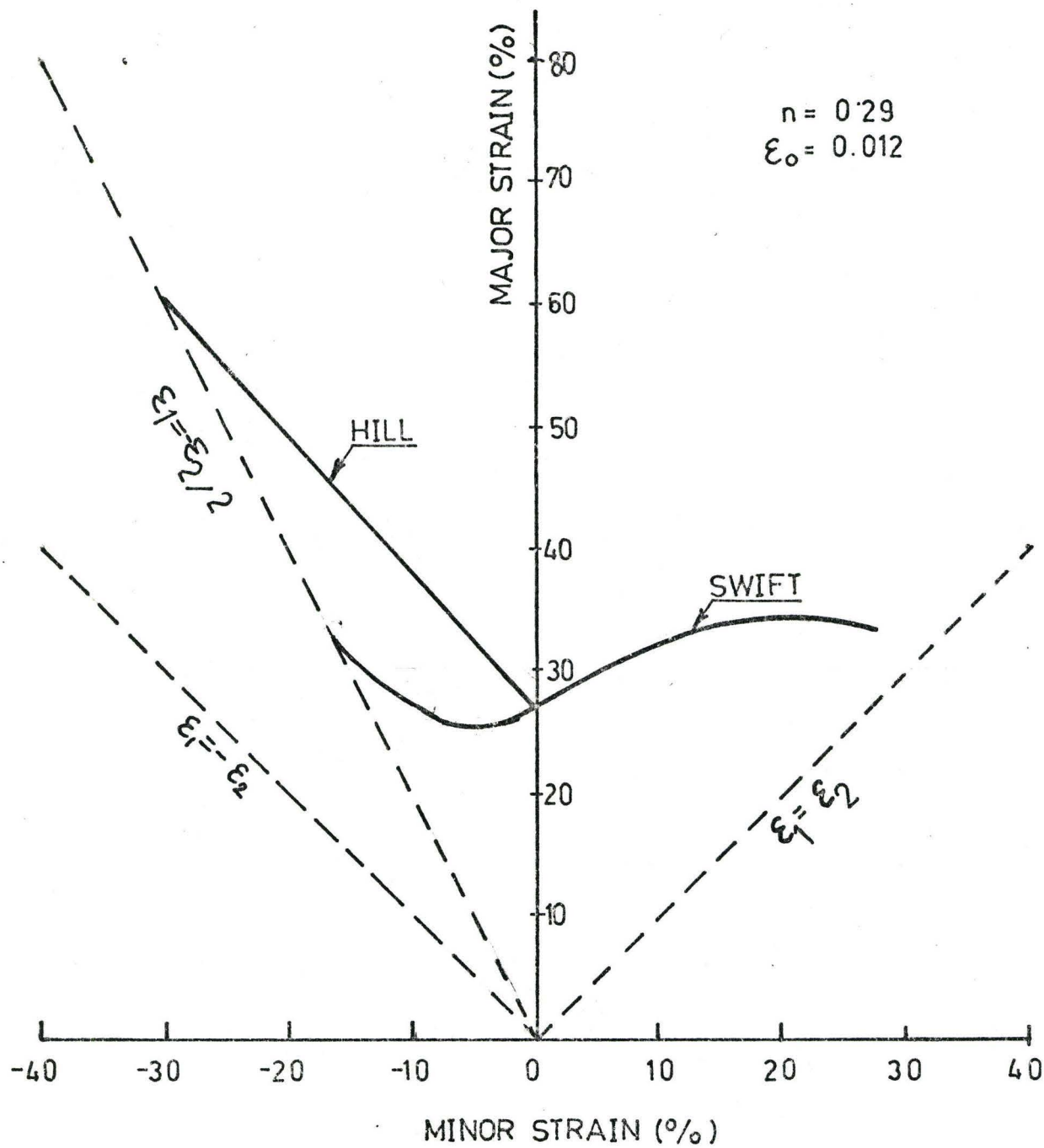

FIGURE 23 FLD OBTAINED FROM INSTABILITY ANALYSIS OF HILL AND SWIFT

concentration becomes slower and larger limit strains are achieved. According to Marciniak's theoretical predictions 'm' is capable of altering both the shape and level of the FLD as illustrated in Figure 21. Unfortunately, there appears to be no commercial materials that fit the postulated empirical constitutive equations (for high m values) in order to check out the theoretical predictions. Note also that the results in Figure 21 are normalised and thus the effect of increasing limit strains with increasing m is masked.

The influence of the fracture thickness strain, ε_{3f}, is illustrated in Figure 22. Here again these curves are normalised but the effect of decreasing ε_{3f} is to lower the useful straining limits, as one would expect.

Increasing the n value increases the level of the FLD and this would appear to be in keeping with all the current experimental data.

In summary the various material parameters and the loading path can have a marked effect upon the shape and level of the FLD. It is not claimed that the Marciniak analysis is capable of describing the behaviour of all materials, at best it predicts some of the observed trends. Undoubtedly there is scope for further theoretical development in order to provide more accurate descriptions of material behaviour.

3.5 Theoretical Prediction of FLD using Instability Criterion

In this appendix the expressions for instability strain given by the Hill and Swift models for localized and diffuse necking are provided.

The original analysis was for isotropic materials but can be extended to cover the case of anisotropic materials.

Case I

ISOTROPIC MATERIALS

(i) Expressions for equivalent stress and strain can be witten for a plane stress case $\sigma_3=0$, for isotropic material

$$\bar{\sigma} = (\sigma_1^2 - \sigma_1\sigma_2 + \sigma_2^2)^{\frac{1}{2}} \tag{A.1}$$

$$d\bar{\varepsilon} = \sqrt{\frac{2}{3}}\,(d\varepsilon_1^2 + d\varepsilon_2^2 + d\varepsilon_3^2)^{\frac{1}{2}} \tag{A.2}$$

(ii) The principal strains ε_1 and ε_2 can then be calculated assuming proportional loading and using the Levy-Mises flow rule.

$$\varepsilon_1 = \frac{(2-\alpha)\,\bar{\varepsilon}}{2(1-\alpha+\alpha^2)^{\frac{1}{2}}} \tag{A.3}$$

$$\varepsilon_2 = \frac{(2\alpha-1)\,\bar{\varepsilon}}{2(1-\alpha+\alpha^2)^{\frac{1}{2}}} \tag{A.4}$$

where $\alpha = \dfrac{\sigma_1}{\sigma_2}$ is the principal stress ratio.

(iii) The constitutive equation of the material is taken

to be

$$\bar{\sigma} = k\,\bar{\varepsilon}^{\,n} \qquad \text{(a)}$$

$$\bar{\sigma} = k\,(\varepsilon_o + \bar{\varepsilon})^n \qquad \text{(b)} \qquad \text{(A.5)}$$

Localized Necking

Using Hill's Model for localized necking and equations (A.1) and (A.5a), the equivalent strain for localized neck can be calculated as

$$\bar{\varepsilon}_\ell = \frac{2n\,(1-\alpha+\alpha^2)}{(1+\alpha)} \qquad \text{(A.6)}$$

The principal strains $\varepsilon_{1\ell}$ and $\varepsilon_{2\ell}$ for localized neck can then be obtained by substituting the value of equivalent strain in equations (4.3) and (A.4). The results obtained are

$$\varepsilon_{1\ell} = \frac{n\,(2-\alpha)}{(1+\alpha)} \qquad \text{(a)}$$

$$\varepsilon_{2\ell} = \frac{n\,(2\alpha-1)}{(1+\alpha)} \qquad \text{(b)} \qquad \text{(A.7)}$$

Hill's model is strictly applicable to cases when principal surface strains are of opposite signs and thus is appropriate to predicting the left hand side of the FLD. These results are plotted in Figure 23 using equation (A.7) for $o < \alpha < \frac{1}{2}$.

Diffuse Necking

Using Swift's model for instability the equivalent strain ε_d for diffuse necking can be predicted using

equations (A.1) and (A.5a).

$$\varepsilon_d = \frac{4n\ (1-\alpha+\alpha^2)^{3/2}}{4\alpha^3-3\alpha^2-3\alpha+4} \qquad (A.8)$$

The principal strains ε_{1d} and ε_{2d} for diffuse necking can be obtained by substituting the value of equivalent strain in corresponding equations (A.3) and (A.4). The results obtained are

$$\varepsilon_{1d} = \frac{2n\ (2-3\alpha+3\alpha^2-\alpha^3)}{(4\alpha^3-3\alpha^2-3\alpha+4)} \qquad \text{(a)}$$

$$\varepsilon_{2d} = \frac{2n(2\alpha^3-3\alpha^2+3\alpha-1)}{(4\alpha^3-3\alpha^2-3\alpha+4)} \qquad \text{(b)} \qquad (A.9)$$

Swift's model, based on diffuse necking, can cover the full range of FLD but generally tends to be conservative since it predicts the onset of diffuse necking and this does not necessarily mark the end of useful straining of the material. This appears to be particularly true on the right hand side of the FLD (the stretch-stretch mode). The results using equation A.9 for $o<\alpha<1$ are shown in Figure 23.

Case II

ANISOTROPIC MATERIAL

(i) Expressions for equivalent stress and equivalent strain can be written down for anisotropic materials

from the theory proposed by Hill [28] as follows:-

$$\bar{\sigma} = \{\frac{3}{2(F+G+H}\ [F(\sigma_y-\sigma_z)^2 + G\ (\sigma_z-\sigma_x)^2 + H\ (\sigma_x-\sigma_y)^2 + 2L\ \tau^2_{yz} + 2M\ \tau^2_{zx} + 2N\ \tau^2_{xy}]\}^{\frac{1}{2}} \qquad (A.10)$$

$$d\bar{\varepsilon} = [\frac{2}{3}\ (F+G+H)]^{2/3}\ \{[F(Gd\varepsilon_y - Hd\varepsilon_z)^2 + G(F\ d\varepsilon_x - Hd\varepsilon_z)^2 + H(Fd\varepsilon_x - Gd\varepsilon_y)^2] + \frac{2d\gamma^2_{yz}}{L} + \frac{2d\gamma^2_{zx}}{M} + \frac{2d\gamma^2_{xy}}{N}\}^{\frac{1}{2}} \qquad (A.11)$$

where F,G,H,L,M and N are parameters of anisotropy.

(ii) The principal strains ε_1 and ε_2 can be calculated assuming proportional deformation and using Levy-Mises flow rule

$$\varepsilon_1 = \frac{\bar{\varepsilon}[(\frac{G}{H} + 1)\ \alpha - 1]}{\{\frac{2}{3}\ (\frac{F}{H} + \frac{G}{H} + 1)[\frac{G}{H}+1)\alpha^2 - 2\alpha + (\frac{F}{H}+1)]\}^{\frac{1}{2}}} \qquad (A.12)$$

$$\varepsilon_2 = \frac{\bar{\varepsilon}[(\frac{F}{H} + 1) - \alpha]}{\{\frac{2}{3}\ (\frac{F}{H} + \frac{G}{H} + 1)\ [(\frac{G}{H} + 1)\ \alpha^2 - 2\alpha + (\frac{F}{H}+1)^{\frac{1}{2}}} \qquad (A.13)$$

Localized Neck

Venter and deMalherbe [34] have extended the instability analysis of Hill [26] to include the anisotropy of the material. Using the equation for equivalent stress (A.10) and power hardening law described in equation (A.5a) the

representative strain for diffuse necking has been obtained and is of the following form

$$\bar{\varepsilon}_{\ell} = \frac{n\left\{\frac{2}{3}\left(\frac{F}{H}+\frac{G}{H}+1\right)\left[\left(\frac{G}{H}+1\right)\alpha^2-2\alpha+\left(\frac{F}{H}+1\right)\right]\right\}^{\frac{1}{2}}}{\frac{G}{H}\alpha+\frac{F}{H}} \quad (A.14)$$

The expressions for principal strains $\varepsilon_{1\ell}$ and $\varepsilon_{2\ell}$ and $\varepsilon_{2\ell}$ can be obtained by substituting equation A.14 in A.12 and A.13 respectively.

Diffuse Necking

Moore and Wallace [9] and Venter and deMalherbe [34] have extended the instability analysis of Swift [27] to include the anisotropy of the material. Proceeding in similar manner as for isotropic material, the expression for equivalent strain in diffuse necking $\bar{\varepsilon}_d$ is obtained as follows

$$\bar{\varepsilon}_d = n\left[\frac{2}{3}\left(\frac{F}{H}+\frac{G}{H}+1\right)\right]^{\frac{1}{2}} \times \frac{\left[\left(1+\frac{G}{H}\right)\alpha^2-2\alpha+\left(1+\frac{F}{H}\right)\right]^{3/2}}{\left(1+\frac{G}{H}\right)^2\alpha^3-\left(1+\frac{2G}{H}\right)\alpha^2-\left(1-\frac{2F}{H}\right)\alpha+\left(1+\frac{F}{H}\right)} \quad (A.15)$$

Which can then be substituted in equations (A.12) and (A.13) to calculated ε_{1d} and ε_{2d} respectively.

From the preceding analysis it is clear that the level of the theoretical limit strain increases with the n value as shown in Figure 24. The influence of normal anisotropy ($\bar{r}$) on the limit strain is shown in Figure 25. It

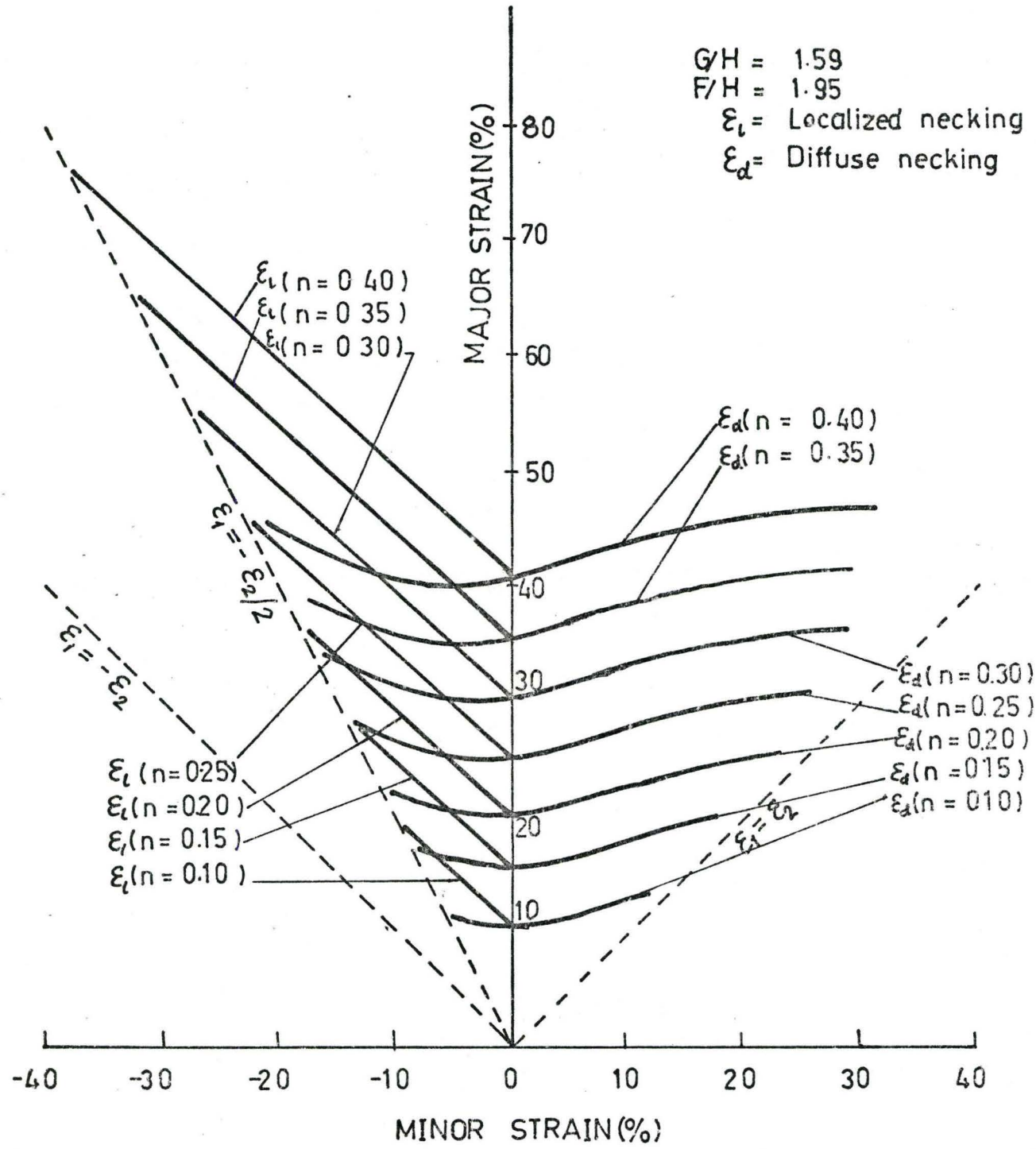

FIGURE 24 EFFECT OF 'n' ON THE POSITION OF FLD

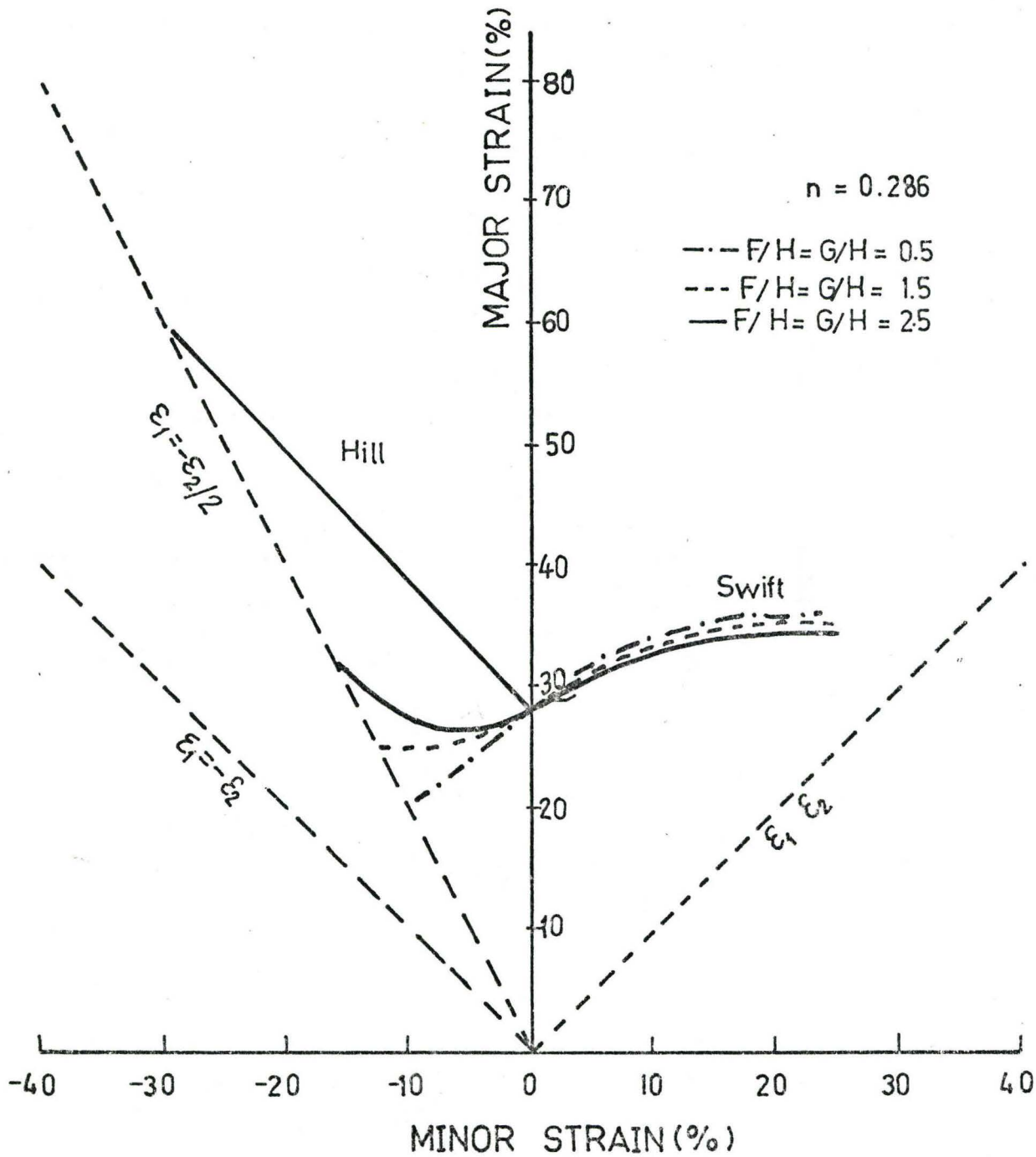

FIGURE 25 EFFECT OF ANISOTROPY ON THE POSITION OF FLD

would appear that $\bar{r}$ exerts a stronger influence on the limit strain for diffuse necking in the tension-compression (left hand side) region of the FLD.

Hasak [35] has developed a set of computer programs based on the preceding analyses whereby the influence of the various material parameters on the limit strains can be readily determined.

CHAPTER IV

EXPERIMENTS AND EXPERIMENTAL RESULTS

4.1 Materials

Six different materials were chosen for testing.

All samples were commercially produced cold rolled sheet received in an essentially stable condition ready for forming. The thickness of all sheets was in the range of 0.032 to 0.036 inches.

AKDQ - An aluminum killed drawing quality mild steel, annealed and skin rolled, this material is free from strain aging and has the best forming behaviour of the commonly used steels.

3003-0 - An aluminum-manganese alloy fully annealed and specially processed to give good forming characteristics.

3003-H14 An alloy of the same nominal composition as 3003-0 hardened by cold work. The particular sample was of commercial quality, not intended for deep drawing.

5182-0 An aluminum-magnesium alloy of drawing quality and in the fully annealed state.

2036-T4 An aluminum-copper-magnesium alloy of drawing quality. Solution treated and aged at room temperature.

TABLE I

	Cr	% Cu	% Mn	% Si	% P	% S	% C	% Al	% Fe	% Mg
AKDQ		-	0.33	0.010	0.005	0.019	0.054	0.035	Re-mainder	-
3003-0	1.02	0.11	1.08	0.24	-	-	-	Remainder	0.63	0.035
5182-0			0.45					Remainder		4.0
2036-T4		2.70	0.26	0.26	-	-	-	Remainder	0.28	0.40

4.2 Tensile Test

All the tensile tests were performed on a Model TTS INSTRON Universal Testing Machine. Instron wedge action grips, type 10F, were used throughout. Using the facility of the servo-controlled chart activated by a type F-51-15A strain gauge extensometer attached to the specimen, an autographic load vs extension curve was produced for each test.

4.2.1 Specimens

General requirements

i) The specimens are to be sheared individually from the sheet in different directions with respect to rolling direction (as shown in Fig. 26) and then machined in packs to remove cold worked edges due to shearing.

ii) The specimen should include the full thickness of the sheet.

iii) Within the gauge length parallelism must be maintained so that no two width measurement differ by more than 0.1% of the measured width.

The shape, dimensions and gauge length section are shown in Fig. 27 in accordance with ASTM specifications.

4.2.2 Measuring Devices

The measurement of the specimens before the after deformation were performed on a tool makers microscope which had a least count of 0.0001 in. The load-extension record was read using a digitizer having a least count of 0.0001 in.

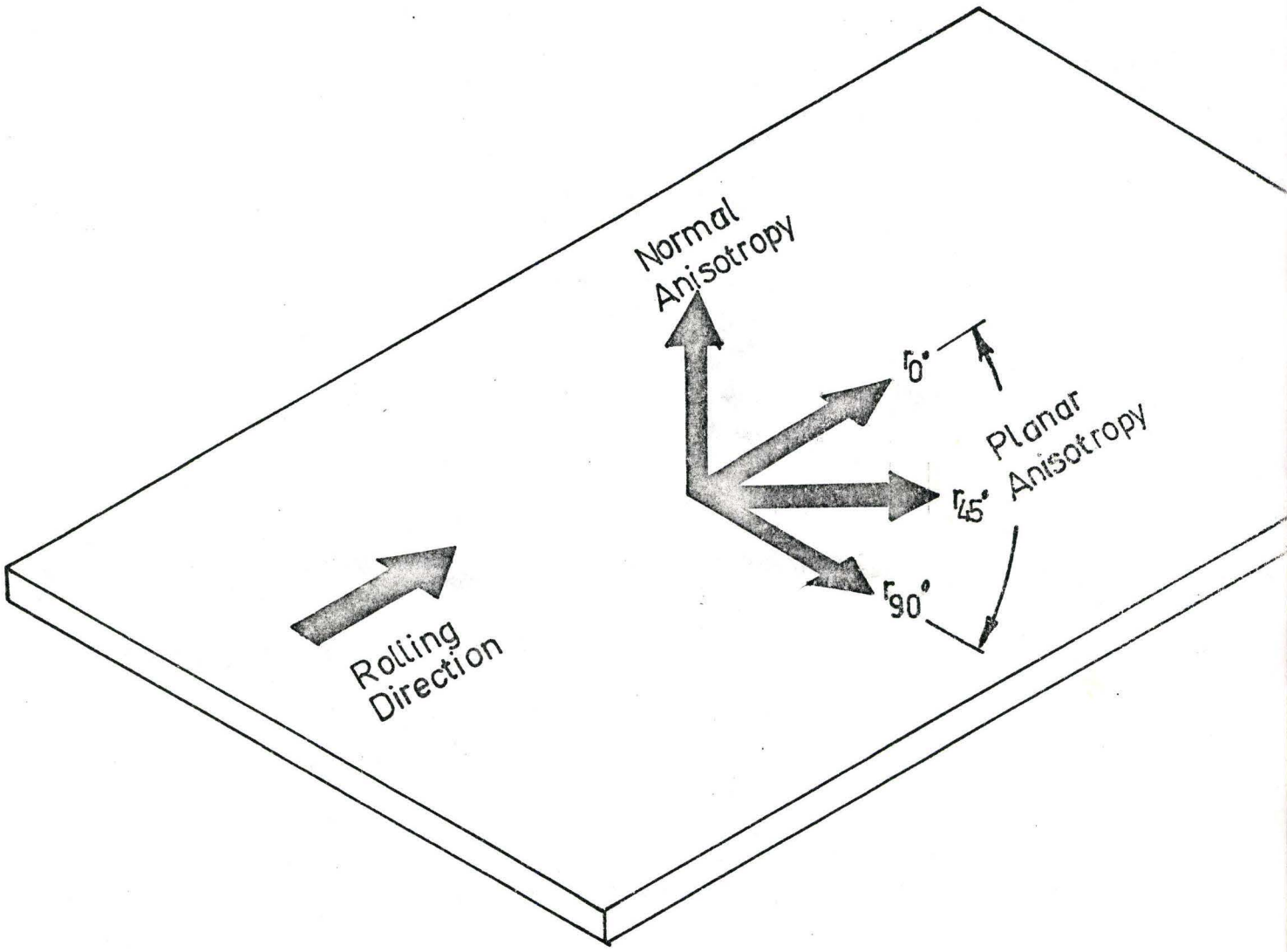

EIGURE 26 TENSILE SPECIMEN IN THREE DIFFERENT DIRECTIONS WITH RESPECT TO ROLLING DIRECTION OF THE SHEET METAL TO DETERMINE ANISOTROPY

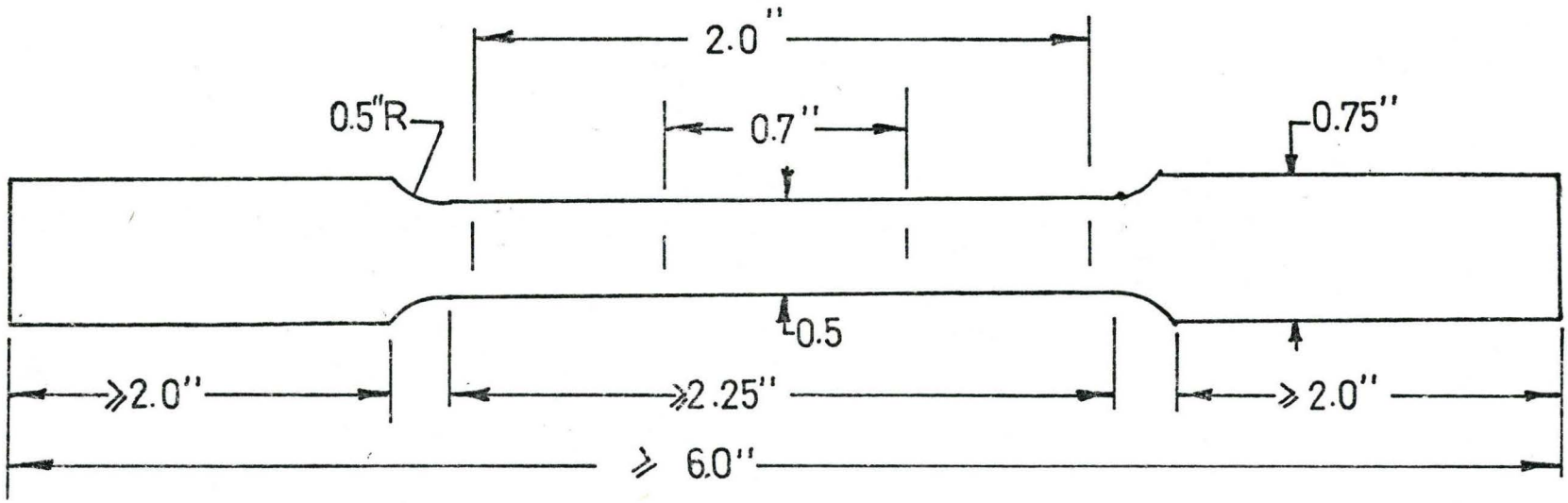

FIGURE 27 TENSILE TEST SPECIMEN

4.2.3 Test Procedure

The specimens were pulled to fracture, and on the basis of the autographic chart the yield stress and ultimate tensile strength were determined; the chart was read using the digitizer. The computer program EVAL (given in Art.4.8 was designed to convert load-extension data to true stress-natural strain and to fit these data with the equation

$$\sigma = k\ (\varepsilon_o + \varepsilon)^n \qquad (4.1)$$

This curve fitting was made by the method of least squares given in Article 4.9. The same test pieces were used to determine limit strain (uniform elongation), total elongation and fracture strain. Uniform elongation, ε_u, was defined as

$$\varepsilon_u = \ln \frac{l}{l_o} \qquad (4.2)$$

Note in this case the gauge section is chosen well removed from the diffuse necked zone.

The total elongation was determined from equation (2.8) where the final gauge length was measured after placing the two halves of the fractured specimen together.

The fracture strain was determined from equation (2.11). Measurements of the final thickness were taken using a toolmakers microscope. The thickness was measured at a number of points at the fractured edge and an average value was taken.

The degree of anisotropy was determined by calculating the r value from equation (2.7). Tensile specimens were

TABLE II TENSILE TEST RESULTS

MATERIAL	TEST DIRECTIONS	YS ksi	UTS ksi	K ksi	n	ε_o	m	r	ε_u	ε_t (%)	ε_{3f}
3003-0	0	7.35	16.9	29.6	.2434	0.000		.6745	.269	31.4	1.502
	45	6.74	15.2	27.3	.2348	0.000	.006	.7769	.229	31.17	1.349
	90	6.30	14.5	30.4	.2481	0.000		.4020	.270	31.40	1.614
	av			20.7	.240	0.000		.658	.249	31.6	1.453
3003-H14	0	17.9	24.4	28.7	.0382				0.020		1.1901
	45	18.2	23.9	28.8	.0414		.007		0.011		1.1423
	90	18.6	24.6	32.1	.0620				0.020		1.1959
	av	18.2	24.2	29.6	.046				0.016		1.168
5182-0	0	22.9	44.0	93.9	.3323	.000	-.0105	.6299	.1861	22.0	.9092
	45	22.2	42.3	89.7	.3315	.000	-.0073	1.0648	.218	23.4	.8615
	90	22.8	42.5	91.5	.3416	.000	-.0152	.8068	.202	23.36	.8140
	av	22.5	42.8	91.2	.334	.000	-.0101	.892	.206	23.0	.8740
5182-H111	0	20.9	43.4	82.9	.2735	.0013	-.0100	.6764	.2110	23.4	.9055
	45	19.7	42.7	82.1	.2813	.0030	-.0100	1.0040	.2014	27.0	.8486
	90	20.3	42.7	85.1	.2999	.0035	-0.0102	.7020	.2090	21.8	.8092
	av	20.1	42.9	83.1	.284	.0027	-.010	.847	.206	24.8	.853
2036-T4	0	31.9	52.5	102.8	.2930	.0087		.6464	.215	22.1	.653
	45	30.5	50.5	99.1	.2969	.0120	-.0032	.0170	.2381	26.0	.717
	90	30.2	50.4	103.2	.3218	.0140		.7076	.209	22.0	.609
	av	30.8	51.0	101.1	.302	.012		.747	.225	24.0	.674
AKDQ* Steel	av	25.9	44.0		.205			1.918		35.7	2.194

* Results are taken from Reference 16

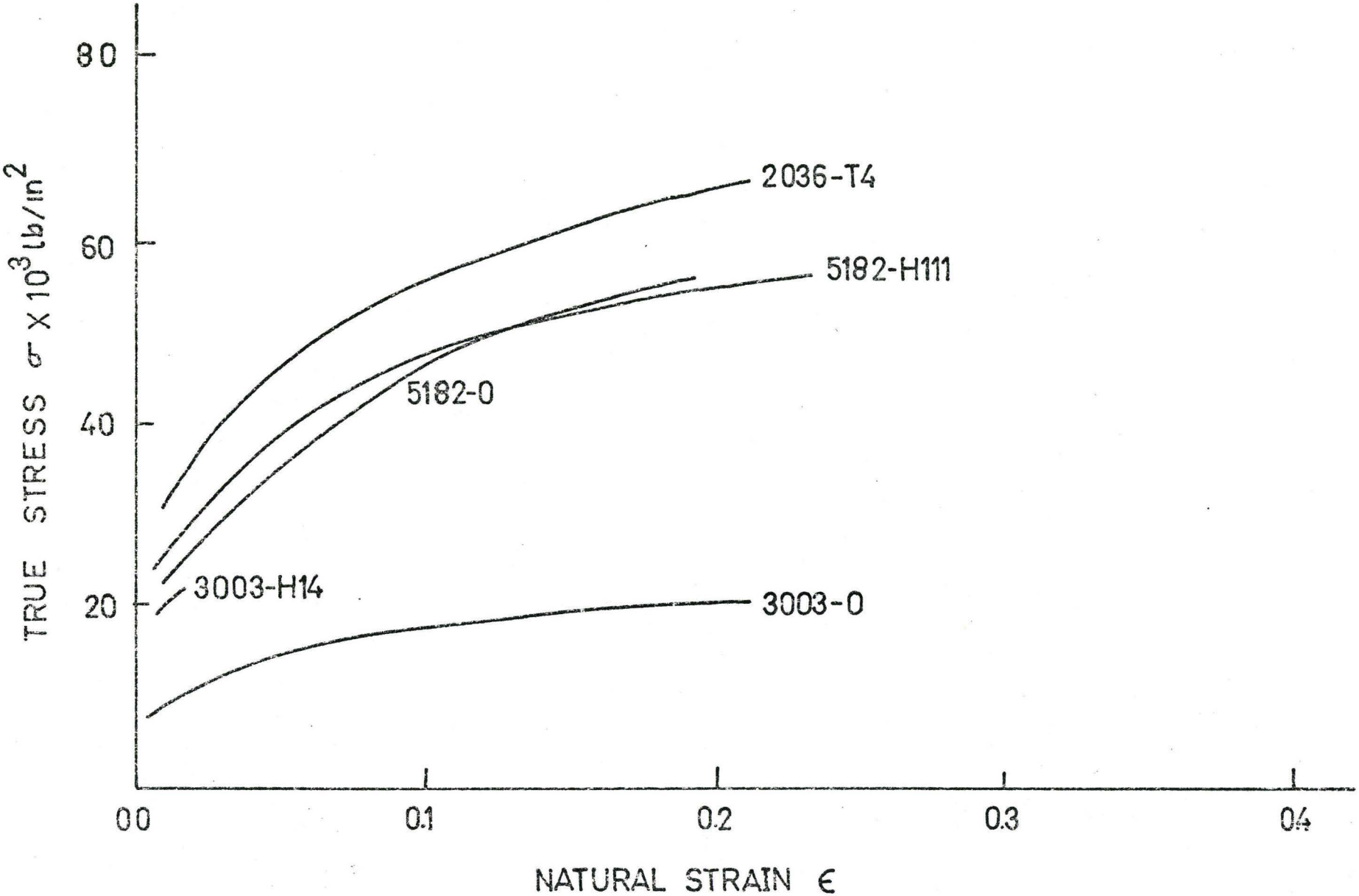

FIGURE 28 TRUE STRESS / STRAIN CURVE OBTAINED FROM TENSILE TEST

cut from the sheet, at 0, 45 and 90 degrees with respect to the direction of rolling, as shown in Fig. 26. Each specimen was deformed to about 15 per cent plastic strain, but never exceeding the uniform strain, and removed from the testing machine for measuring. The longitudinal strain was determined by measuring the final dimension of a 2 in. gauge length using a tool makers microscope. The change in width of the specimen was measured at three points over the gauge section and an average value computed. The thickness strain was then computed on the basis of constant volume of material within the gauge section and the "r" value finally determined from equation (2.7).

4.2.4 Tensile Test Results

Tensile test results are presented in Table II. The stress strain curves computed from load-extension autograph up to a maximum load are plotted in Figure 28.

All materials show a good strain hardening capability and uniform strain except the cold worked 3003-H14 alloy. The 3003-0 is clearly very soft compared with other materials, while 2036-T4 alloys appears to be the strongest among the materials tested.

The strain hardening index, n, and the, r, value could not be determined with any accuracy for the 3003-H14 material since the uniform elongation was only 2 per cent. With the stronger alloys 5182 and 2036 it was noticeable that the uniform strain, ε_u, was consistently lower than the

n value. Note this is in contradiction to the simple instability theory which predicts $\varepsilon_u = n$.

The r values for the aluminum alloys are all less than unity. The variation of r with orientation of the test piece provides some information about the existence of planar anisotropy.

The only material showing a significant yield point elongation or Lüders strain was the 5182-0 and both this and the 5182-H11 shows appreciable serrated yield throughout the tensile test, a manifestation of the Portevin-Le Chatelier (P-L) effect.

The measured fracture strains are the largest with the lower strength alloys and decrease as the strength of the alloy decreases. Previous investigations, as well as work conducted here at McMaster, indicate that these higher strength alloys exhibit a slight negative strain rate sensitivity index, m; while m appears to be positive for the softer materials. It is not clearly established how strain rate sensitivity affects the magnitude of the fracture strain in these particular alloys.

It is generally felt that a positive strain rate sensitivity index is beneficial in prolonging the extent of the deformation but this conclusion is based generally on the forming characteristics of the so called "superplastic" alloys. As stated above the degree of correlation between m and the level of formability and fracture strain has not been veri-

fied for common engineering materials.

4.3 Bulge Test

The bulge testing machine developed at McMaster University and described in reference [18], was employed.

The equipment includes a mechanical spherometer and extensometer which determine the radius of curvature and the strain over the pole of the dome [18]. Refer also to Figure 29.

4.3.1 Specimens

The specimen need not be cut to an exact circular shape, a typical blank is shown in Figure 30.

The grids were photographically printed on the specimen using the Kodak Photoresist method [36]. Grids of this type can be applied with great precision and do not affect the deformation or fracture behaviour of the specimens.

4.3.2 Test Procedure

The thickness of the specimen was measured before it was loaded into the die. After sufficient clamping was achieved the biaxial test unit (with dial gauges set to zero) was placed into the locating ring, the pressure was supplied and the readings of pressure, spherometer and extensometer gauges were taken at regular intervals. Bulging process was performed up to the fracture of the specimen. The readings of pressure, spherometer and extensometer gauges were converted into true stresses and natural strains using computer program EVAL (App.B) and the data was fitted to an equation of the

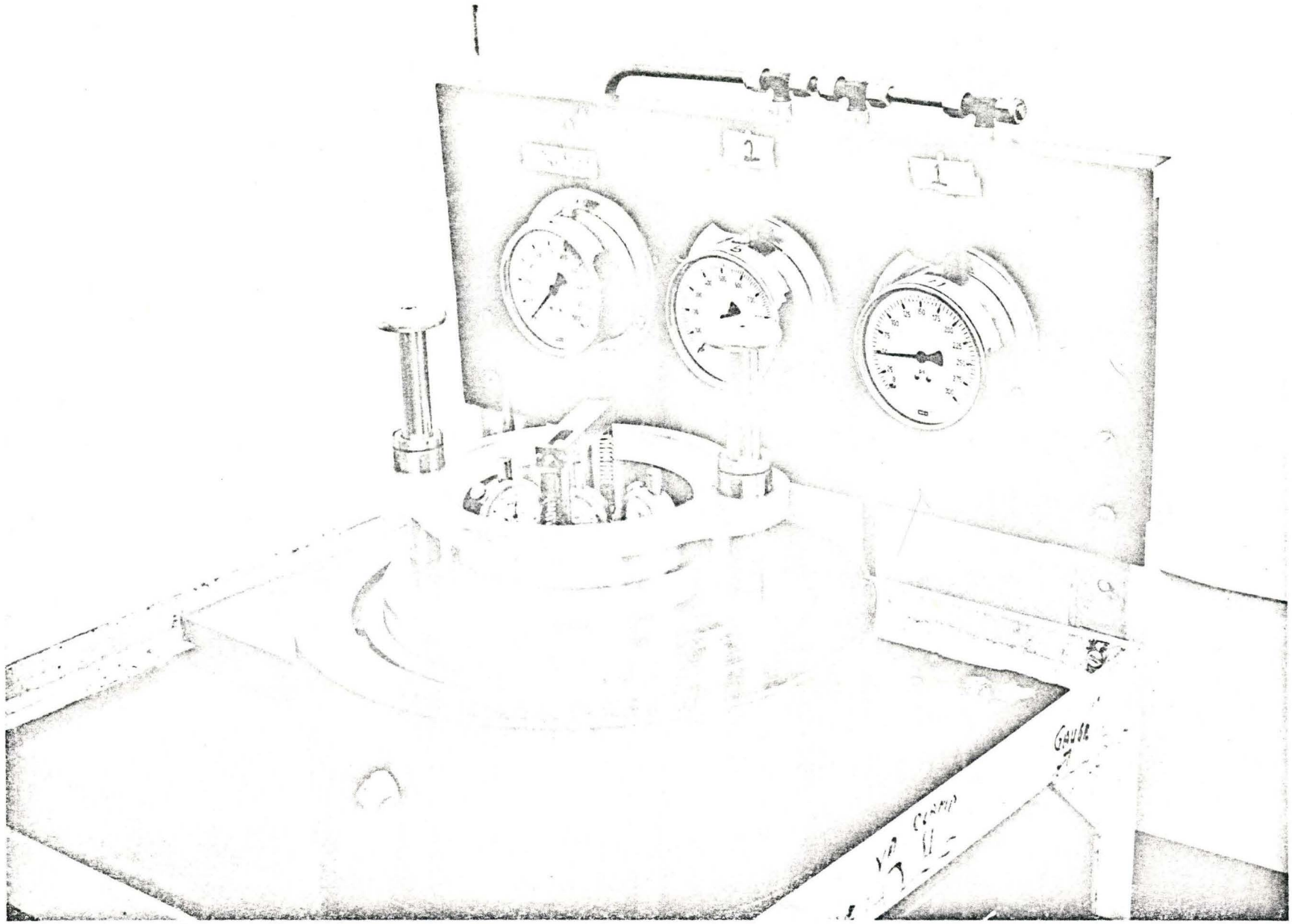

FIGURE 29 BULGE TEST EQUIPMENT

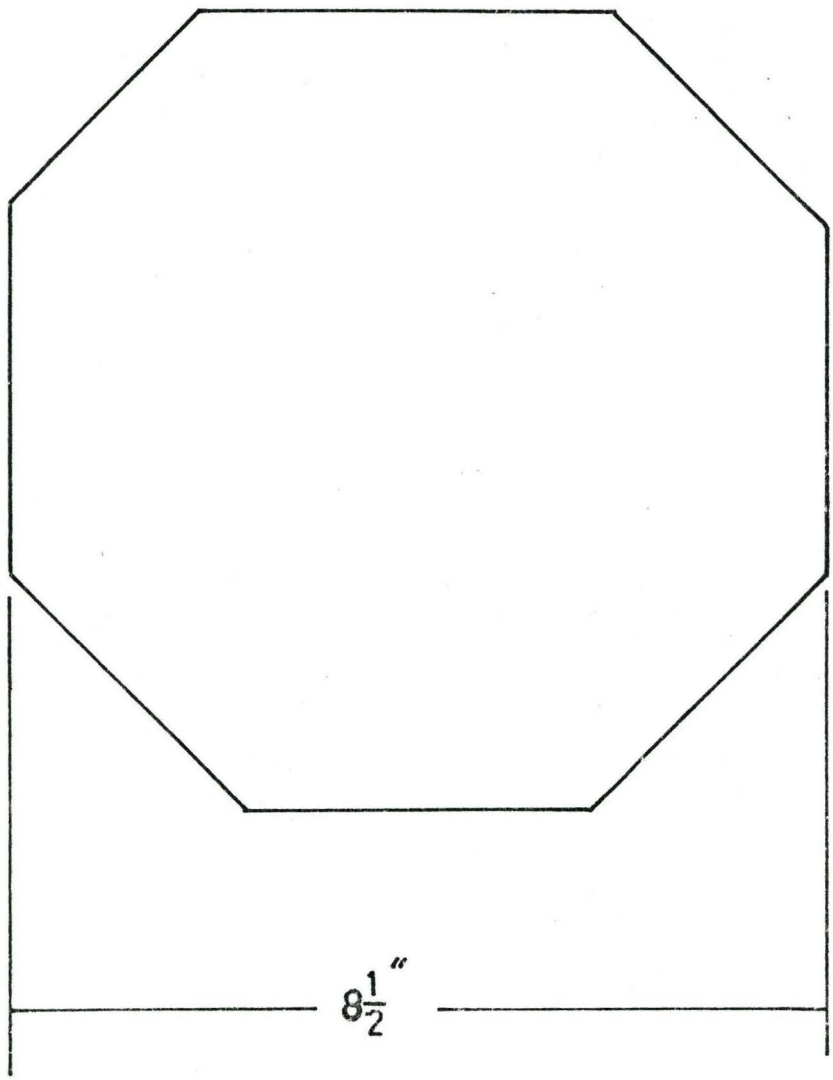

FIGURE 30 SPECIMEN FOR BULGE TEST

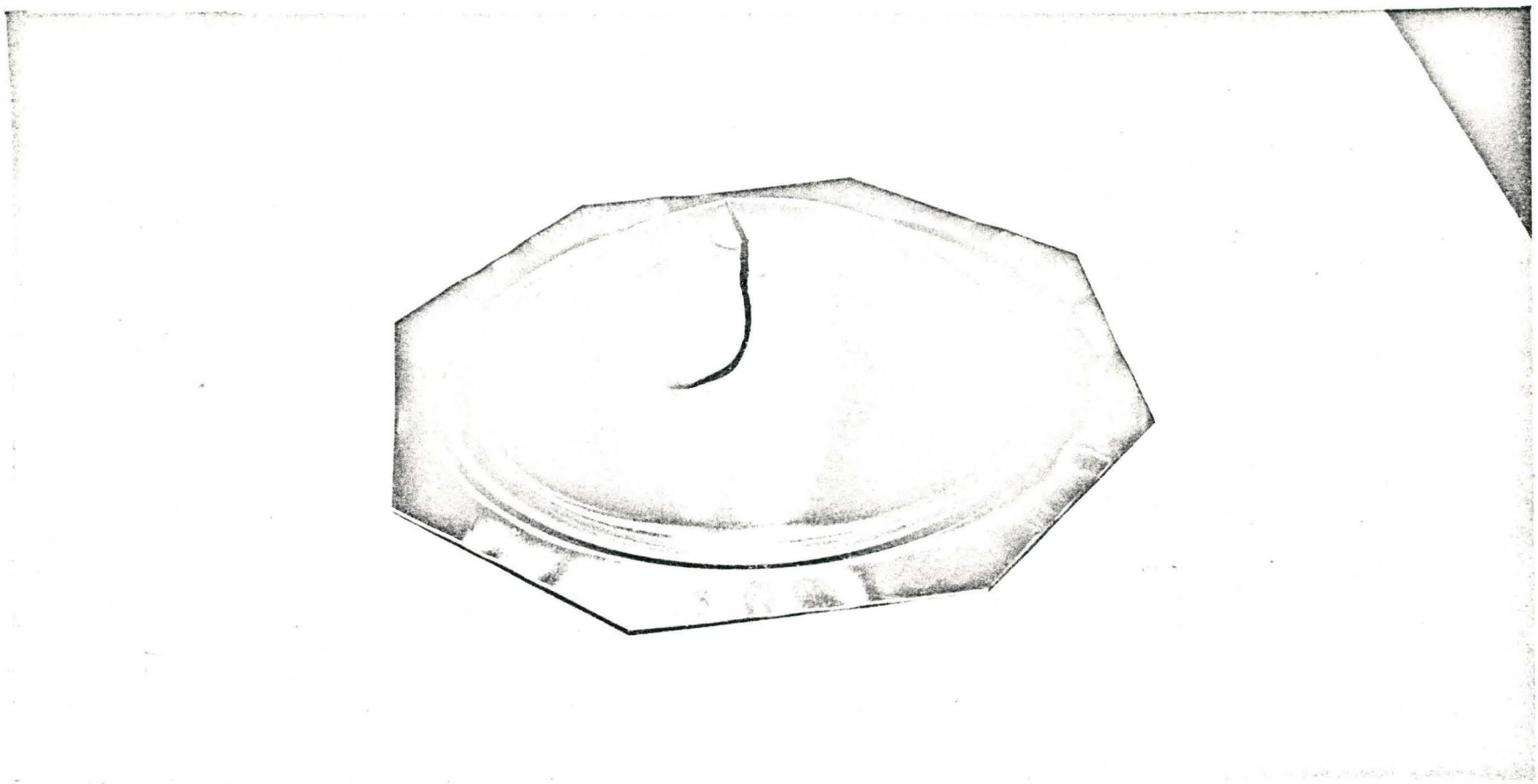

FIGURE 31 BULGED SPECIMEN - MATERIAL 5182-0 AL.

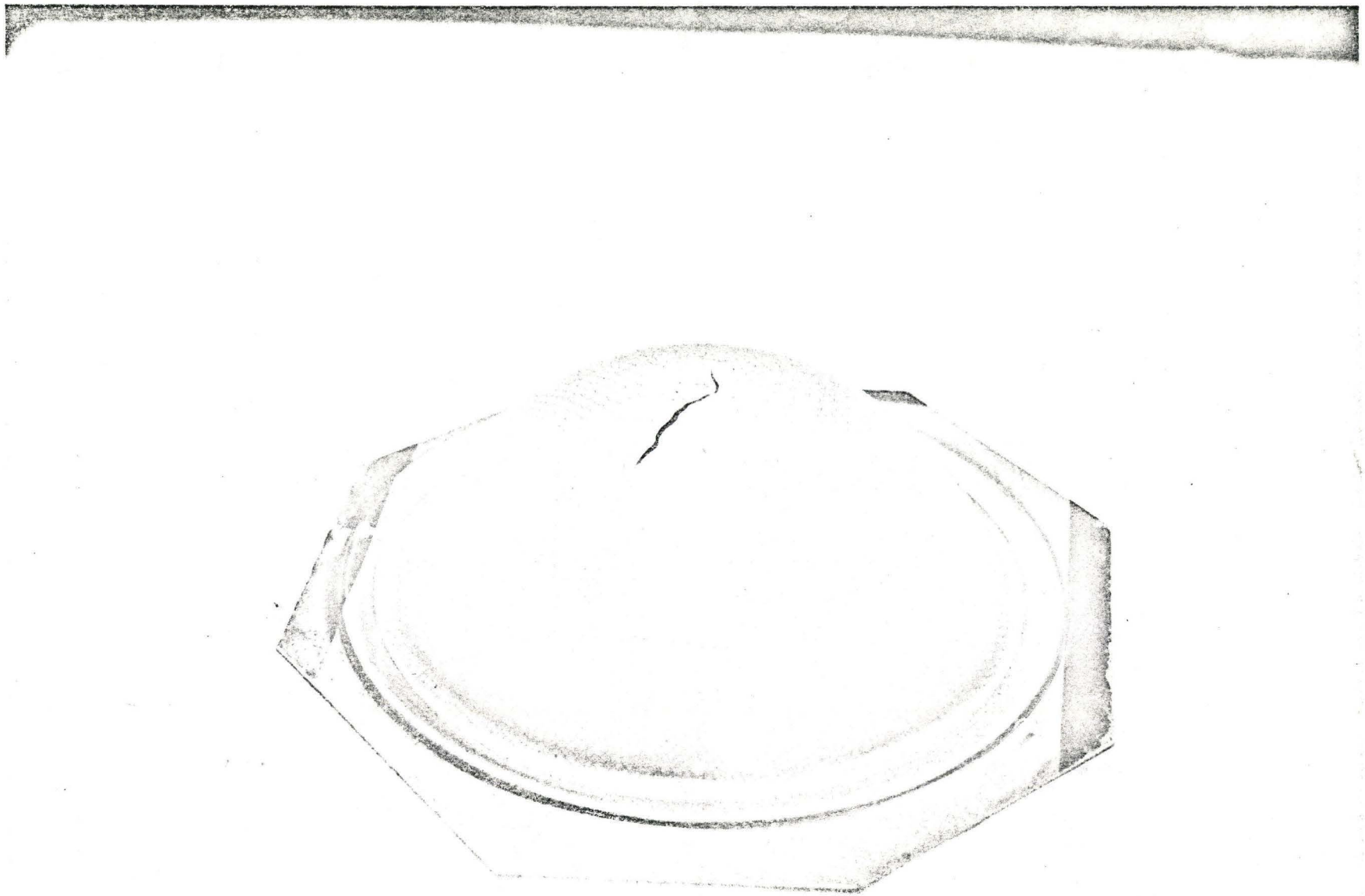

FIGURE 32 BULGED SPECIMEN — MATERIAL 3003-0 AL.

TABLE III BULGE TEST

MAT	n	ε_o	K ksi	ε_1^*	ε_2^*	ε_t^*	ε_{3f}
3003-0	.2095	.010	25.33	.457	.449	.906	2.09
3003-H14	.0494	.020	25.75	.270	.270	.540	1.44
5182-0	.2575	.000	82.96	.250	.230	.480	.86
5182-H111	.2386	.000	74.35	.1905	.1905	.381	.83
2036T4	.3029	0.010	99.6	.292	.232	.531	.717

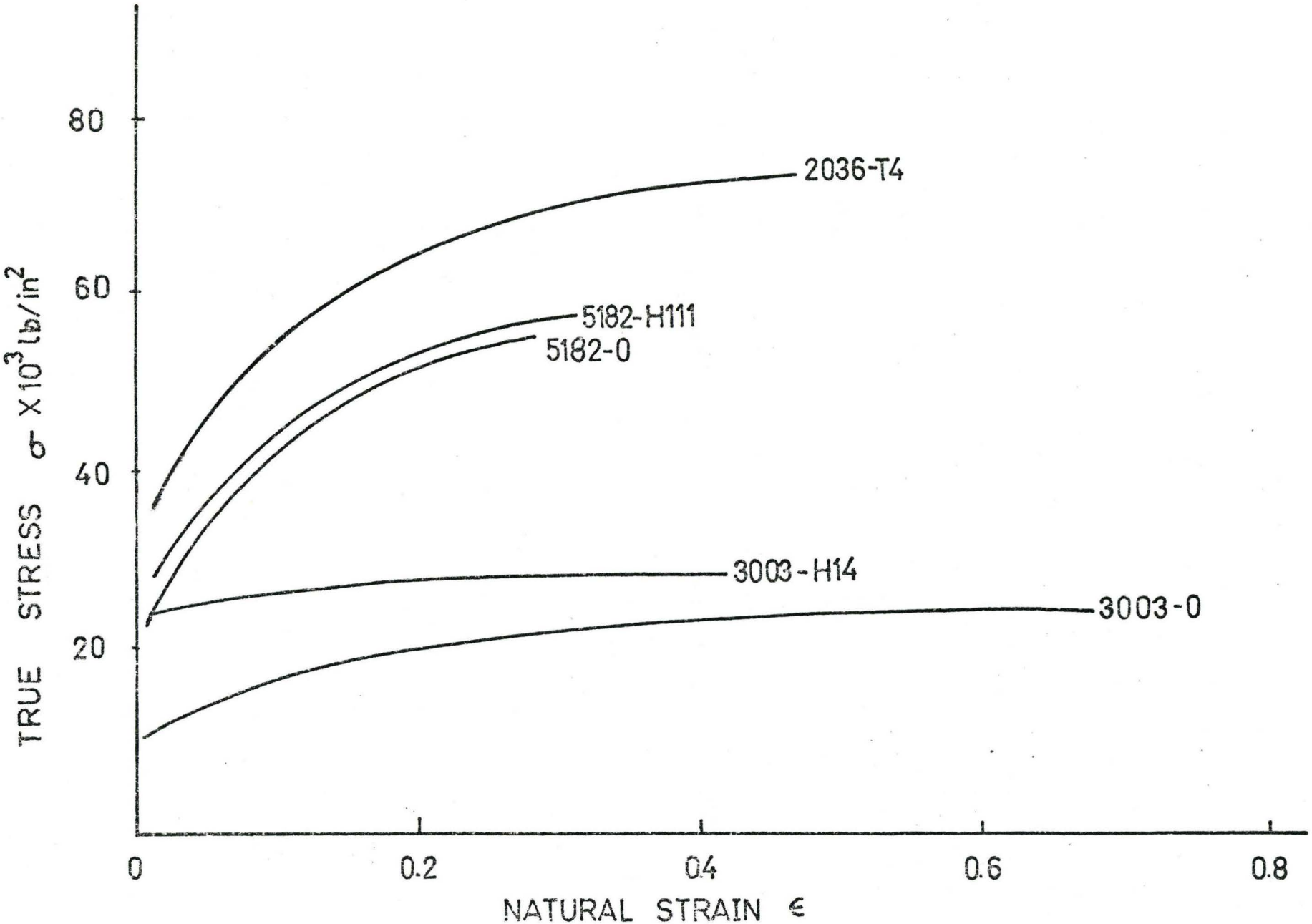

FIGURE 33 TRUE STRESS/STRAIN CURVES OBTAINED FROM BULGE TEST

form,

$$\sigma = k(\varepsilon+\varepsilon_o)^n$$

The limit strains were determined by measuring the grid circle close to the necked zone. Figs. 31 & 32 show details of a fractured bulge specimen and the retention of the photo-grid. The fracture thickness strain is determined by measuring the thickness at several points along the fractured edge using a toolmakers microscope and averaging the results. In order to perform these measurements invariably a piece of material has to be cut from the specimen to provide access to the fractured edge.

4.3.3 Bulge Test Results

In an isotropic material a plot of membrane stress versus thickness strain should be equivalent to tensile stress strain curve and the data plotted on this basis are presented in Figure 33. As this test is not limited by diffuse necking, a longer stress strain curve is generally obtained particularly in materials having a low strain hardening index. This is particularly apparent with 3003-H14 which has a maximum uniform strain of 0.02 in uniaxial tension and 0.54 in the bulge test.

The bulge test data is summarized in Table III. The limit thickness strain is defined as ε_t^* and this is calculated from the sum of the two limit surface strains ε_1 and ε_2. Ideally for the bulge test ε_1 and ε_2 should be equal and this is verified by the results of TableIII. The thickness fracture

strain ε_{3f} (measured at the point of fracture) is also given in the table.

4.4 Torsion Test

The apparatus available in the metalworking laboratory at McMaster is an instrument that has been developed and designed at the Technical University of Warsaw [19] and shown in Figure 34. The line diagram of the instrument is shown in Figure 3.

4.4.1 Specimens

The specimen had a shape of a rectangle 50 x 75 mm cut from the sheet metal.

4.4.2 Test Procedure

The specimen was rigidly clamped in the machine and twisted in its plane until fracture occurred at the edge of the inner clamps. Two measuring drums enable the permanent reading of angles θ_B and θ_D during the deformation process to be taken.

On the basis of θ_D and θ_B values the fracture strain and work hardening exponent were determined.

In order to avoid computations, tables can be provided to give the desired parameters for a measured θ_D and θ_B.

4.4.3 Torsion Test Results

Table IV shows the results obtained from torsion test. The work hardening index shows a good agreement for 3003 alloys, whereas for high strength alloys the value of n from torsion tests is lower than that obtained from tensile

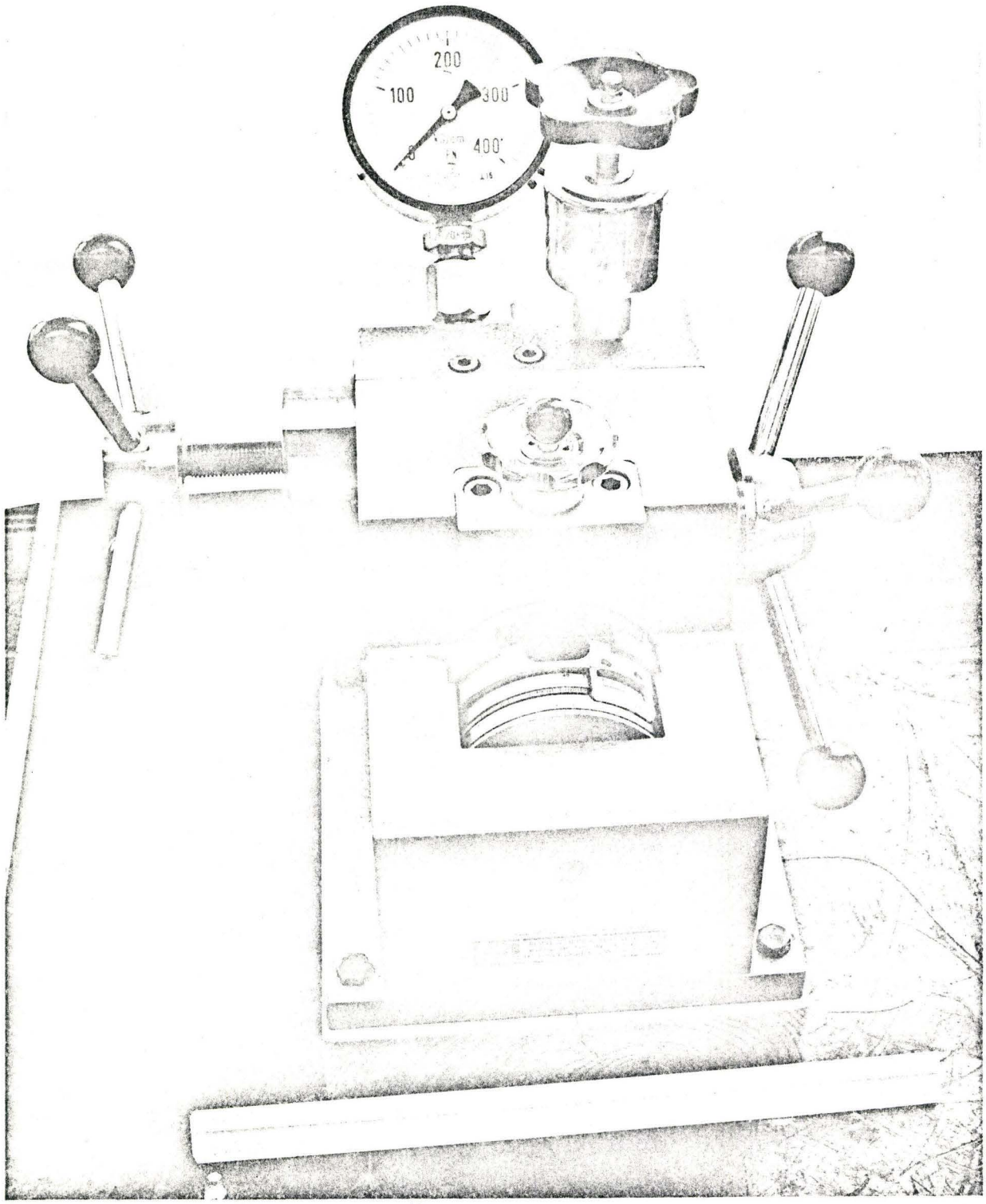

FIGURE 34 MARCINIAK TORSION TESTING MACHINE

TABLE IV TORSION TEST RESULTS

MATERIAL	3003-0	3003-H14	5182-0	5182-H111	2036-T4
n	.235	.135	.200	.175	.181
$\bar{\varepsilon}_{3f}$	1.30	1.84	.82	.99	.33

tests. This might be attributed to strain rate-sensitivity effect. The high strength aluminum alloys show significantly lower fracture strains than the 3003 alloy.

4.5 Hecker Test for Determination of FLD

The test to determine FLD has been discussed earlier in article 2.4.1 of Chapter II.

The testing was performed on a Hille 20 ton universal sheet metal testing machine. Since the blank diameter which can be accommodated on a Hille press was 6.5 inches; the tooling and the specimen size had to be modified as follows.

(i) The diameter of the hemispherical punch was chosen to be 3" instead of 4" as suggested by Hecker [13].

(ii) The clamping of the specimen was obtained by providing serrated matching faces of the die, as shown in Figure 35.

(iii) The maximum size of the specimen used was 6" square. The other specimen were made 6" long and the width varied from 6" down to 1" in steps of 1".

(iv) All specimen were gridded photographically using a Kodak Photo-resist Method [36]. The diameter of the grid circle for this series of tests was 0.0285".

4.5.1 Test Procedure

Each specimen was securely clamped at the periphery (clamping pressure 10 tons) and stretched to failure without load interruption. The average speed of the punch was 1.2"/min.

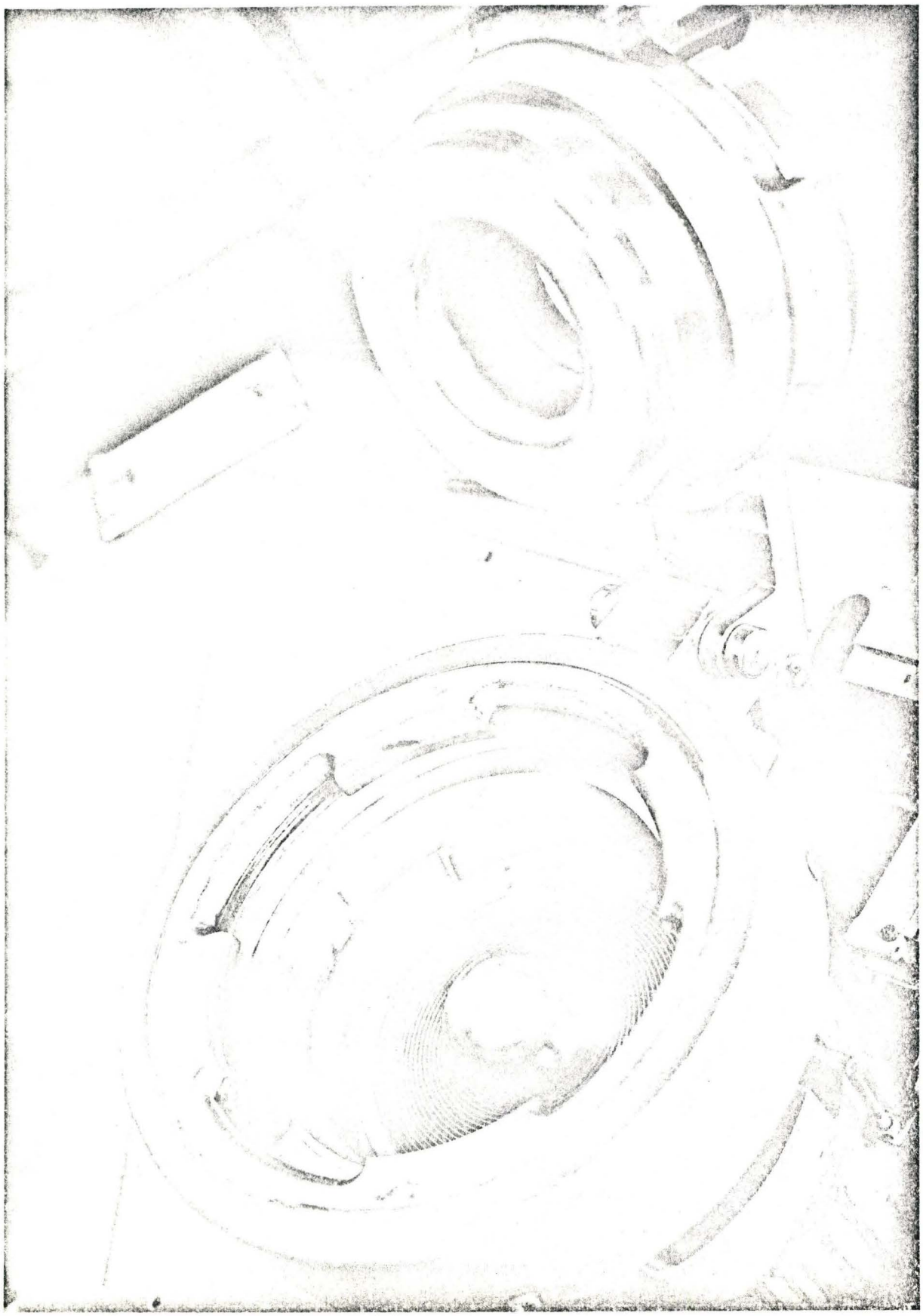

FIGURE 35 EXPERIMENAL SET UP FOR HECKER TEST

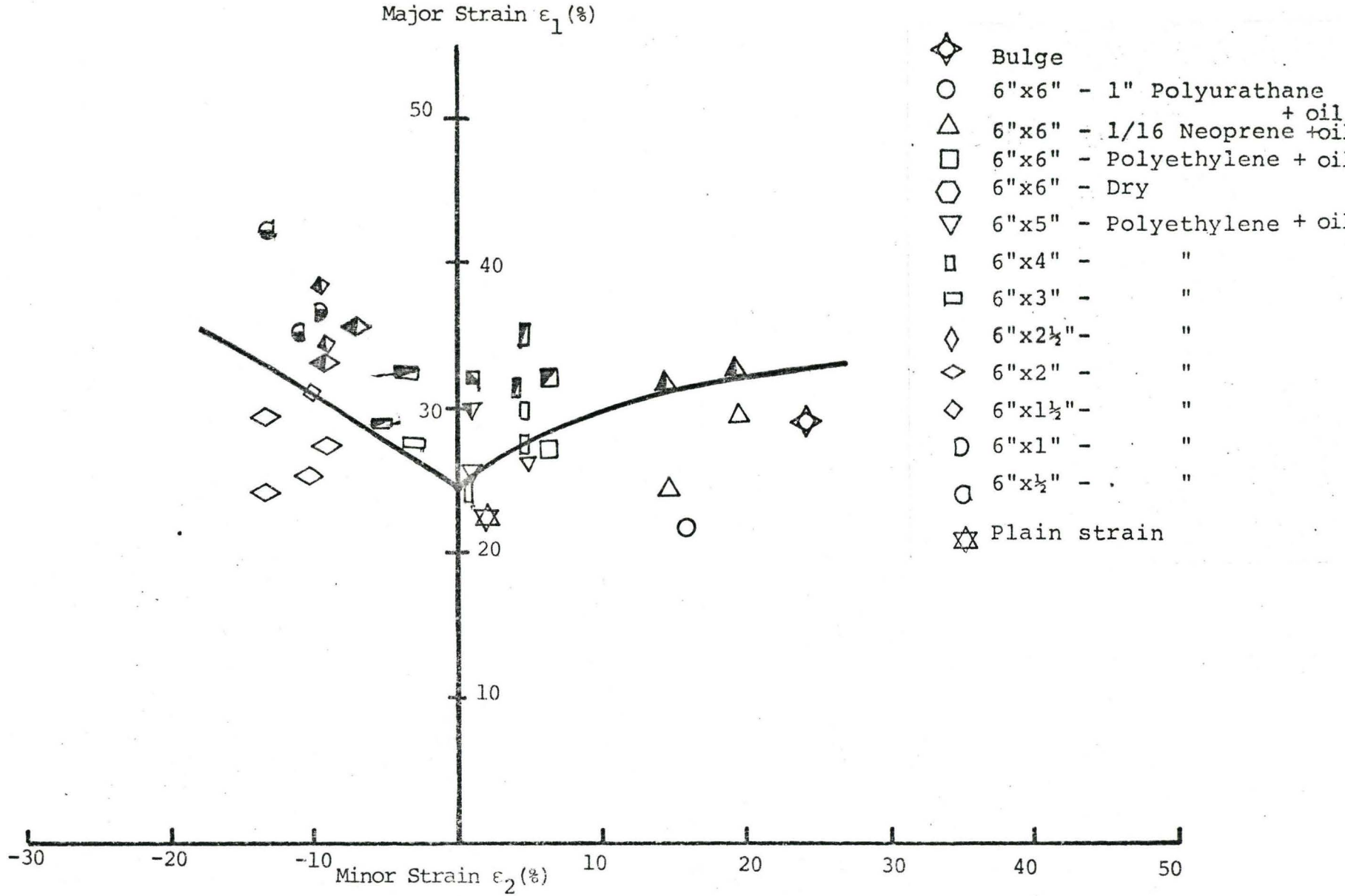

FIGURE 36 - FLD for 2036-T4 Aluminum Alloy

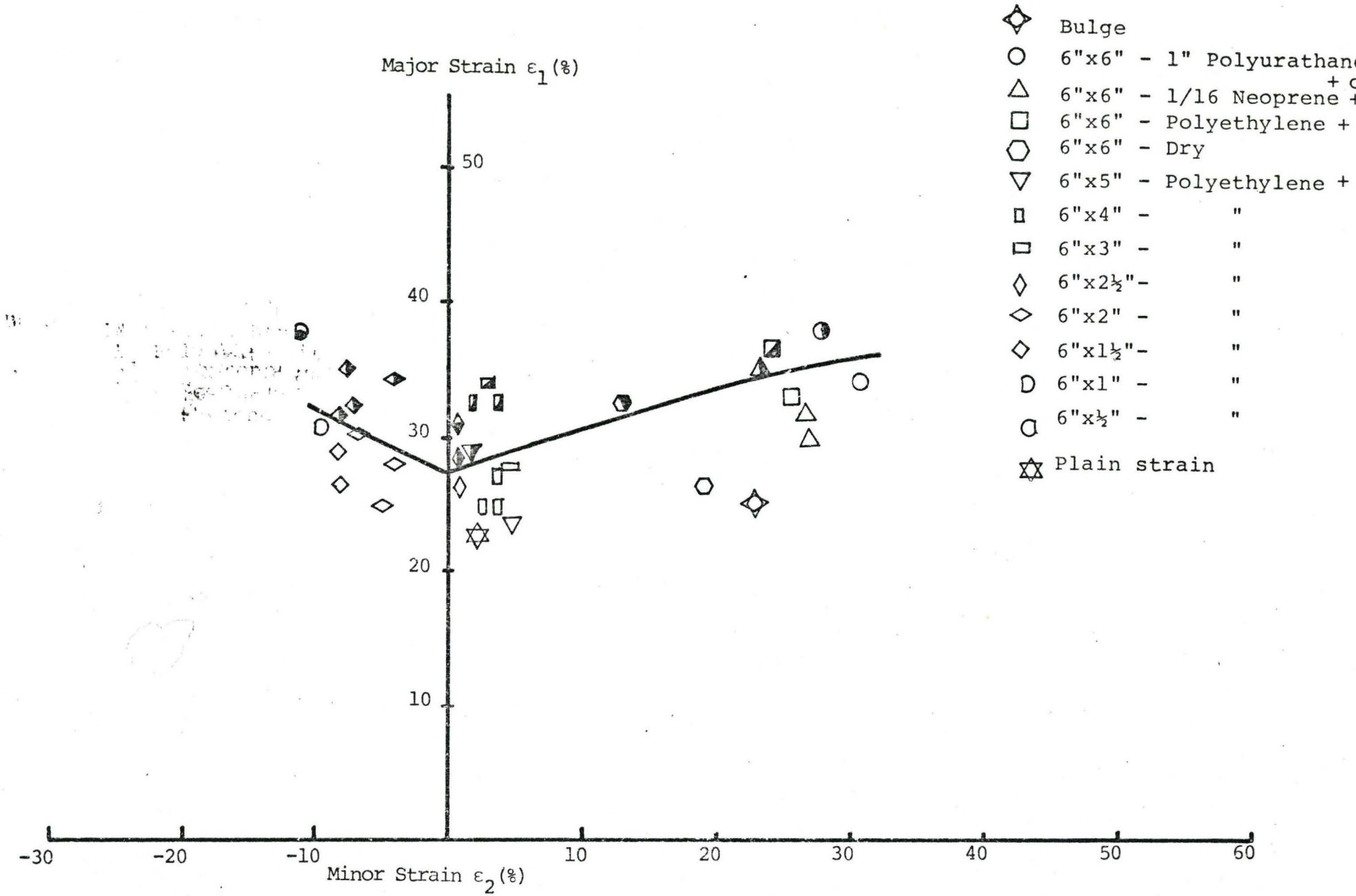

FIGURE 37 - FLD for 5182-0 Aluminum Alloy

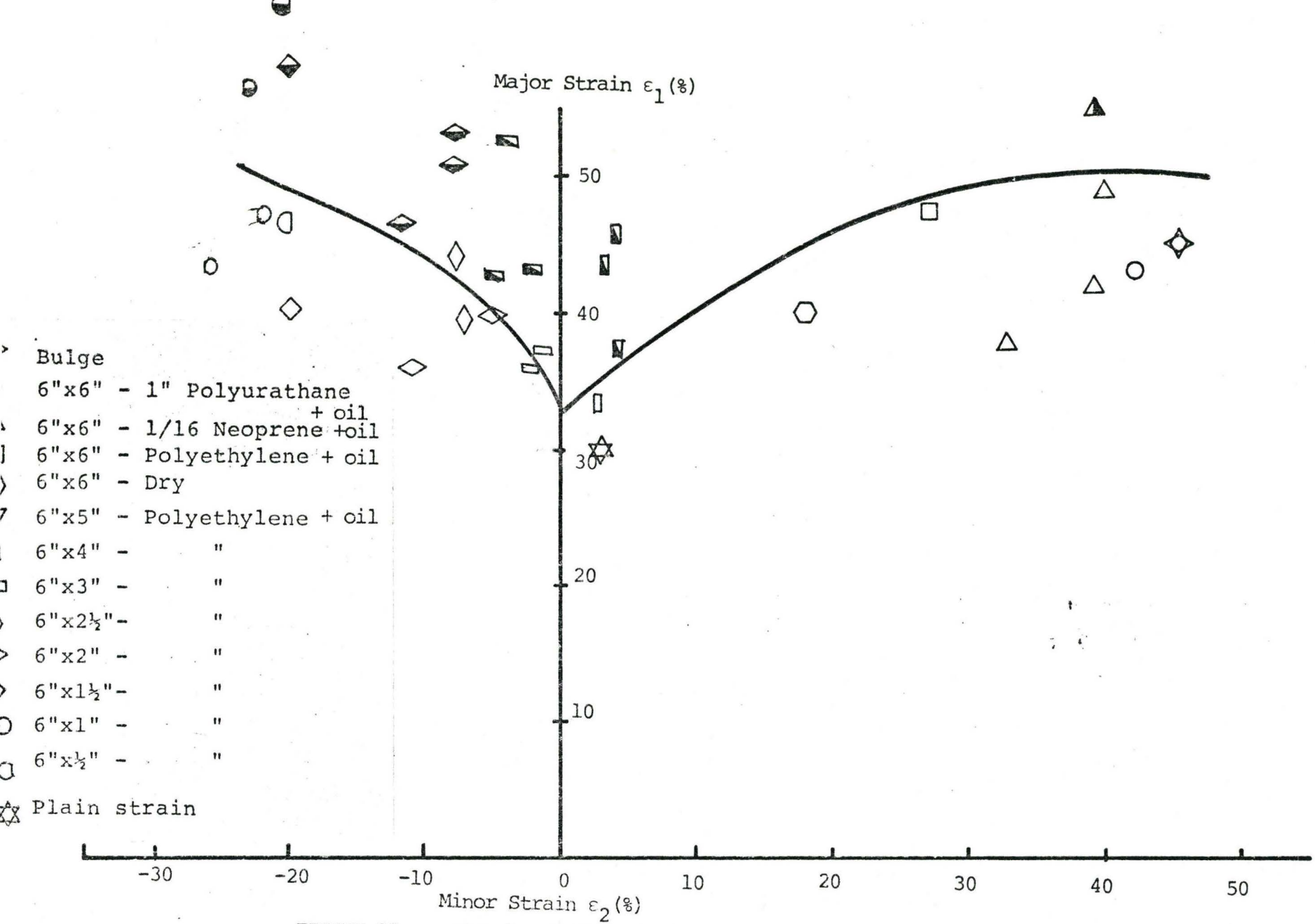

FIGURE 38 - FLD for 3003-0 Aluminum Alloy

To determine the FLD, failures were generated to cover the entire range of strain ratios ie $-\frac{1}{2} < a < 1$ by altering either the lubrication conditions or width of the specimen.

The surface strains ε_1 and ε_2 and the FLD was obtained as described in article 2.4.1.

4.5.2 Test Results

Figures 36 to 38 show the FLD's for aluminum alloys 2036-T4, 5182-0 and 3003-0 respectively.

The FLD's for stronger alloys are flatter and do not show an appreciable increase in major strain as the process goes from plane strain to balanced biaxial straining.

The limit strain for plane strain condition is higher than "n" value for soft and ductile aluminum alloy 3003-0 but for stronger alloys 5182-0 and 2036-T4 the strain is lower than "n" value.

4.6 Plane Strain Test

The detailed description of this test is given in article 2.3.6 of Chapter II. This test was also carried out on the 20T Hille Press.

Figure 9 shows a schematic diagram of the tooling designed for this test. The surface area of the rectangular punch was chosen to be equal to the surface area of a 2" diameter flat bottom punch.

All specimens were 6½" x 4½" and cut from the plane of the sheet, they were gridded with 0.0285" diameter circular

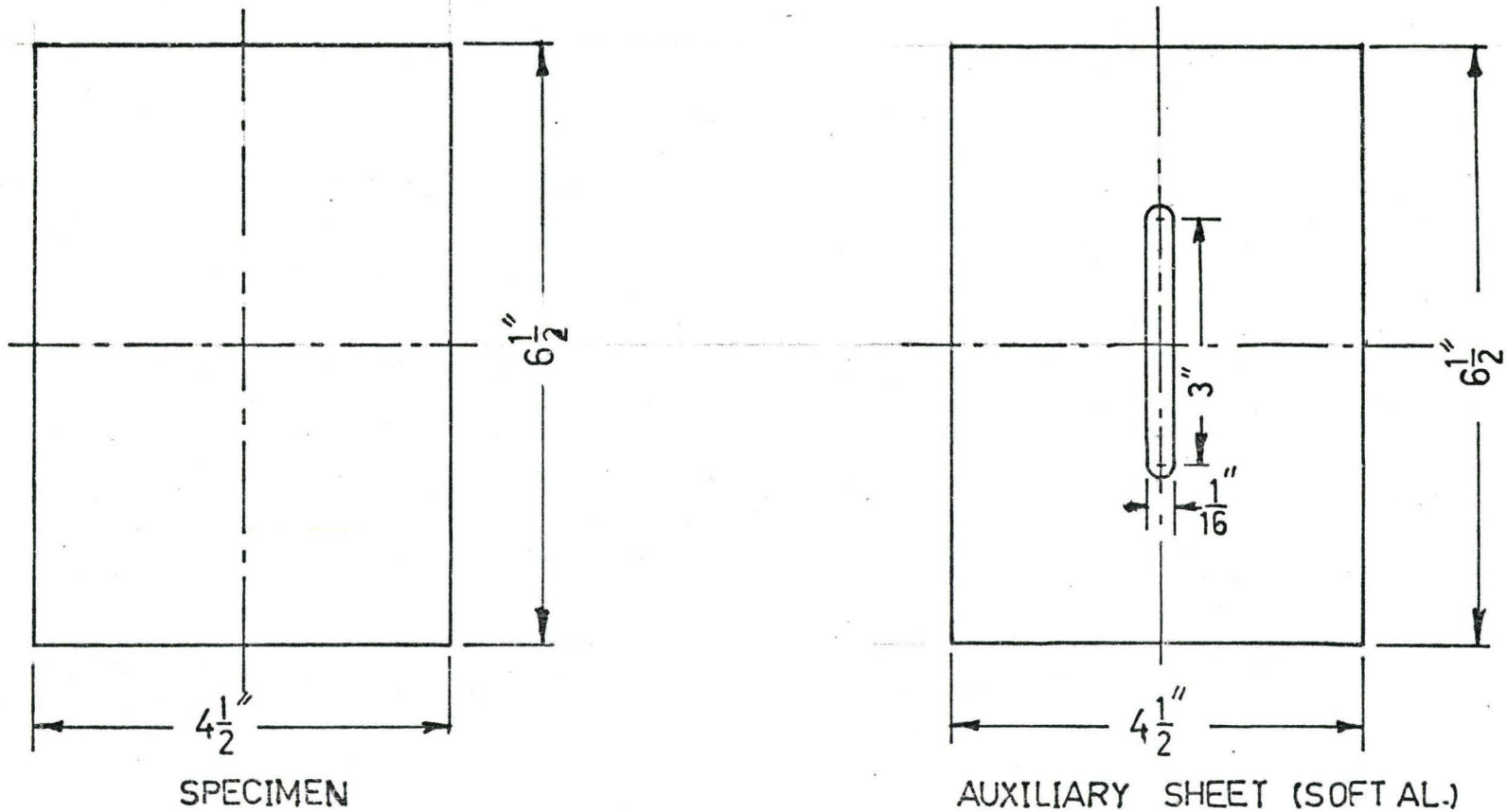

FIGURE 39 SPECIMEN FOR PLANE STRAIN TEST

TABLE V PLANE STRAIN TEST

MATERIAL	ε_1	ε_2	$\bar{\varepsilon}$	a	ε_{3f}
3003-0	.299	.025	.3435	.084	1.47
3003-H14	.098	.011	.1217	.113	1.498
5182-0	.2386	.0210	.2735	.088	.757
2036	.221	.0175	.2498	.08	0.38

grid.

An auxiliary sheet of soft aluminum (6½" x 4½") with a slit (3" x $\frac{1}{16}$") along the centre line was used to promote plane strain failure in the specimen under investigation.

Figure 39 shows the specimen and auxiliary sheet.

4.6.1 Test Procedure

The test procedure is exactly the same as described for the Hecker Test (article 4.5.1).

4.6.2 Results

The limit strains obtained by this test are shown in Table V, they are generally lower than the values obtained in the Hecker Test. Such a descrepancy is normally expected because the geometry of deformation in the two kinds of tests is different. This is supported by Ghosh and Hecker [37] who show a higher value of limit strain for out of plane stretching over in plane stretching, under identical degrees of biaxiality.

4.7 Measurement of Strains at Fracture Site

The principal strains are measured for specimens failed under different conditions of biaxial loading. The purpose here is to investigate the influence of loading path on the strains at fracture.

The fracture thickness strain, ε_{3f}, can be obtained by measuring the thickness of the specimen at fracture site. The surface strains ε_{2f} parallel to fracture can be

TABLE VI - Principal Surface Strain at the Fracture Site and the Limit Strain (FLD) for 3003-0 Aluminum Alloy

Specimen No.	ε_1^*	ε_2^*	$a=\frac{\varepsilon_2}{\varepsilon_1}$	ε_{1f}	ε_{2f}	ε_{3f}
1	.427	-.213	-.5	1.94	-.22	-1.72
2	.430	-.189	-.44	1.81	-.23	-1.58
3	.390	-.123	-.32	1.76	-.13	-1.63
4	.359	-.111	-.30	1.78	-.12	-1.66
5	.371	-.032	-.087	1.76	-.025	-1.735
6	.378	.041	.108	1.70	.03	-1.73
7	.547	.439	.80	1.45	.44	-1.89
8	.415	.38	.92	1.54	.33	-1.87

TABLE VII - Principal Surface Strains at the Fracture Site and the Limit Strains (FLD) for 5182-0 Aluminum Alloy

Specimen No.	ε_1^*	ε_2^*	a	ε_{1f}	ε_{2f}	ε_{3f}
1	.311	-.095	-.305	.79	-.11	-.68
2	.3365	-.065	-.19	.86	-.10	-.76
3	.25	-.05	-.2	.83	-.10	-.73
4	.285	-.007	-.0245	.72	-.03	-.69
5	.258	.027	.105	.69	.02	-.71
6	.277	.045	.162	.65	.04	-.69
7	.334	.266	.72	.56	.24	-.80
8	.264	.191	.79	.53	.18	.71
9	.336	.32	.96	.54	.25	.79

TABLE VIII - Principal Surface Strains at the Fracture Site and the Limit Strains (FLD) for 2036-T4 Aluminum Alloy

Specimen No.	ε_1^*	ε_2^*	$a=\frac{\varepsilon_2}{\varepsilon_1}$	ε_{1f}	ε_{2f}	ε_{3f}
1	.277	-0.100	-.36	.407	-0.077	-0.33
2	.331	-0.100	-.30	.574	-0.107	-0.467
3	.296	-0.058	-.195	.496	-0.073	-.423
4	.321	0.139	.043	.498	0.000	.498
5	.309	0.045	.144	.426	0.055	.481
6	0.309	0.048	.155	.464	0.017	-.481
7	.247	.147	.595	.564	0.116	-.68
8	.253	.156	.617	.503	.128	-.631
9	.298	.194	.65	.499	.185	-.684

obtained by measuring the grid diameter at the fracture site. Since the strain gradient is very high near the fracture site, ε_{1f} can not be computed by measuring the deformed grid at the fracture site. However, ε_{1f} can be computed by assuming volume consistancy ie,

$$\varepsilon_{1f} + \varepsilon_{2f} + \varepsilon_{3f} = 0 \qquad 4.3$$

or

$$\varepsilon_{1f} = - (\varepsilon_{2f} + \varepsilon_{3f})$$

Tables VI,VII & VIII show the principal surface strains at the fracture site and the surface limit strains (FLD) compiled from all the tests conducted on materials 3003-0, 5182-0 and 2036-T4.

Figures 40 to 42 show the plot of fracture strain, ε_{3f}, versus the strain ratio, a, for the same three materials, which Figures 43 to 45 show the variation of the fracture surface strains, ε_{1f} and ε_{2f}, for the materials.

To analyse the failure mode and strain gradients existing at the fracture site a number of specimens, failed under different conditions of loading, were chosen. Each specimen was cut perpendicular to the plane of the sheet and to the fracture line. These specimens were then mounted for examination under the optical microscope.

Figures 46 to 50 show a series of photographs taken

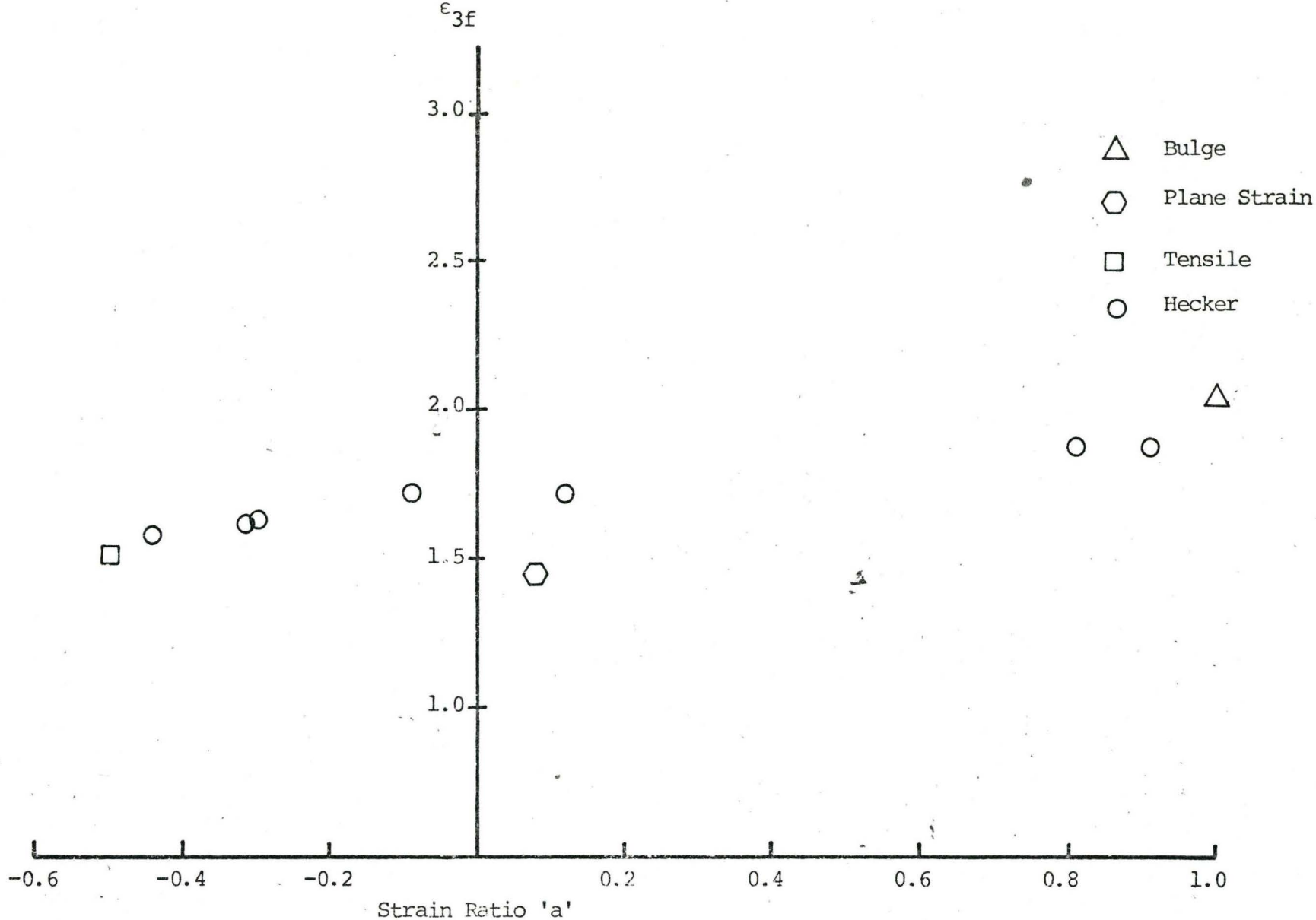

FIGURE 40 - Fracture Strain ε_{3f} Versus Strain Ratio 'a' for 3003-0 Aluminum Alloy

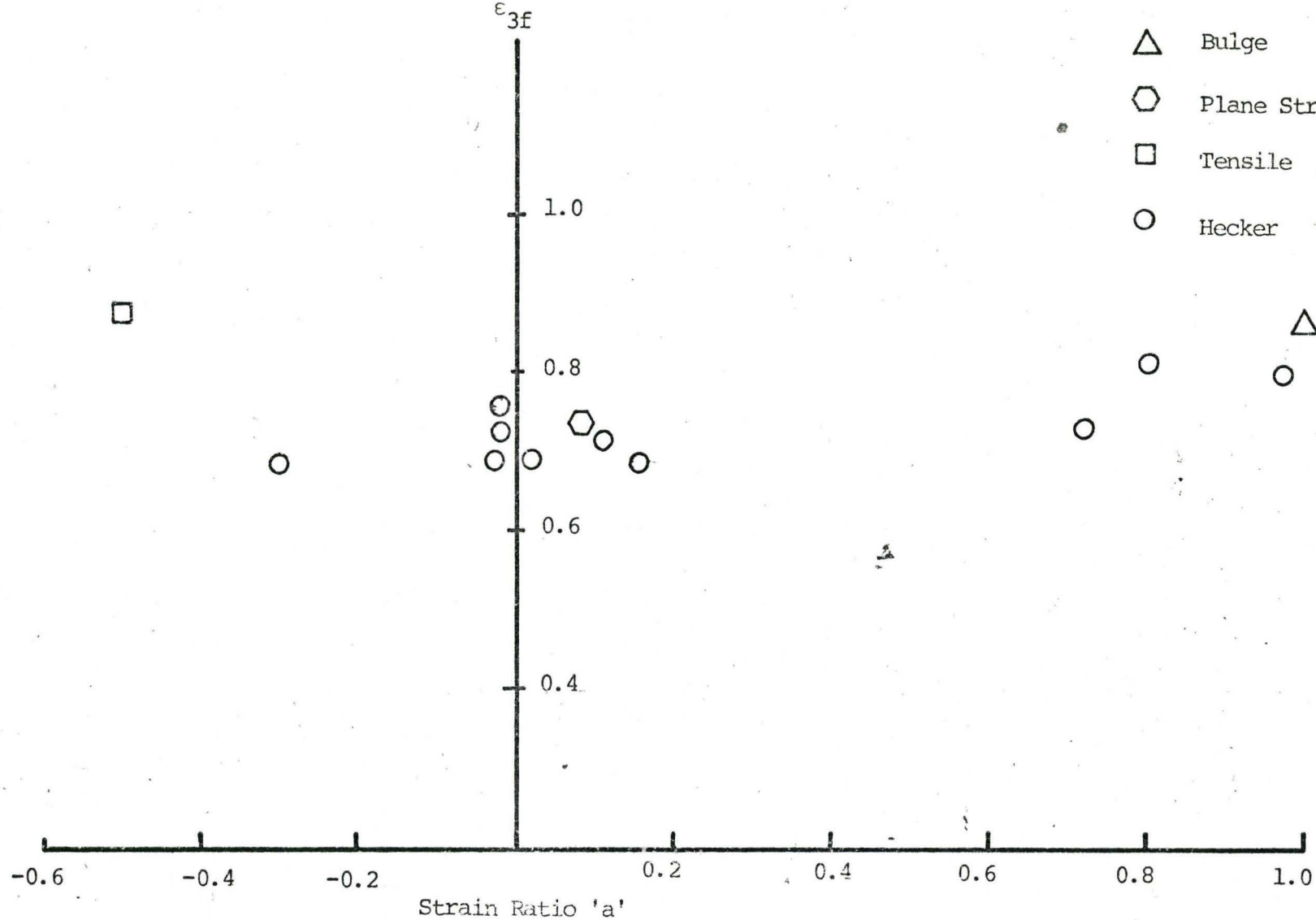

FIGURE 41 - Fracture Strain ε_{3f} Versus Strain Ratio 'a' for 5182-0 Aluminum Alloy

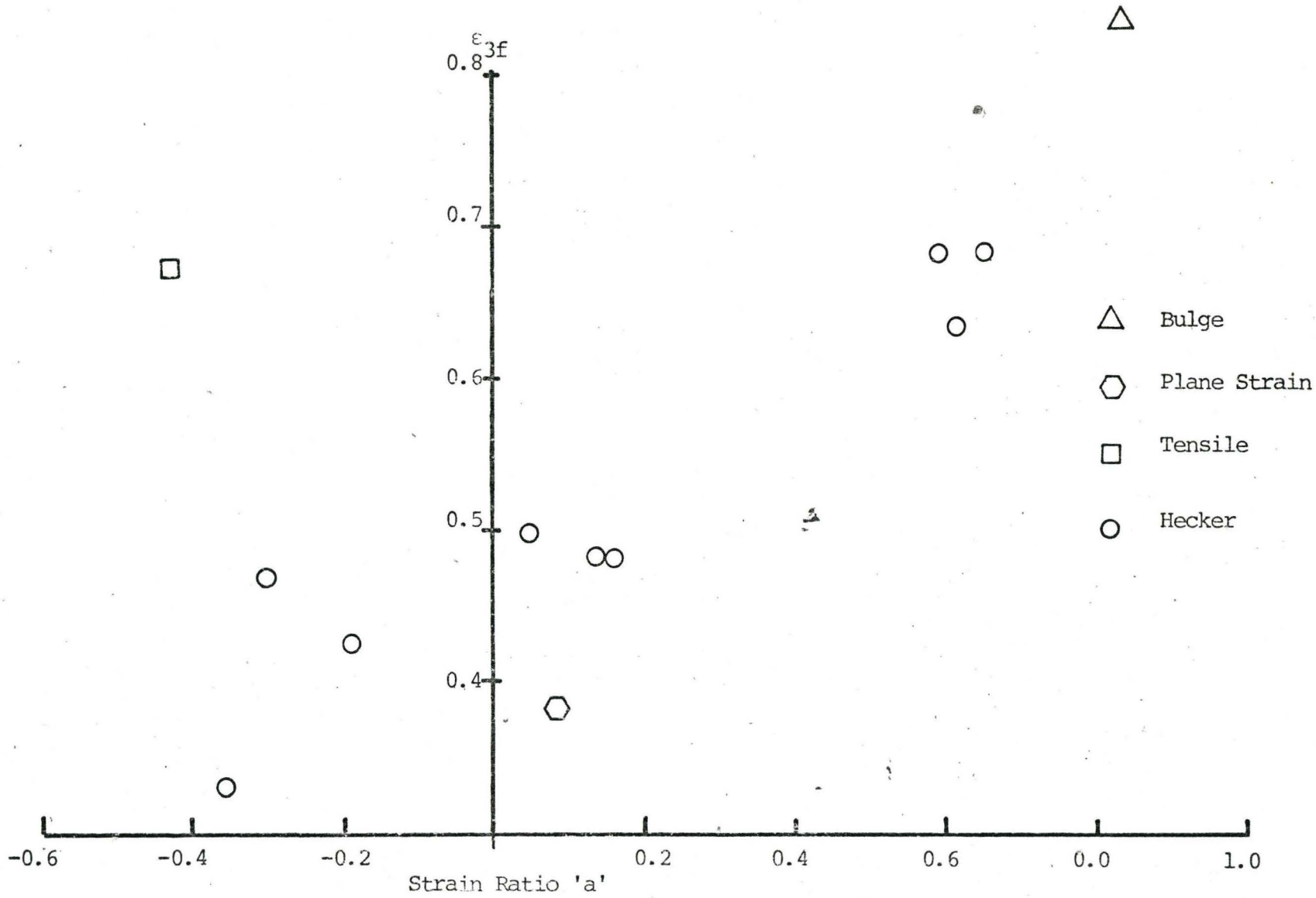

FIGURE 42 - Fracture Strain ε_{3f} Versus Strain Ratio 'a' for 2036-T4 Aluminum Alloy

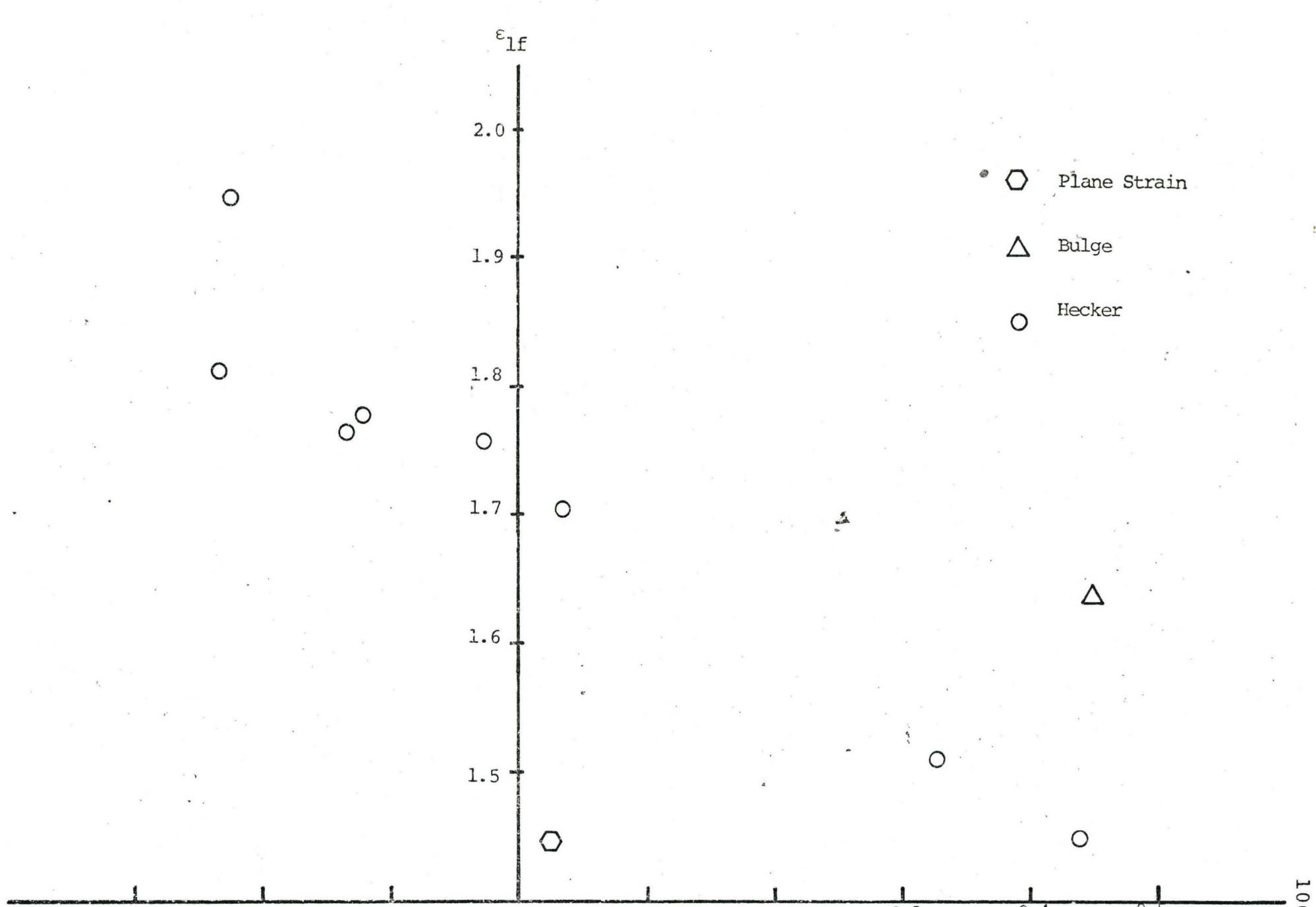

FIGURE 43 - Fracture Surface Strains ε_{1f} Versus ε_{2f} for 3003-0 Aluminum Alloy

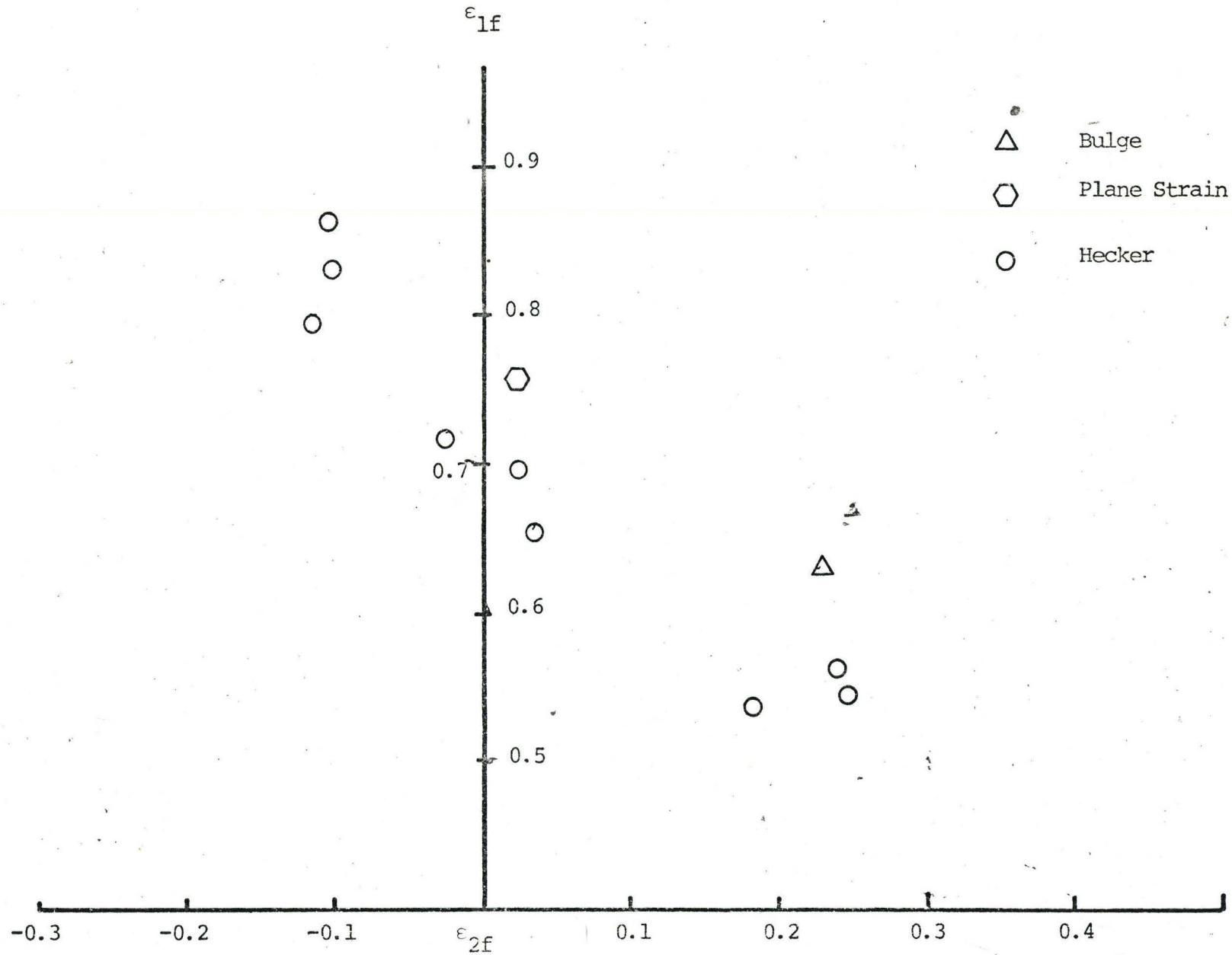

FIGURE 44 - Fracture Surface Strains ε_{1f} Versus ε_{2f} for 5182-0 Aluminum Alloy.

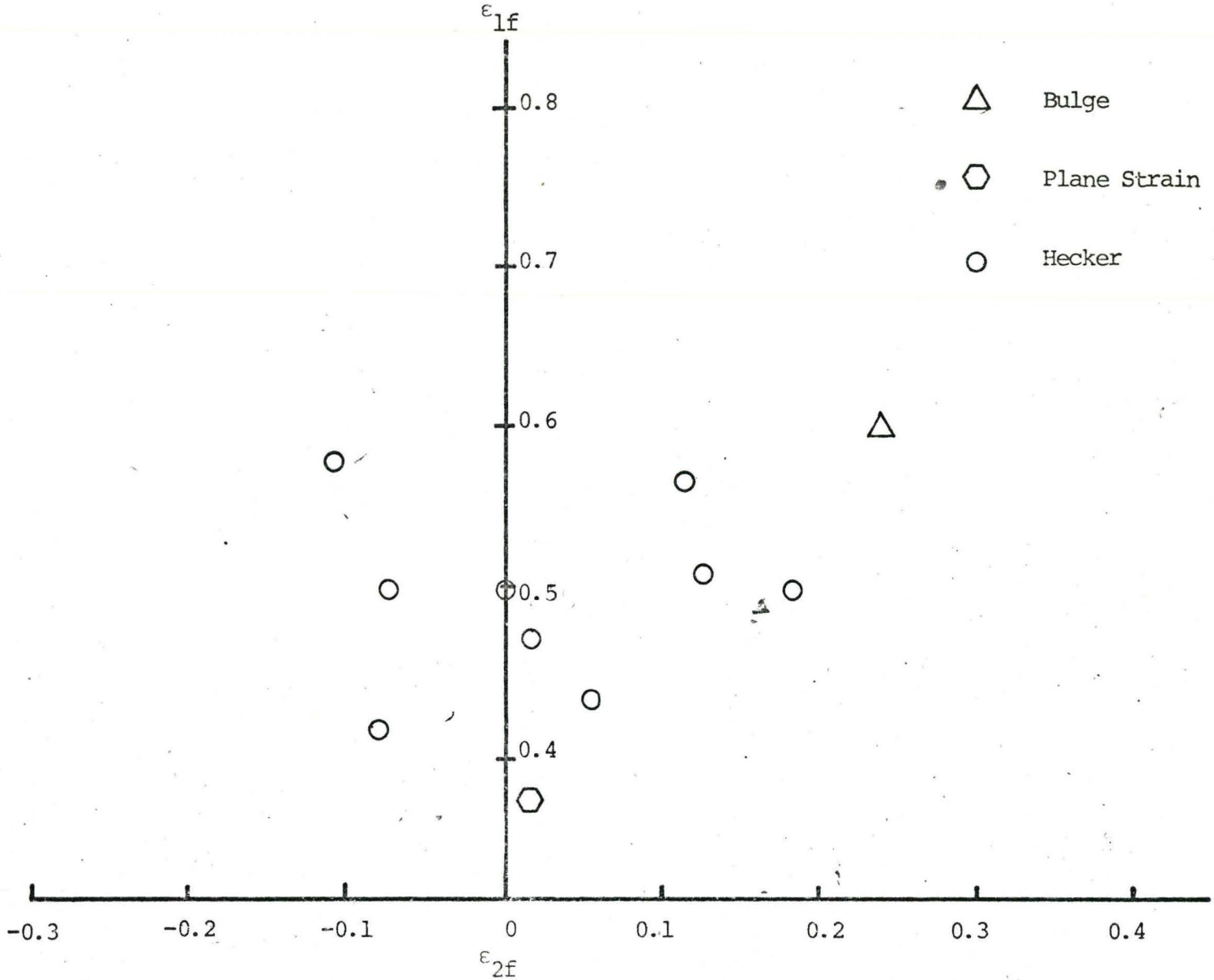

FIGURE 45 - Fracture Surface Strain ε_{1f} Versus ε_{2f} for 2036-T4 Aluminum Alloy

TENSILE SPECIMEN

a = ½

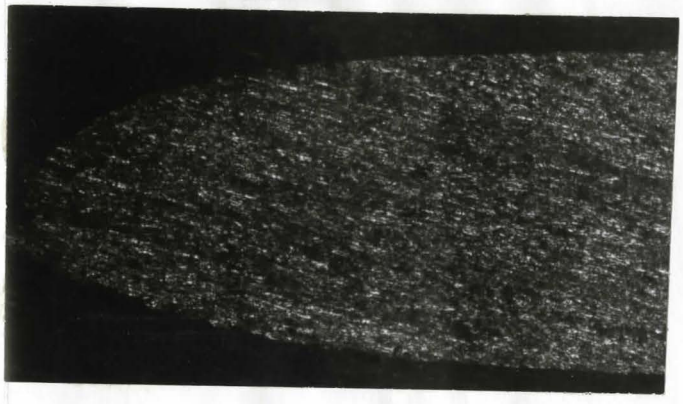

PLANE STRAIN

a = .08

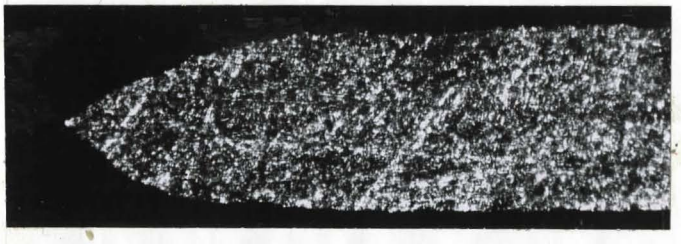

BULGE

a=1

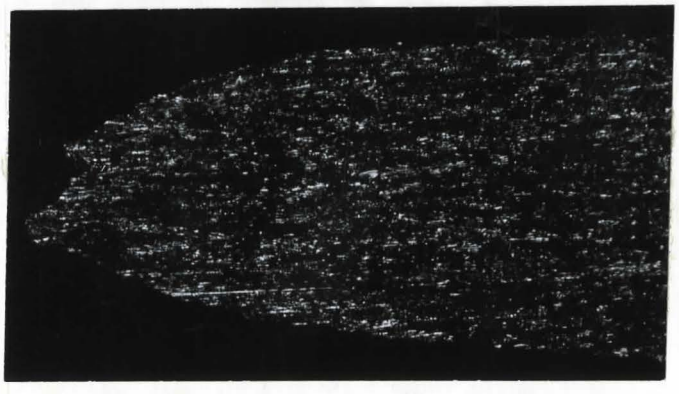

HECKER TEST

a = -½

FIGURE 46 For Thickness Profile at Fracture Site
Material 3003 - Aluminum Alloy, 66X

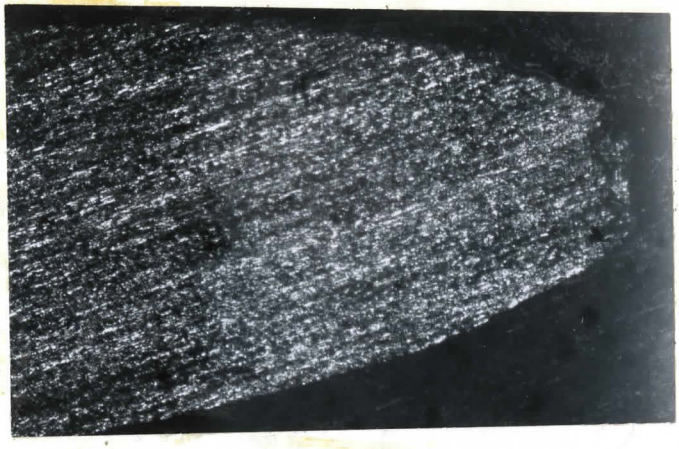

TENSILE SPECIMEN

a = -½

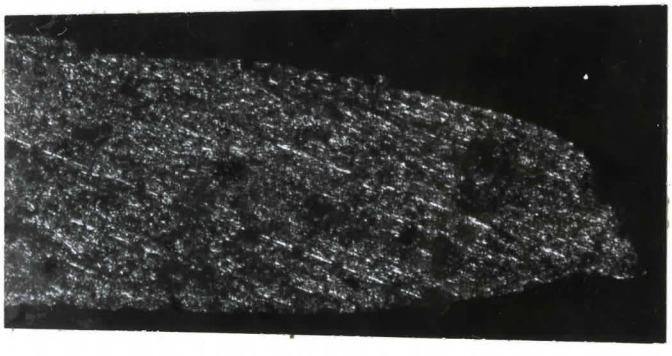

BULGE

a=1

FIGURE 47 Thickness Profile at Fracture Site for Material 3003 H14 Aluminum Alloy, 66X

TENSILE TEST SPECIMEN

a = .5

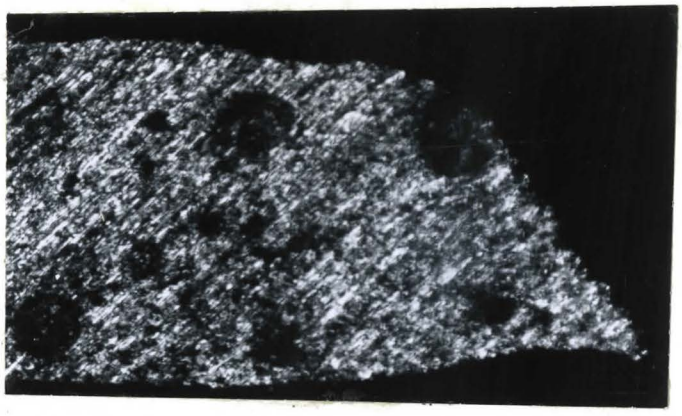

PLANE STRAIN TEST SPECIMEN

a = .08

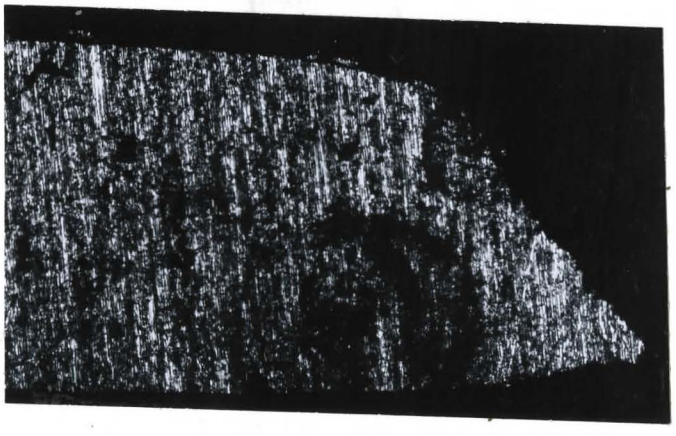

HECKER TEST SPECIMEN

a = .12

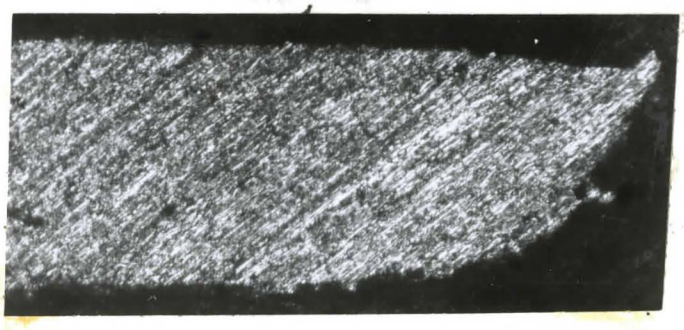

BULGE TEST SPECIMEN

a = 1

FIGURE 48 Thickness Profile at Fracture Site for 5182-0 Aluminum Alloy, 66X

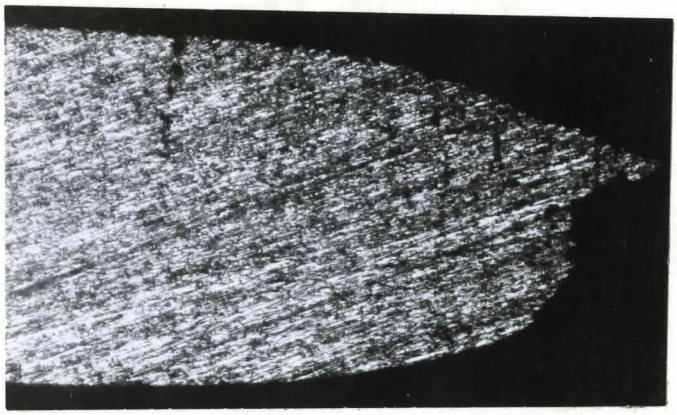

TENSILE TEST
SPECIMEN

a = -½

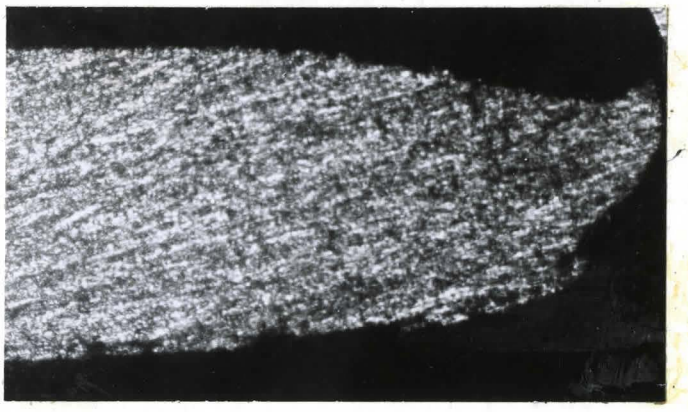

BULGE TEST
SPECIMEN

a=1

FIGURE 49 - Thickness Profile at Fracture Site for 5182-H111 Aluminum Alloy, 66X.

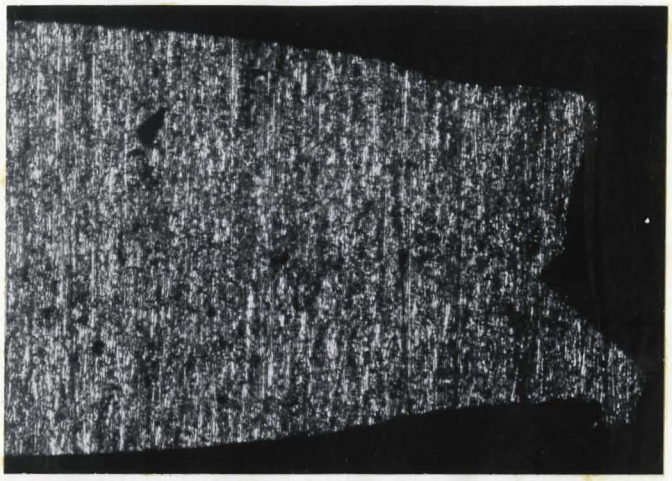

TENSILE TEST SPECIMEN

a = ½

PLANE STRAIN TEST SPECIMEN

a = .08

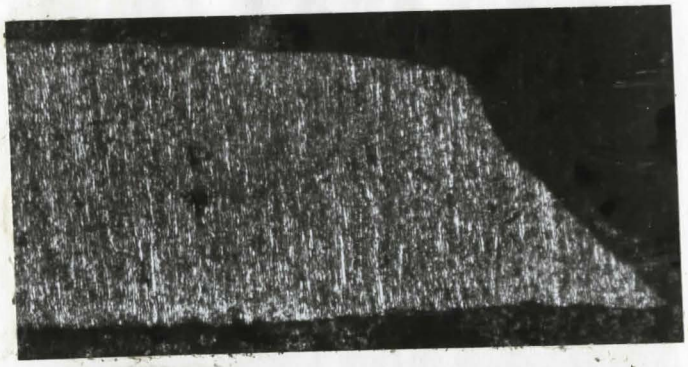

BULGE TEST SPECIMEN

a=1

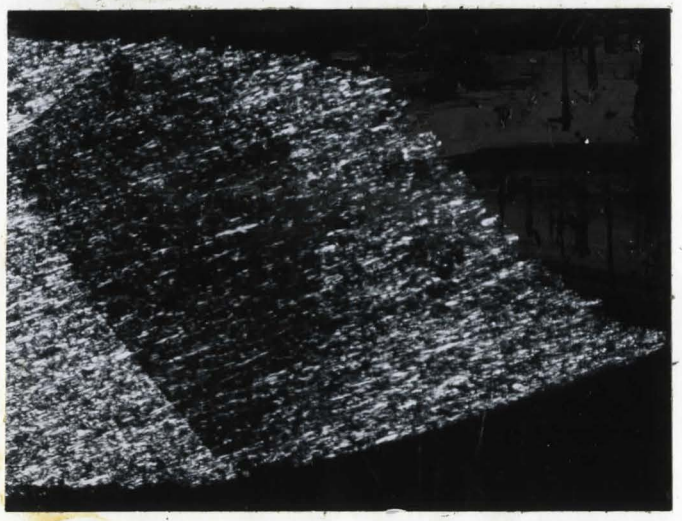

HECKER TEST SPECIMEN

a=.155

FIGURE 50 - Thickness Profile at Fracture Site for 2036-T4 Aluminum Alloy, 66X

from optical microscope with a magnification of 66. It can be seen from Figures 46 and 47 that alloys 3003-0 and 3003-H14 show a steep strain gradient and pronounced localized neck at the fracture site. The fracture appears to have all the characteristics of a ductile failure mode.

Figures 48, 49 and 50 show the thickness profiles at fracture site for 5182-0, 5182-H111 and 2036-T4 aluminum alloys. Even with different loading conditions these alloys do not show much strain gradient at the fracture site and the fracture mode appears to be of a shear type. Certainly, these materials do not show the same propensity to develop high strain gradients at fracture as the 3003 alloys.

4.8 Computer Program for Predicting True stress - True Strain

The program EVAL is designed to convert either load and percent elongation in a Tension Test or pressure, extensometer readings and spherometer readings from a Bulge Test, to True Stress and True Strain.

```
      PROGRAM EVAL(INPUT,OUTPUT,TAPE5=INPUT,TAPE6=OUTPUT,TAPE10)
C  EVALUATION OF WORK-HARDENING EXPONENT *N*,INITIAL STRAIN
C  *EPSO* AND STRENGTH CONSTANT *C* FROM BULGE TEST OR/AND
C  TENSILE TEST BY METHOD OF LEAST SQUARES
C
C  VARIABLES LIST
C
C  NTR  =NUMBER OF TRIALS FOR WHICH RESULTS ARE TO BE CALCULATED
C  N    =NUMBER OF OBSERVATIONS IN THIS TRIAL
C  IFLAG=PARAMETER INDICATING KIND OF TEST,IT TAKES VALUE *0* FOR
C        TENSILE TEST, AND ANY INTEGER NUMBER FOR BULGE TEST
C   A1      =INITIAL THICKNESS OF SPECIMEN (IN.)
C   A2      =INITIAL WIDTH OF SPECIMEN(IN.) FOR TENSILE TEST ,FOR BULGE A2 =0.
C  P    =READING OF PRESSURE GAUGE (PSI)
C   RLG    =READING OF LEFT EXTENSOMETER DIAL GAUGE(IN.)
C    RRG   =READING OF RIGHT EXTENSOMETER DIAL GAUGE (IN.)
C  H    =READING OF SPHEROMETER DIAL GAUGE (IN.)
C    D0    =INITIAL GAP OF EXTENSOMETER
C
C
C
      DIMENSION X(50),Y(50),TITLE(4)
      COMMON A1,A2,TITLE,EXPON,   STR,STCOF
      READ (5,10) NTR
      READ(5,90)TITLE,A1,A2
      M1=0
      M2=0
      D0=1.193
      DO 200 II=1,NTR
      READ (5,11) N,IFLAG
```

```
      IF (IFLAG.EQ.0) GOTO 51
      TO=A1
      M1=M1+1
      WRITE (6,20) M1
      WRITE(6,99)TITLE,A1,A2
      NN=0
      DO 40 L=1,N
      READ(5,12)  P,RLG,RRG,H
      A=RLG+RRG
C
C     REJECT DATA POINTS WITH STRAIN VALUES LESS THAN  3 PERCENT
C
      IF (A.LE.0.0054) GOTO 55
      D=D0+3.125*A
C
C   PRESSURE GAUGE CALIBERATION
      IF(P.LT.300.0)PT=(P+3.60)*.996
      IF(P.GE.300.0)PT=(P-0.3)/0.994
      IF(P.GE.1000.0)PT=(P-22.1)/0.997
      I=L-NN
C
C  CALCULATE REPRESENTATIVE STRESS AND STRAIN
      X(I)=2.0*ALOG(D/D0)
      RS=(1.056+H*H)/(2.0*H)
      T=TO*(D0/D)**2.0
      Y(I)=(PT*RS)/(2.0*T)
      WRITE(6,96)X(I),Y(I)
C  Y(I) AND X(I) ARE REPRESENTATIVE STRESS AND STRAIN RESPECTIVELY
C
      GOTO 40
```

```
 55   NN=NN+1
 40   CONTINUE
      N=I
C  PERFORM LEAST SQARES FIT OF RESULTS TO SIGMA=C*(EPSO+EPSILON)**N
      CALL STATS (X,Y,N)
      GOTO 200
 51   M2=M2+1
      WRITE (6,27) M2
      WRITE(6,99)TITLE,A1,A2
      A=A1*A2
C
C  Y(I),X(I) = LOAD (LBS) AND EXTENSION (PER CENT) READ
C  FROM INSTRON TESTING MACHINE PLOT
      READ (5,14) (X(I),I=1,N)
      READ (5,14) (Y(I),I=1,N)
      DO 60 I=1,N
C  CALCULATE REPRESENTATIVE STRESS AND STRAIN
      X(I)=ALOG(1.0+X(I)/100.0)
      Y(I)=Y(I)*EXP(X(I))/A
      WRITE(6,96)X(I),Y(I)
 96   FORMAT(F12.6,4X,F12.6)
C  Y(I) AND X(I) ARE REPRESENTATIVE STRESS AND STRAIN RESPECTIVELY
C
 60   CONTINUE
C  PERFORM LEAST SQARES FIT OF RESULTS TO SIGMA=C*(EPSO+EPSILON)**N
      CALL STATS(X,Y,N)
200   CONTINUE
 10   FORMAT (I4)
 11   FORMAT (2I4)
 12   FORMAT(F6.2,4X,3F10.8)
```

```
 13  FORMAT (2F8.5,F5.3)
 14  FORMAT (5F12.6)
 15  FORMAT (F8.5)
 20  FORMAT (1H1,* BULGE TEST RESULTS   *,*  TRIAL NO. *,I4/)
 21  FORMAT(* INITIAL THICKNESS OF SPECIMEN= *,F7.5,* IN.*,/)
 27  FORMAT (1H1,* TENSILE TEST RESULTS   *,*  TRIAL NO. *,I4/)
 90  FORMAT(4A10,2F10.4)
 99  FORMAT(1H1,4A10,F10.4,1H*,F10.4//)
     STOP
     END
```

4.9 Computer Program for Curve Fitting and Plotting the true stress - strain data

The relationship between true stress and natural strain data obtained from tensile or bulge test is expected to be linear when plotted logarithmically.

With data that can be correlated by a straight line, there is one straight line for which the sum of squares of deviations of one of the variables is a minimum. Such a straight line will be a least squares line, reference [38].

If the pairs of the variables associated with each data point are designated as x_i and y_i, with y designated as the independent variable, a straight line through the data is expressed as

$$y = a + bx \qquad \text{(C1)}$$

where

y - estimated value of y for an observed value of x

a - intercept, giving estimated value of y at x = 0

b - slope of line of regression coefficient.

The values of a and b corresponding to the line with minimum-squared deviation of y from y have been well established.

These are

$$a = \bar{y} - b\,\bar{x} \tag{C2}$$

$$b = \frac{\sum_{i=i}^{N} (x-\bar{x})\ (y-\bar{y})}{\sum_{i=i}^{N} (x - \bar{x})^2} \tag{C3}$$

where

$$\bar{x} = \frac{1}{N} \sum_{i=i}^{N} x_i$$

$$\bar{y} = \frac{1}{N} \sum_{i=i}^{N} y_i$$

N - number of data points

As a measure of goodness of the correlation, a correlation coefficient R has been taken as

$$R = b \frac{\sum_{i=i}^{N} (x_i-\bar{x})^2}{\sum_{i=i}^{N} (y_i - \bar{y})^2} \tag{C4}$$

The correlation coefficient ranges from 1.0 to 0.0 depending on the goodness of the fit of the line.

The correlation coefficient R of 1.0 indicates a perfect association between the variables, the correlation coefficient R of 0.0 indicates a completely random relation.

In our case equation (C1) takes the form

$$\log \sigma = \log k_1 + n \log (\varepsilon_0+\varepsilon) \tag{C5}$$

where

$$k_1 = k\ \dot{\varepsilon}^{\,m}$$

according to the generalized material behaviour law,

$$\sigma = k\ (\varepsilon_o + \varepsilon)^n\ \dot{\varepsilon}^{\,m}. \qquad (C6)$$

In order to fit the experimental data to equation (5) a computer program is provided.

The experimental data (load and extension) are first transformed into true stresses and natural strains by program EVAL (App. B1). For the bulge test data points for $\varepsilon < 0.03$ are removed due to the large scatter within that range.

The least squares fit is performed then by subroutine STATS in two stages:

1. Computation of n, k_1, and R, according to equations (2), (3), (4), (5) for $\varepsilon_o = 0.0$. At this stage the data points deviating by $\pm$ 3% from the least squares line are removed.

2. Successive computation of n, k and R for ε_o increased in steps of 0.001. The execution of the program is stopped when R reaches a maximum magnitude, the values of n, k_1, and R for $\varepsilon_o = 0.0$ and n, k_1, ε_o for maximum value of R are then printed out.

The additional subroutine PLOT is provided to plot the experimental data points and the theoretical curve $\sigma = k_1(\varepsilon_o + \varepsilon)^n$, with true stress and natural strain as co-ordinate axes.

It has to be pointed out that the least squares line corresponding to equation (5) minimizes the squares of deviations of log σ from log σ and not the deviations of σ from σ. This modification is, however, not of significance.

```
      SUBROUTINE STATS (X,Y,N)
C  THIS SUBROUTINE PERFORMS A LEAST SQARES FIT S=C*(EPSO+E)**N
C    VALUES OF EPSO ARE SUGGESTED IN THE STEPS OF 0,001
C
C  AS A CRITERION OF BEST FIT HAS BEEN TAKEN COEFFICIENT
C  OF LINEAR CORRELATION ACCORDING TO *APPLIED STATISTICS
C  FOR ENGINEERS* BY WILLIAM VOLK
C
C  Y(I) AND X(I) ARE REPRESENTATIVE STRESS AND STRAIN RESPECTIVELY
C
      DIMENSION X(50),Y(50),XN(25),C(25),R(25),EPSO(25) ,
     $ TITLE(4),RX(25),RY(25)
      COMMON A1,A2,TITLE,EXPON,   STR,STCOF
      WRITE (6,28)
      M=0
 107  SY=0,0
      SSY=0,0
      DO 70 I=1,N
      SLOG=ALOG10(Y(I))
      FILOG=ALOG10(X(I))
      SY=SY+SLOG
      SSY=SSY+SLOG*SLOG
      IF (N,EQ,0) GOTO 70
      WRITE (6,23)  Y(I),X(I),SLOG,FILOG
  70  CONTINUE
      RSSY=SSY-(SY*SY)/N
      R(1)=0,0
      EPSO(1)=0,0
      JJ=0
      DO 35 K=2,22
```

```
      SX=0.0
      SSX=0.0
      SXY=0.0
      DO 45 I=1,N
      FILOG=ALOG10(X(I)+EPSO(K-1))
      SLOG=ALOG10(Y(I))
      SX=SX+FILOG
      SSX=SSX+FILOG*FILOG
   45 SXY=SXY+SLOG*FILOG
      RSSX=SSX-(SX*SX)/N
      RSXY=SXY-SX*SY/N
      XN(K)=RSXY/RSSX
      C(K)=10**(SY/N-XN(K)*SX/N)
      IF (M.EQ.1) GOTO 105
      NN=0
      DO 90 L=1,N
      YY=C(K)*X(L)**XN(K)
      A=ABS(YY-Y(L))-.03*YY
      IF (A) 101,102,102
  102 NN=NN+1
C
C  DATA POINTS REJECTED BY CURVE FITTING AS THEY LIE 3 PCNT OUTSIDE
C
      JJ=JJ+1
      RX(JJ)=X(L)
      RY(JJ)=Y(L)
      GOTO 90
  101 I=L-NN
      Y(I)=Y(L)
      X(I)=X(L)
```

```
   90  CONTINUE
       N=I
       M=1
       GOTO 107
  105  R(K)=XN(K)*SQRT(RSSX/RSSY)
       IF(R(K)-R(K-1)) 100,110,110
  110  EPSO(K)=EPSO(K-1)+.001
   35  CONTINUE
  100  WRITE(6,24)
       WRITE (6,25)
       WRITE (6,26) XN(2),EPSO(1),C(2),R(2)
       WRITE (6,26)  XN(K-1),EPSO(K-2),C(K-1),R(K-1)
            STR=EPSO(K-2)
       EXPON=XN(K-1)
       STCOF=C(K-1)
   23  FORMAT (F15.4,F13.4,F15.4,F13.4/)
   24  FORMAT (1H1)
   25  FORMAT      (9X,2HXN,8X,4HEPSO,7X,5HCONST,7X,1HR/)
   26  FORMAT (F12.4,F11.4,F12.3,F10.3/)
   28  FORMAT (6X,12HSTRESS(PSI ),2X,11HTRUE STRAIN,3X,11HLOG(STRESS),2X,
      111HLOG(STRAIN)/)
C
C  CALLING PLOTTING SUBROUTINE
C
       CALL PLOTSO(X,Y,N,RX,RY,JJ)
       RETURN
       END
```

```
      SUBROUTINE  PLOTSQ(X,Y,N,RX,RY,JJ)

 THIS SUBROUTINE USES A PLOTING AREA 6IN BY 6IN

      DIMENSION X(50),Y(50),RX(25),RY(25),TITLE(4)
      COMMON A1,A2,TITLE,EXPON,   STR,STCOF

 SEARCHING FOR MAX VALUE S OF X AND Y

      XMAX=0.0
      YMAX=0.0
      DO 51 I=1,N
      IF (X(I).GT.XMAX)  XMAX=X(I)
      IF (Y(I).GT.YMAX) YMAX=Y(I)
   51 CONTINUE
      DO 52 I=1,10
      IF (YMAX .LT. 10000.0*FLOAT(I)) GO TO 53
   52  CONTINUE
   53 YMAX=10000.0*FLOAT(I)
      DO 54 J=1,15
      IF (XMAX.LT. 0.05*FLOAT(J)) GO TO 55
   54 CONTINUE
   55 XMAX=0.05*FLOAT(J)

 CHOOSING SCALES

      XSCALE=6.0/XMAX
      YSCALE=6.0/YMAX
      CALL PLOT(0.0,0.0,3)
      CALL LETTER(6,0.3,90.0,3.0,4.0,6HSAREEN )
```

```
      CALL PLOT(4.0,0.5,-3)
      CALL LETTER(40,0,1,90,0,0.2,0.5,TITLE)
      ENCODE(20,96,A3) A1,A2
   96 FORMAT(2F10.6)
      CALL LETTER (20,0,1,90,0,0,2,5,0,A3)
      CALL LETTER (6,0,2,0,0,5,0,0,0,6HSTRAIN)
C    CHOOSING NEW ORIGEN
      CALL PLOT(3,0,1.5,-3)
C    PLOTTING THE AXIS
      CALL PLOT(0,0,6.0,3)
      CALL PLOT(0.0,0,0,2)
      CALL PLOT (6.0,0,0,2)
C   CALIBERATING THE AXIS
      DO 56 I=1,10
      Q=(YMAX*FLOAT(I))/10.0
      YS=Q*YSCALE
      ENCODE(8,57,AODE) Q
   57 FORMAT(F8.1)
      CALL LETTER(8,0,1,0,0,-1,0,YS,AODE)
   56 CONTINUE
      DO 58 J=1,10
      P=(XMAX*FLOAT(J))/10.0
      XS=P*XSCALE
      ENCODE(6,59,ST) P
   59 FORMAT(F6.3)
   58 CALL LETTER(6,0,1,90,0,XS,-1,0,ST)
C    PLOTTING DATA POINTS USED IN CURVE FITTING
      DO 61 I=1,N
      XS=X(I)*XSCALE
      YS=Y(I)*YSCALE
```

```
 61   CALL MATH(XS,YS,0,1,0,0,5HPOINT)
      CALL PLOT(0,0,0,0,3)
C    PLOTTING DATA POINTS  REJECTED BY CURVE FITTING
      IF(JJ,EQ,0)GO TO 79
      DO 62 I= 1,JJ
      XS=RX(I)*XSCALE
      YS=RY(I)*YSCALE
 62   CALL MATH(XS,YS,0,1,0,0,5HDELTA)
      CALL PLOT(0,0,0,0,3)
 79   DX=XMAX*0,05
       WRITE(6,211) EXPON,STR,STCOF
 211  FORMAT(4X,F12,6,4X,F12,6,4X,F12,4)
      DO 63 I=1,20
      XB=DX*(FLOAT(I))
      YB=STCOF*((XB+   STR)**EXPON)
      XS=XB*XSCALE
      YS=YB*YSCALE
 63   CALL PLOT(XS,YS,2)
C  WRITING THE EQUATION OF THE CURVE FITTED
      ENCODE(10,64,KAPA) STCOF
 64   FORMAT(F10,3)
      ENCODE(6,65,EO)    STR
 65   FORMAT(F6,4)
      ENCODE(6,66,COF) EXPON
 66   FORMAT(F6,4)
      CALL GREEK(7,0,0,0,0,1,90,0,5HSIGMA )
      CALL MATH(7,0,0,5,0,1,90,0,5HEQUAL)
      CALL LETTER(10,0,1,90,0,7,0,1,0,KAPA)
      CALL MATH (7,0,2,2,0,2,90,0,6HLPAREN)
      CALL GREEK (7,0,2,5,0,1,90,0,6HEPSLON )
```

```
      CALL MATH(7,0,2,8,0,1,90,0,4HPLUS)
      CALL LETTER(6,0,1,90,0,7,0,3,0,EO)
      CALL MATH (7,0,3,7,0,2,90,0,6HRPAREN )
      CALL LETTER(6,0,1,90,0,6,8,4,0,COF)
C  CLOSING THE TAPE
      CALL PLOT(14,0,-2,0,3)
      CALL PLOT(0,0,0,0,999)
      RETURN
      END
```

CDTOT 99

CHAPTER 5

Discussions and Conclusions

The tensile data for the aluminum alloys illustrate that 3003-0 Al-Mn alloy is soft and ductile. The increase in strength and attendant decrease in ductility through cold working is clearly demonstrated by the 3003-H14 material. The strength of the 5182 Al-Mg alloy is about the same as that of AKDQ steel, while the 2036-T4 Al-Mg-Cu alloy is somewhat stronger. The degree of uniform straining (i.e. strain prior to necking) was about the same for the higher strength alloys and was comparable to that of mild steel. Thus on the basis of the tensile data it would appear that the objective of developing formable alloys with strength levels similar to that of AKDQ steel can be achieved.

With the higher strength alloys there was a tendency to show a slight yield point elongation. However, this was not manifest by unsightly Lüders band markings on the specimen during the early stage of the tensile test for 2036-T4 alloy. The 5182 aluminum alloy shows both yield point elongation and serrated yielding and hence shows both Type A and Type B band marks. Stretch formed components with this material are likely to show band marks, inclined at 45 degrees to the rolling direction, in the

lower strained regions.

It has become customary to attempt to fit tensile data with empirical power hardening laws and suppliers of the sheet metal to quote a strain hardening index ('n' value) for the material. The curve fitting programmes have been developed in this thesis, specifically for the ease of extracting this sort of information.

As described in the thesis, simple instability analysis will predict that the uniform strain is equal to 'n' value. However, all the higher strength aluminum alloys showed a uniform strain smaller than the predicted 'n' value, even though excellent correlation was obtained between the actual data and the fitted curves. This author acknowledges that the discrepancy could be credited to the empiricism in the curve fitting techniques. Nevertheless it illustrates a deviation from the practise that has been established for mild steels.

In attempting to explain this discrepancy, values of fracture strain were obtained for these higher strength alloys. The reasoning being that if low fracture strains are exhibited then there will be attendant decrease in the level of uniform strain. Certainly, the fracture strains were lower for the 5182 and 2036-T4 alloys as given in Table II and the mode of fracture is different for the alloys

as seen by comparing Figures 46 to 50. This difference in fracture behaviour was also demonstrated in the Load versus Extension Curve, since the post necking domain (region beyond the maximum load point) was virtually non-existent with the higher strength alloys. However, a maximum load point was always obtained and the materials did not fracture under a rising load. It is to be noted that none of these observations in themselves predict the level of uniform strain.

Some investigators have postulated that the discrepancy may be associated with the strain rate sensitivity characteristics of the material. Attempts have been made to ascertain the strain rate sensitivity factor 'm' through "change speed" tests on a tensile testing machine. This technique was also performed in this present work and it was found that for the 5182 and 2036-T4 alloys, the 'm' value was slightly negative (in the order of .003 to .01), while for the other material 'm' appeared to be positive. Whatever the influence 'm' exerts on the useful levels of formability, it is the opinion of this author that the answer will not be found by conducting instability analysis (based on a maximum load criterion) using an empirical constitutive law of the type

$$\sigma = K(\varepsilon_o+\varepsilon)^n \dot{\varepsilon}^m$$

The 'm' value always appears to be too small, vis a vis the 'n' value, to exert a strong influence.

The strain hardening index 'n' was also obtained from the "In-plane" torsion test and bulge test, see Tables III and IV. These 'n' values are somewhat lower than those obtained from the tensile test data. The bulge and torsion test may be interpreted as giving an average 'n' value, since they reflect the behaviour of the whole sheet and not a specified orientation as in the tensile test. Differences in stress-strain behaviour of a material as observed from different test methods is usually attributed to the anisotropy of the material, and in turn this is reflected by variations in 'n'. However, the differences in 'n' as observed in these current experiments are somewhat larger than anticipated. The bulge test extends the stress-strain data beyond that obtainable with the tensile test and it was noticed that over the latter portion of the curve a change in gradient was observed. This suggests that 'n' value is not constant over the entire range as obtained by fitting a power hardening law to the data. In fact the correlation of the fitted curve was not as good in the case of the bulge test. Some authors have suggested taking two values of 'n' for the bulge test data, one for the initial portion of the curve and a second value for the

final region. In the opinion of this present author, this might be a pragmatic approach but begs the question as to what is the cause of such behaviour.

The materials were anisotropic as illustrated in Table II. Variations in 'r' within the plane of the sheet will generally be reflected by 'earing' in the drawing test. The fact that 'r' is lower than unity for all orientations indicates that these materials will have inferior drawability to AKDQ steel. Varification of these statements are to be found in the deep drawing tests conducted by Cloke [16].

As explained in this thesis much higher limit strains are generally obtained in the bulge test vis a vis the tensile test. In this present work it was found that the surface limit strains were marginally bigger (and about the same for 5182 H111) for the higher strength alloys. It appears that lower thickness fracture strains 'ε_{3f}' for these alloys limits the uniform straining that can be obtained.

From a theoretical point of view localized necks (as they are generally understood) would not occur in the bulge test. However, a pronounced local neck is observed with the 3003 alloys as illustrated in Figures 46 and 47, the effect of strain localization at fracture is less apparent with the higher strength alloys as illustrated in Figures

48 to 50.

The forming Limit Curves for the higher strength alloys, as determined from the Hecker test (see Figures 36 and 37),are all lower than that of AKDQ steel for $-\frac{1}{2}<a<1$. In the stretch-stretch mode ($o<a<1$) the curves for the high strength alloys are rather flat indicating little change in formability with the strain path. However, the apparent formability is a function of the deformation geometry and loading conditions as is evident from the following considerations.

i) A condition of plane strain was obtained by the Hecker test (stretching over a hemispherical punch) and from the Marciniak test (stretching the material in its plane). Lower values of limit strain are always obtained from the Marciniak test.

ii) Balanced biaxial tension was achieved by three methods:

a) The Hecker Test

b) The Marciniak Stretch Test

c) The Bulge Test.

Lower values of limit strains were always obtained with tests b) and c).

It is the opinion of this author that although differences in deformation geometry play a role, a significant factor in the improved formability with the Hecker test is

the interfacial punch pressure. In other words the punch exerts a high compressive stress on the material over its region of contact. Evidence exists which illustrates that even small compressive stresses superimposed on a tensile loading system enhances the uniform straining in a tensile specimen [39,40]. In a recent paper, Pearce and Ganguli [41] have presented data which also confirms the improved level of FLD obtained with the Punch Test over that achieved when bulging (with oil pressure) elliptical diaphragms of different aspect ratio.

This investigation has provided results of the fracture strains under different loading conditions, which has hitherto been unreported. The thickness fracture strain 'ε_{3f}' for the 3003 alloys are the highest and this value remains relatively constant over the whole range of loading conditions as shown in Figure 40. At the point of fracture severe strain gradients are present with this material and the failure mode appears to be ductile.

For the higher strength alloys the thickness fracture strain 'ε_{3f}' is much smaller. These alloys do not exhibit large strain gradients at fracture and show a shear type of failure mode. With the 5182-0 alloy, the thickness fracture strain shows a slight upward trend towards balanced biaxial tension, Figure 41. The results for the 2036-T4 alloy show a great deal of scatter but ε_{3f} appears to be

minimised in the region of plane strain and maximised towards balanced biaxial and uniaxial tension. At this stage author is incapable of explaining this behaviour except commenting that ε_{3f} is very sensitive to the loading conditions for this alloy.

It is to the belief of this author that this work has highlighted some of the differences that exist in the formability of high strength aluminum alloys and AKDQ steel. From the tensile test data alone good strength and high 'n' values are obtained for 5182 and 2036 alloys. However, low FLD's, low fracture strains and low 'r' values have also been revealed and these findings indicate inferior press performance for the 5182 and 2036-T4 alloys in all modes of sheet forming. Hence, to extend the use of aluminum alloys for automotive stamping, it will be necessary to avoid localization of deformation through less severe part design, through redesigning of dies and proper control of other process variables such as lubrication and hold-down pressures.

REFERENCES

1. S.P. Keelar, "Determination of Forming Limits in Automotive Stampings", Sheet Metal Ind., 683, (1965).

2. S.P. Keelar, "Understanding Sheet Metal Formability", Series of Six Articles, Machinery (1968).

3. G.M. Goodwin, "Application of Strain Analysis to Sheet Metal Forming Problems in the Press Shop", SAE Paper 680093.

4. R. Pearce and J. Woodthorpe, "An Aid to Practical Sheet Metal Forming", J. Mech. Eng. Sci., 12, 443, (1970).

5. R. Pearce, "A Users Guide to Forming Limit Diagrams", Sheet Metal Ind., 943, (1971).

6. R.L. Whitely, "The Importance of Directionality in Drawing Quality Steel", Trans. ASME, 52, 154, (1960).

7. J. Woodthorpe and R. Pearce, "The Effect of $\bar{r}$ and n upon the FLD of Sheet Steel", Sheet Metal Ind., 1061, (1969).

8. S.P. Keelar and W.A. Backofen, "Plastic Instability and Fracture in Sheets Stretched over Rigid Punches", Trans. ASME, 56, 25, (1963).

9. G.G. Moore and J.F. Wallace, "The Effect of Anisotropy on Instability in Sheet Metal Forming", J. Inst. of Metals, 93, 33, (1964).

10. M. Azrin and W.A. Backofen "The Deformation and Failure of a Biaxially Stretched Sheet", Met. Trans., 1, 2857, (1970).

11. Z. Marciniak and K. Kuczynski, "Limit Strains in the Process of Stretch Forming Sheet Metal", Int. J. Mech.

Sci., 9, 609, (1967).

12. Z. Marciniak, K. Kuczynski and T. Pokora, "Influence of Plastic Properties of a Material on the Forming Limit Diagram for Sheet Metal in Tension", Int. J. Mech. Sci., 15, 789, (1973).

13. S.S. Hecker, "A Simple Forming Limit Curves Technique and Results on Aluminum Alloys", Proc. 7th Biennial Congress of IDDRG., Amsterdam, Oct. 9-10, (1972).

14. S.S. Hecker, "Formability of Aluminum Alloys", Trans. ASME, 97, Series H, 66, 1975.

15. A.S. Kasper, D.G. Adams and J.A. Dicello, "Sheet Metal Forming Limits with Manufacturing Applications", Proc. 21st Sagamore Army Materials Research Conf., Aug. (1974).

16. W.T. Cloke, "Formability of Aluminum and Steel in Drawing Square Cups", M.Eng. Thesis, McMaster University, Hamilton, Ontario, Canada. (1975).

17. R. Sowerby and W. Johnson, "A Review of Texture and Anisotropy in Relation to Metal Forming", Mats. Sci. and Eng., 20, 101, (1975).

18. P.H. Albertin, "Development of the Biaxial Stress Test for Sheet Material", M. Eng. Thesis, McMaster University, Hamilton, Ontario, Canada (1972).

19. Z. Marciniak and J. Kolodziejski, "Assessment of Sheet Metal Failure Sensitivity by Method of Torsioning the Rings", Proc. 7th Biennial Congress of the IDDRG, Amsterdam, Oct. 9-10, (1972).

20. M. Atkinson, "Assessing Normal Anisotropic Plasticity of Sheet Metals", Sheet Metal Ind., 167, (1967).

21. D.K. Uko, "The Bending Under Tension Test", M.Eng. Thesis, McMaster University, Hamilton, Ontario, Canada, (1975).

22. S.S. Hecker, "A Cup Test for Assessing Stretchability", Metals Engineering Quat., 30, Nov.(1974).

23. N. Chung, J.D. Embury, J.E. Evensen, R.G. Hoagland and C.M. Sargent, "Unstable Shear Failure in a 7075 Aluminum Alloy" (To be published).

24. A Considere, Ann Ponts et Chaussees, 9, Sec. 6, (1885).

25. Z. Marciniak, "Aspects of Material Formability", McMaster University, Hamilton, Ontario, Canada (1974).

26. R. Hill, "Discontinuous Plastic States: Localized Necking of Thin Sheets", J. Mech. and Phy. of Solids, 1, 19, (1952).

27. H.W. Swift, "Plastic Instability under Plane Stress", J. Mech. and Phy. of Solids, 1, 1, (1952).

28. R. Hill, "A General Theory of Uniqueness and Stability in Elastic-Plastic Solids", J. Mech. and Phy. of Solids, 6, 236, (1958).

29. R. Hill, "A Theory of the Plastic Bulging of a Metal Diaphragm by Lateral Pressure", Phil. Mag., (Sec 7) 41, 1133, (1950).

30. W. Johnson and P.B. Mellor, "Plasticity for Mechanical Engineers", Von Nostrand (1962).

31. Z. Marciniak, "Analysis of Necking Preceding Fracture of Sheet Metal Under Tension", La Metallurgia italiana, 8, 701, (1968).

32. R. Sowerby and J.L. Duncan, "Failure in Sheet Metal in Biaxial Tension", Int. J. Mech. Sci., 13, 217, (1971).

33. R. Hill, "Mathematical Theory of Plasticity", Oxford University Press, Ely House London, (1950).

34. R.D. Venter and M.C. deMalherbe, "Theoretical Estimate of the Keelar-Goodwin Formability Curve", SMI, (1971).

35. V. Hasek, "Influence of Different Factors on the Position and Form of FLD", Proc. of NAMW Res. Conf., McMaster University, Hamilton, Ontario, Canada, 35 (1973).

36. G.L. Baraya, J. Parker and J.W. Flowett, "Mechanical and Photographic Processes for Producing Grid of Lines", Int. J. Mech. Sci., 5, 365, (1963).

37. A.K. Ghosh and S.S. Hecker, "Stretching Limits in Sheet Metals: In plane Versus Out of Plane Deformation", Met. Trans., 5, 2161, (1974).

38. W. Volk, "Applied Statistics for Engineers", McGraw Hill, (1958).

39. A. Taraldsen, "Stabilized Tensile Testing", Material Testing, 6, 189, (1964).

40. J.D. Benedyk, "The Significance of Tensile Necking Retardation on Sheet Metal Formability", Proc. of NAMW Res. Conf. II, Wisconsin Univ., 381, (1974).

41. R. Pearce and D. Ganguli, "The Forming Limits of Aluminum - Magnesium Alloy Sheet in Biaxial Tension", J. of Inst. of Metals, 100, 289, (1972).